Impurity Redistribution During Silicon Epitaxial Growth And Semiconductor Device Processing.

Citation

LANGER, PAUL H. *Impurity Redistribution During Silicon Epitaxial Growth And Semiconductor Device Processing.* 1973, https://preserve.lehigh.edu/lehigh-scholarship/graduate-publications-theses-dissertations/theses-dissertations/impurity.

INFORMATION TO USERS

This material was produced from a microfilm copy of the original document. While the most advanced technological means to photograph and reproduce this document have been used, the quality is heavily dependent upon the quality of the original submitted.

The following explanation of techniques is provided to help you understand markings or patterns which may appear on this reproduction.

1. The sign or "target" for pages apparently lacking from the document photographed is "Missing Page(s)". If it was possible to obtain the missing page(s) or section, they are spliced into the film along with adjacent pages. This may have necessitated cutting thru an image and duplicating adjacent pages to insure you complete continuity.

2. When an image on the film is obliterated with a large round black mark, it is an indication that the photographer suspected that the copy may have moved during exposure and thus cause a blurred image. You will find a good image of the page in the adjacent frame.

3. When a map, drawing or chart, etc., was part of the material being photographed the photographer followed a definite method in "sectioning" the material. It is customary to begin photoing at the upper left hand corner of a large sheet and to continue photoing from left to right in equal sections with a small overlap. If necessary, sectioning is continued again – beginning below the first row and continuing on until complete.

4. The majority of users indicate that the textual content is of greatest value, however, a somewhat higher quality reproduction could be made from "photographs" if essential to the understanding of the dissertation. Silver prints of "photographs" may be ordered at additional charge by writing the Order Department, giving the catalog number, title, author and specific pages you wish reproduced.

5. PLEASE NOTE: Some pages may have indistinct print. Filmed as received.

Xerox University Microfilms
300 North Zeeb Road
Ann Arbor, Michigan 48106

73-23,808

LANGER, Paul H., 1941-
IMPURITY REDISTRIBUTION DURING SILICON
EPITAXIAL GROWTH AND SEMICONDUCTOR DEVICE
PROCESSING.

Lehigh University, Ph.D., 1973
Engineering, metallurgy

University Microfilms, A XEROX Company, Ann Arbor, Michigan

IMPURITY REDISTRIBUTION DURING SILICON EPITAXIAL GROWTH AND SEMICONDUCTOR DEVICE PROCESSING

by

Paul H. Langer

A Dissertation

Presented to the Graduate Committee

of Lehigh University

in Candidacy for the Degree of

Doctor of Philosophy

in

Metallurgy and Materials Science

Lehigh University

1973

(5-1-73)

Approved and recommended for acceptance as a dissertation in partial fulfillment of the requirements for the degree of Doctor of Philosophy.

April 11, 1973

Dr. J. I. Goldstein
J. I. Goldstein

Accepted, May 1, 1973

Special Committee directing
the doctoral work of
Mr. Paul H. Langer

J. I. Goldstein Chairman J. I. Goldstein

W. C. Hahn W. C. Hahn
S. R. Butler S R Butler
M. Charles M. Charles
K. E. Benson K E Benson

ACKNOWLEDGMENTS

The author wishes to acknowledge the advice and encouragement of his doctoral committee. He wishes to especially thank his advisor Dr. J. I. Goldstein for his continued interest and encouragement. The help of Dr. K. E. Benson in supplying the experimental apparatus was greatly appreciated.

He also wishes to thank Mr. W. R. McCormack of Western Electric who allowed the author the time and support necessary to accomplish this investigation. He would also like to thank Mr. C. L. Paulnack, N. Fichter, Mr. S. Boehn and Mr. A. Kaminsky of Bell Telephone Laboratories for their aid in the construction of the experimental apparatus.

Finally the author wishes to thank his wife and family for their continued devotion, patience, and encouragement which made this work possible.

TABLE OF CONTENTS

LIST OF FIGURES

LIST OF TABLES

ABSTRACT

A model has been developed that can account for both front and back "autodoping" effects during epitaxial growth as well as impurity redistribution during further high temperature processing. The model incorporates three dopant fluxes, i.e., 1) the flux from the solid into the gas phase at the rear of the wafer, 2) the flux from the solid to the front surface of the wafer, and 3) the flux from the bulk gas phase into the boundary layer near the front surface of the wafer in which transport of dopant occurs by diffusion only. The redistribution of impurities both within the solid semiconductor and in the gas phase are investigated from a theoretical viewpoint. Numerical solutions are obtained using the Crank-Nicolson method. A computer program is presented that can handle the simultaneous redistribution of five dopant elements, during processing steps such as epitaxial growth, oxidation, and ion implantation. Implications of differences between this approach and previous work is discussed. Calculated results are presented to illustrate the variety of problems that may be solved using this mathematical approach.

The evaporation coefficient of boron in silicon in a hydrogen ambient was experimentally determined to be,

$$h = 1.674 \times 10^{7} e^{-2.48/kT}$$

where h is in microns/min, the energy is expressed in eV., and temperature is in ^{o}K. This equation was determined in the temperature range

from 1190 to 1380 C. These results allowed the accurate prediction of boron back surface "autodoping" effects during epitaxial growth. Radial as well as in depth concentration versus distance plots were experimentally determined illustrating boron autodoping for both lightly and heavily doped substrates. Excellent agreement between the numerically determined concentration profiles and the experimental data for boron autodoping is obtained using the experimentally determined values of the evaporation coefficient.

INTRODUCTION

The distribution of impurities in epitaxial grown silicon layers plays a major role in the operation of diodes, transistors, and integrated circuits. The impurity redistribution that occurs during silicon epitaxial processing and semiconductor device fabrication is dependent upon processing times and temperatures, diffusivities, evaporation rates, and segregation coefficients of the dopants in the solid and gaseous phases. A model for the redistribution process would enable one to assess the critical steps in the fabrication sequence and predict the effect of process changes on the impurity distribution in the semiconductor. A typical device processing sequence may consist of fifteen discrete high temperature steps that affect the impurity redistribution. Since the results of the prior step form the initial conditions for the present step analytical solutions to the diffusion or transport equations are not available. Therefore a sequential numerical technique is the obvious choice to solve this type of processing problem. At present only fragmentary parts of this problem have been solved and no complete model exists.

The purpose of this dissertation is to derive the boundary conditions necessary to describe the epitaxial growth and device fabrication process, and then to solve the diffusion equation in the solid in conjunction with these boundary conditions using a numerical solution. In order to test the numerical model the evaporation coefficient of boron in silicon will be experimentally determined. Using this evaporation data predictions concerning the transport of boron during epitaxial growth will be made and tested against experimentally determined concentration profiles of boron in the epitaxial layer. Once the accuracy of the computer model has been established experimentally a number of semiconductor processing problems will be simulated and the calculated impurity concentration versus depth results will be compared with the experimental values.

Background - Epitaxial Growth

Since the largest single unknown in calculating the impurity redistribution during device fabrication is the redistribution due to epitaxial growth this process step will be treated in great detail. The prior efforts on modeling the substrate and layer impurity redistribution during epitaxial silicon growth can be divided into three categories based upon the source of the impurity. The first and earliest approach involved the transfer of dopant from the front surface of the substrate,(1-2) mixing of this dopant with the gas phase, and subsequent reincorporation of this dopant into the growing epitaxial layer. This treatment completely ignored solid state diffusion as the other major mechanism for dopant transport. The second approach to the redistribution involved the transport of dopant by diffusion in the solid only.(3-4) The effects of the ambient gas phase were neglected. A more detailed analysis of this approach was made by Abe, et al.(5) A numerical approach was used in order to treat the steps prior to the deposition of the epitaxial layer. The influence of the gas phase on the redistribution process was ignored and the case of slow layer growth was not successfully treated. The third approach to the redistribution problem involved the transfer of dopant from the back surface of the wafer into the ambient and its subsequent incorporation into the growing epitaxial layer.(6-8) However, the effects of solid state diffusion were ignored.

All three approaches have been used and the results of the models have been verified over a limited range of experimental conditions. The three approaches give a wide range of predictions when applied to any one common system. Since front and back surface evaporation and diffusion of dopant are all occurring simultaneously throughout the epitaxial growth and other high temperature processing steps, a model incorporating all of the three approaches would provide a better description of the process.

The type of dopant transport phenomenon that will predominate in a given epitaxial deposition cycle is a function of the distribution of dopant in the substrate along with the dopant intentionally added to the gas phase. Three dopant fluxes must be considered to completely define the boundaries of the gas solid composite system. The first flux is that between the solid and the gas at the back boundary. This flux is the one that has been treated by Joyce et al.,(6) Shepherd,(7) and Skelly(8) as the sole contributing factor to the "autodoping" phenomenon. A similar flux existing at the front surface of the wafer gives the rate of transfer of dopant from the solid to the front gas-solid interface. This flux is of great importance in understanding autodoping associated with the first few microns of growth.

After the first few microns of growth in normal epitaxy (i.e., lightly doped layer on highly doped substrate) the back transport effect predominates. The third flux is that flux which controls the rate of transport of dopant from the bulk of the gas phase to the gas phase boundary layer near the front interface. In the gas phase boundary layer, diffusion is the sole transport mechanism. This flux can include intentionally added dopant as well as the dopant released at the back surface.

The following treatment will determine the three dopant fluxes and establish the boundary conditions for the problem. The doping of a layer with the same dopant as in the substrate as well as different dopant species is considered. Also non-uniform initial conditions are treated by the numerical method employed to solve Fick's Second Law in the solid.

THEORY

The solution of the problem will involve the treatment of three regions, 1) bulk gas phase where all the dopant is uniformly distributed, 2) gas phase boundary layer where transport of dopant is by diffusion only, and 3) the solid where transport of dopant occurs only by diffusion. Figure 1 depicts a section of an epitaxial reactor with the wafer on a heated susceptor. The various sources of dopant are shown schematically. To reduce this situation to a one dimensional case consider a line z=zo, perpendicular to the wafer in the plane A-A. Figure 2 shows the concentration distribution along the line z=zo from the wall of the reactor, x=w to the back surface of the wafer, x=b. This line also passes through the boundaries x=d and x=i which respectively separates the bulk gas phase from the gas phase boundary layer, and the gas phase boundary layer from the front surface of the wafer. All subsequent analysis of impurity redistribution problems will refer to the dopant movement along the line z=zo. A mathematical model describing the redistribution sequence can be formulated since the impurity redistribution with the solid and within the gas phase boundary layer is diffusion controlled. For a diffusion controlled process Fick's Second Law (for constant diffusivity, D) in one dimension is,

$$\frac{\partial C(x,t)}{\partial t} = D \frac{\partial^2 C(x,t)}{\partial x^2} \tag{1}$$

where C(x,t) is the concentration and x and t are the spatial and time

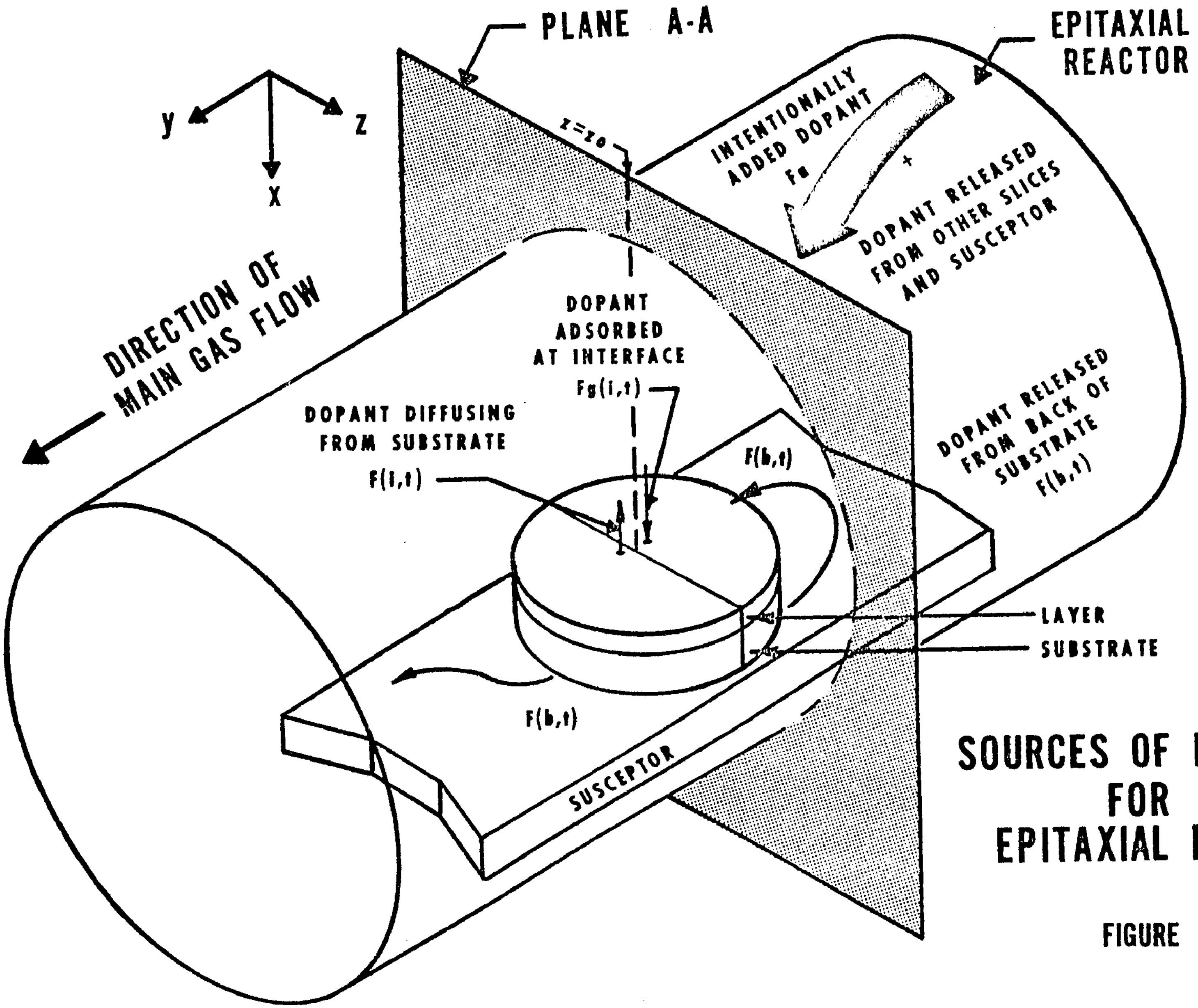

SOURCES OF DOPANT
FOR
EPITAXIAL LAYER

FIGURE 1

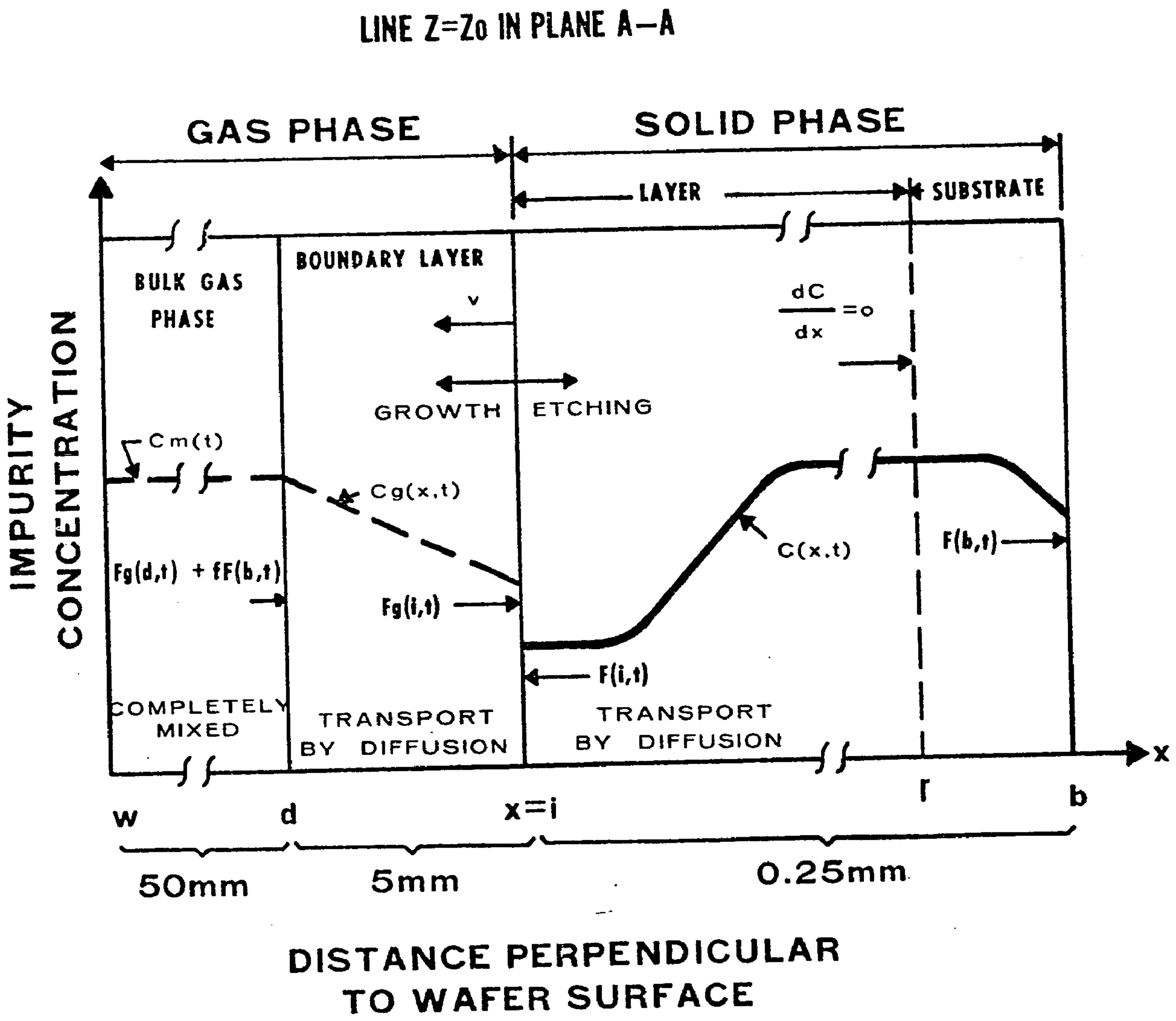
LINE Z=Zo IN PLANE A—A
GAS PHASE
SOLID PHASE
LAYER
SUBSTRATE
BULK GAS PHASE
BOUNDARY LAYER
v
dC/dx =o
GROWTH
ETCHING
Cm(t)
Cg(x,t)
C(x,t)
F(b,t)
Fg(d,t) + fF(b,t)
Fg(i,t)
F(i,t)
COMPLETELY MIXED
TRANSPORT BY DIFFUSION
TRANSPORT BY DIFFUSION
IMPURITY CONCENTRATION
x
w
d
x=i
r
b
50mm
5mm
0.25mm
DISTANCE PERPENDICULAR TO WAFER SURFACE

FIGURE 2

variables respectively. The one dimensional assumption is applicable to the case of uniformly doped epitaxial structures normally encountered in semiconductor device fabrication since the diameter to thickness ratio of the wafer is usually greater than 150 to 1. For analysis of sub-diffused substrates encountered in integrated circuit fabrication the one dimensional analysis does not strictly apply since transport of dopant from the diffused regions to the non-diffused areas occurs parallel to the surface of the wafer. This dopant transfer may still be analyzed in one dimension by treating the diffused and non-diffused regions as separate structures linked by an intermediate gas phase. In order to obtain the boundary condition at the front gas-solid interface (x=i) the mass balance will be constructed about the interface. The flux F(i,t) in the solid at the interface x=i will then be expressed in terms of solid concentrations and concentrations of dopant in the bulk of the gas phase. Both of these concentrations may be measured experimentally.

As can be seen from Figure 1 there are two sources of dopant that may enter the growing epitaxial layer by way of the gas phase. These sources are the flux of intentionally added dopant, F_a, and the flux of dopant escaping from the back and sides of the wafer F(b,t). These dopant fluxes will be used to define the time rate of change of dopant, $Q' = dQ/dt$, in control region 1 shown in Figure 2A. Let one consider the dopant flow into and out of region 1. This area is in the x-y plane between x=w to x=d and $y=y_1$ to $y=y_2$. The dopant entering this region consists of the flux of intentionally added

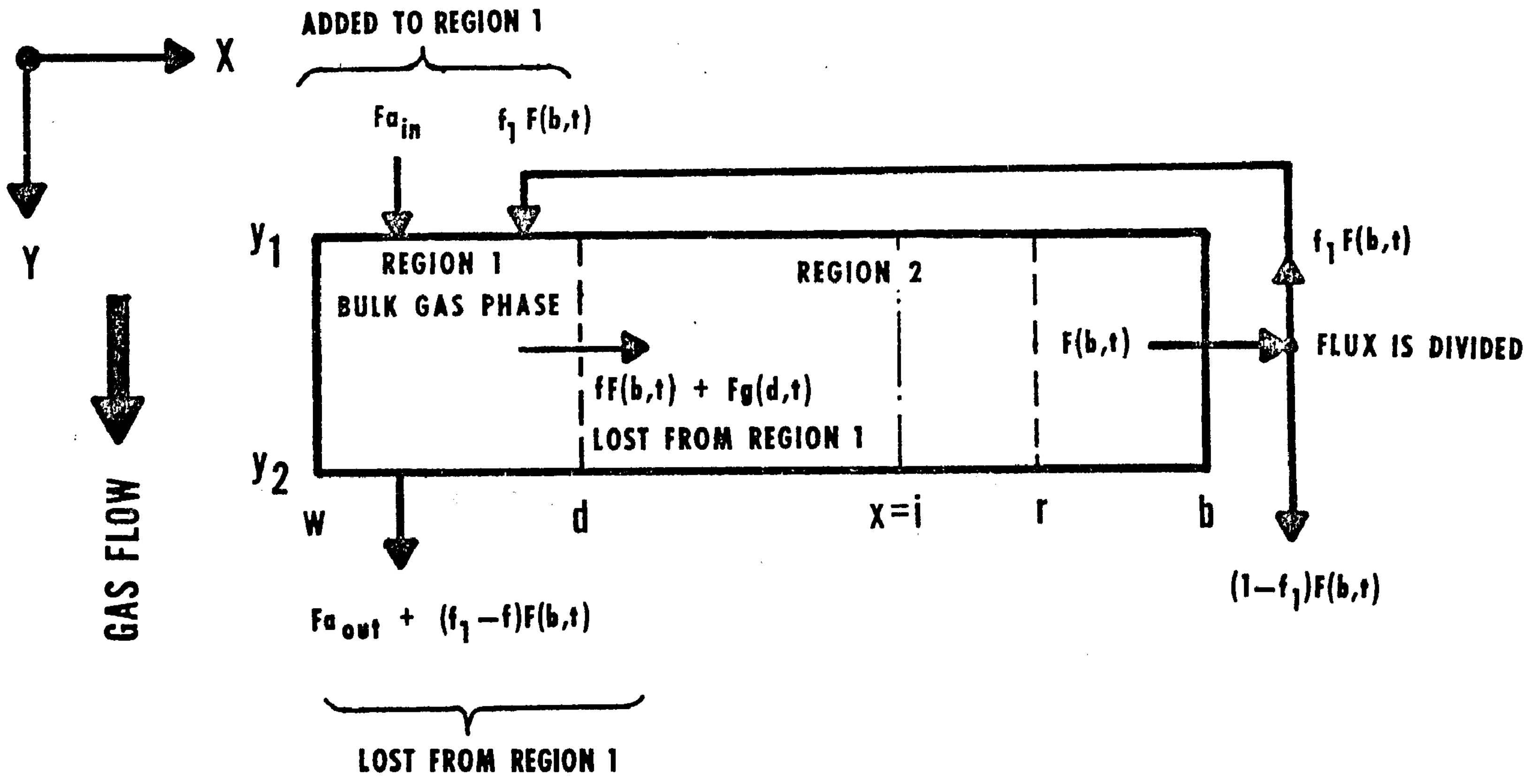

FIGURE 2A CONTROL REGION

impurities, $F_{a_{in}}$, plus some fraction (f_1) of the flux of dopant escaping from the back of the wafer $f_1F(b,t)$. Of this dopant entering region 1 across y_1 some will leave in the y-direction across y_2. The rest will enter region 2 in the x-direction, toward the solid, crossing the boundary, x=d.

Therefore the rate of change of dopant in region 1, Q_1', may be written as

$$Q_1' = F_{in} - F_{out} \tag{2a}$$

or

$$Q_1' = \{F_{a_{in}} + f_1F(b,t)\} - \{[F_{a_{out}} + (f_1-f)F(b,t)] + [Fg(d,t) + fF(b,t)]\} \tag{2b}$$

Where "f" is the fraction of dopant from the back of the wafer that is crossing the boundary x=d, in the x-direction and going toward the solid. $Fg(d,t)$ is the fraction of the intentionally added dopant also going toward the solid in the x-direction. Therefore $[Fg(d,t) + fF(b,t)]$ is the flux of dopant leaving region 1 and crossing the boundary, x=d.

Now let one consider the rate of change of dopant Q_2' (region 2, Figure 2A) in the gas-solid composite system between x=d and x=r. "r" is a point in the wafer where the concentration gradient is always equal to zero. For semiconductor device fabrication such a point always exists since wafers are usually ∿ 250 microns thick, while diffusion lengths in the solid are almost never more than 10 microns. To obtain Q_2' one first must integrate the concentration distribution in region 2 to obtain Q_2. Q_2 is the total number of dopant atoms per unit area in region 2.

$$Q_2 = \int_d^i Cg(x,t)\,dx + \int_i^r C(x,t)\,dx \qquad (3)$$

Where the symbol "g" refers to terms in the gas, while the absence of a "g" refers to terms in the solid. To obtain Q_2' one differentiates equation (3) with respect to time.

$$\begin{aligned} Q_2' = {} & \int_d^i \frac{\partial Cg(x,t)}{\partial t}\,dx + Cg(i,t)\,\frac{di}{dt} - Cg(d,t)\,\frac{dd}{dt} \\ & + \int_i^r \frac{\partial C(x,t)}{\partial t}\,dx + C(r,t)\,\frac{dr}{dt} - C(i,t)\,\frac{di}{dt} \end{aligned} \qquad (4)$$

The terms containing the expression $\int_\alpha^\beta \frac{\partial c}{\partial t}\,dx$, when α and β are arbitrary limits can be simplified using the following substitution.

$$\int_\alpha^\beta \frac{\partial C}{\partial t}\,dx = \int_\alpha^\beta D\,\frac{\partial^2 C}{\partial x^2}\,dx = F(\alpha,t)-F(\beta,t)$$

which is the integral of Fick's second law for constant diffusivity. Using the above substitution in equation (4) and defining $v_\alpha = \frac{d\alpha}{dt}$ (where α is the position of a boundary in the x-direction), one obtains:

$$\begin{aligned} Q_2' = & -Fg(i,t) + Fg(d,t) + v_iCg(i,t) \\ & - v_dCg(d,t) - F(r,t) + F(i,t) \\ & + v_mC(r,t) - v_iC(i,t) \end{aligned} \tag{5a}$$

Inspecting equation (5a) there are a number of terms that will go to zero. Since the boundary, x=r, is not moving, v_m is zero. The velocity at x=d is set equal to zero since the movement of the front interface is small compared to thickness of the gas phase boundary layer.(30) Therefore only the velocity v_i is non-zero. Since x=i is the only moving interface the subscript will be omitted. The flux at x=r is zero since "r" was defined as a point where the concentration gradient is always zero. Eliminating the zero terms from Q_2' one obtains

$$\begin{aligned} Q_2' = & -Fg(i,t) + Fg(d,t) \\ & - v[C(i,t) - Cg(i,t)] \\ & + F(i,t) \end{aligned} \tag{5b}$$

Since dopant only enters or leaves region 2 at the boundary x=d, one already knows the flux across "d" from the analysis of region 1, i.e., [Fg(d,t) + fF(b,t)]. This flux may now be set equal to Q_2' to obtain the boundary condition at the front gas-solid interface.

$$\begin{aligned} F(i,t) = & Fg(i,t) + v[C(i,t) - Cg(i,t)] \\ & + fF(b,t) \end{aligned} \tag{6}$$

The assumptions used to simplify Q′ and to derive the boundary condition at the gas-solid interface, (x=i), are summarized below:

1. Bulk gas phase completely mixed at all times.
2. A linear concentration gradient exists across the stagnant gas phase boundary layer.
3. Dopant transport in the solid phase can be characterized by Fick's Second Law.
4. The diffusivity of the dopant is independent of concentration.
5. The dopant escaping from the back surface of the wafer is not influenced by the flux of dopant at the front interface.
6. During growth, etching, or oxidation steps only the front solid interface is moving.

Equation (6) implies that the flux F(i,t) is not only a function of dopant transported from the gas (Fg(i,t)), but is also a function of the dopant leaving the back surface or sides of the wafer (F(b,t)), as well as the velocity of the front gas-solid interface, v.

Equation (6) contains flux terms that cannot be easily evaluated. Therefore the terms F(b,t) and Fg(i,t) will be approximated with the following relationships.

$$F(b,t) = -h[C(b,t) - kCg(b,t)] \tag{7}$$

and

$$Fg(i,t) = h[C(i,t) - kCg(i,t)] \tag{8}$$

These equations assume that the driving force for dopant transport at the interfaces, x=b and x=i respectively, is the concentration difference across the interface. "k" is the equilibrium segregation coefficient defined at zero growth rate as:

$$k = \frac{C(i,\infty)}{Cg(i,\infty)} \tag{9a}$$

and

$$k = \frac{C(b,\infty)}{Cg(b,\infty)} \tag{9b}$$

This type of flux approximation, (equations (7) and (8)) is used to describe a situation, at an interface, where a restriction to dopant transport exists (see Crank(28)). The restriction coefficient "h" has the units of velocity, and will be referred to in this work as the "evaporation coefficient". Grove(29) has incorrectly referred to this constant as the "gas phase mass transfer coefficient in terms of concentrations in the solid. The evaporation coefficient is a constant that depends upon the temperature, pressure, dopant species, wafer orientation, gas velocity, and reactor geometry. "h" effectively keeps the ratio of concentrations on either side of an interface from reaching the equilibrium value as defined in equations 9a and 9b. At long times equilibrium will be reached and the dopant transport across the interface will cease. The evaporation coefficient therefore controls the time rate of approach of the ratio of concentrations on either side of an interface to its equilibrium value.

For large values of "h" (i.e., $h >> \sqrt{D/t}$) the escape of dopant will be diffusion controlled since all the dopant reaching a surface will rapidly transfer into the gas phase. Also for large "h" the back flux term will rapidly approach a constant value and have the same effect as an increased constant concentration level of dopant in the gas phase. For small values of "h" there will be a large time dependence of the flux at the front interface resulting in a graded dopant distribution in the growing layer. Substituting (7) and (8) into (6) and regrouping terms one obtains an equation for the flux in the solid at the front interface in terms of solid and gas phase concentrations and the constants h, v, and f.

$$\begin{aligned} F(i,t) &= h[C(i,t) - kCg(i,t)] \\ &\quad - fh[C(b,t) - kCg(b,t)] \\ &\quad + v[C(i,t) - Cg(i,t)] \end{aligned} \tag{10}$$

Equation (10) still contains terms of Cg(i,t) and Cg(b,t) which cannot be easily measured in practice. Since the distance between the front and back surfaces of the wafer is small compared to the total boundary layer thickness, (30) we will assume Cg(b,t) = Cg(i,t). Equations (7) and (8) still contain a term, Cg(i,t), which cannot be easily measured. One approach to this dilema would be to write the flux across the gas phase boundary layer (x=d to x=i) as

$$F = hg[Cm(t) - Cg(i,t)]$$

where Cm(t) is the mean gas phase concentration and hg is the gas phase mass transfer coefficient. Then one could simultaneously solve the above equation in conjunction with equation (6) to eliminate the term Cg(i,t) in favor of the mean gas phase concentration Cm(t). This is a cumbersome method. Since the diffusivity in the gas is much larger (twelve orders of magnitude) than in the solid, and since the velocity of the gas-solid interface is small compared to the transport across the boundary layer, a simple relationship between the mean gas phase concentration and the gas phase concentration at the interface will be assumed.

$$Cg = k_g\, C_m(t) \tag{11}$$

where "k_g" is an arbitrary constant that will depend upon the gas velocity distribution in the boundary layer. "k_g" is usually very close to unity for most conditions encountered during epitaxial growth and semiconductor processing.

Finally substituting (11) into (10) and assuming Cg(b,t) = Cg(i,t), one obtains the boundary condition at the front interface in terms of readily measurable or easily calculable quantities.

$$\begin{aligned} F(i,t) &= h[C(i,t) - k_e\, C_m(t)] \\ &\quad - fh[C(b,t) - k_e\, C_m(t)] \\ &\quad + v[C(i,t) - k_g\, C_m(t)] \end{aligned} \tag{12}$$

where k_e = kkg. This flux term F(i,t) completely describes the movement of dopant both from the solid and from the gas across the front gas-solid interface. The flux of dopant will only go to zero under a set of stringent conditions. These three conditions must be met simultaneously for a zero flux to occur.

1) The velocity, v, of the gas-solid interface is zero.
2) The concentration in the solid at the front interface must be equal to ke*Cm(t).
3) The concentration in the solid at the back interface must be equal to ke*Cm(t).

If one lets $C_m(t) = 0$ and assumes that no dopant from the back is reincorporated into the growing layer (f=0) then equation (12) reduces to:

$$F(i,t) = (h+v)\ C(i,t)$$

which is Grove's(4) boundary condition for the solid neglecting gas phase contributions.

An alternate approach to the solution of the composite gas-solid system involves the solution of the transport problem in both the gas phase boundary layer and in the solid phase. This approach eliminates the assumptions about the fluxes at x=i and x=b inherent in the method outlined above. For practical reasons as outlined later, the approximation approach was chosen over the solution of the composite system.

The boundary condition at the front gas-solid interface has been developed (equation (12)). Using this boundary condition in conjunction with the boundary condition at the back of the wafer (equation

(7)) one can solve Fick's Second Law (equation (1)) in the solid using numerical techniques. In the next section the numerical solution will be developed to solve this system of equations for the concentration distribution in the solid.

NUMERICAL SOLUTION

A number of numerical techniques have been used in the past to obtain solutions to a parabolic partial differential equation (e.g. equation (1)). The simplest approach is the forward finite difference method (FFDM). This technique suffers in two major respects. The first of these is the poor approximation (only first order correct) to the time derivative of concentration. The second restriction is the limit on the stability criterion which requires that the value of the dimensionless quantity $R = D^*\Delta t/(\Delta x)^2$ can not exceed 0.5, where delta t and delta x are the time and spatial increments respectively. This limit on R forces one to employ very small values of delta t (and use extremely long computation times) if a stable solution is to be obtained. The implicit Crank-Nicolson Method (CNM) has the disadvantage of more mathematical operations than the FFDM but offers higher accuracy for the same total expenditure of computer time. Also there is no bound on the stability parameter "R" for interior points.(11) Some problems may occur at a boundary when large values of R are used especially if a large concentration discontinuity exists. Since the CNM involves analogs for the various concentration derivatives centered in the time interval delta t they are second order correct. Another advantage of the CNM is the ease in which delta x and/or delta t may be varied. It is this flexibility that leads to shorter run times for the same level of accuracy compared to the FFDM. For the initial stages of a problem where large changes in concentration with time are occurring one would like to use small values of delta t. In the final stages of the problem, where little or no concentration changes are taking place a much larger value of delta t would permit substantial savings in computer time. The spatial grid size delta x is usually only limited by the available amount of computer core storage.

The CNM analogs for the concentration derivatives necessary to solve equation (1), using the boundary conditions of (12) and (7), will be derived using a method similar to that employed by von Rosenberg.(11) A plot of concentration C versus the spatial variable i, at different time levels, j, is shown in Figure 3. To find the values of concentration at the points (i+1,j) and (i-1,j) one writes the Taylor series expansion about the point (i,j). These expressions are given below:

$$C(i+1,j) = C(i,j) + \sum_{n=1}^{\infty} \frac{\partial^n C(i,j)}{\partial x^n} \frac{(\Delta x)^n}{n!} \tag{13}$$

and

$$C(i-1,j) = C(i,j) + \sum_{n=1}^{\infty} (-1)^n \frac{\partial^n C(i,j)}{\partial x^n} \frac{(\partial x)^n}{n!} \tag{14}$$

where i and j represent the spatial and time variables. If one subtracts (14) from (13), rearranges terms, and divides both sides by

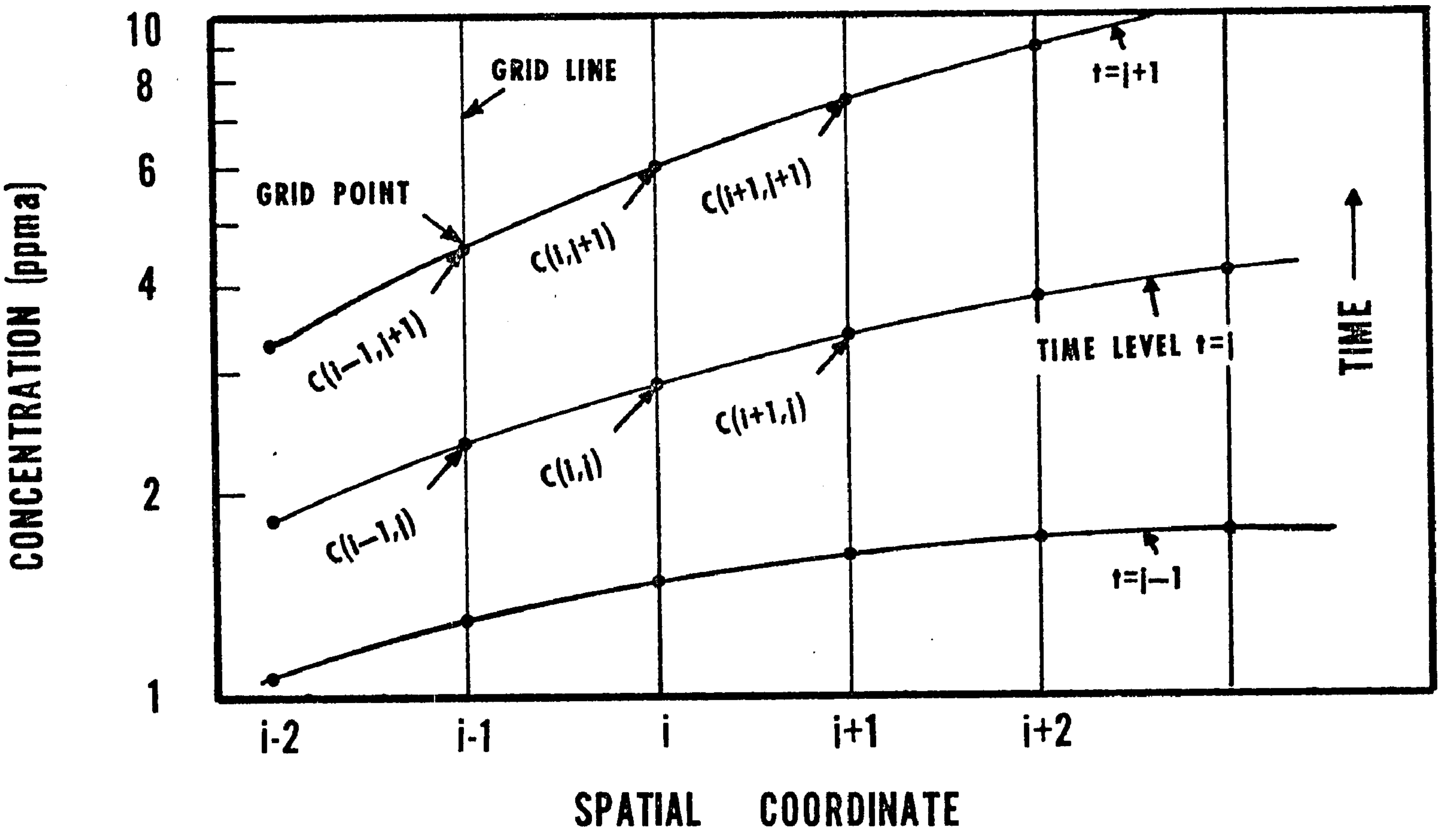

FIGURE 3 CONCENTRATION GRID AT THREE TIME LEVELS

two delta x, the first derivative is obtained.

$$\frac{\partial C(i,j)}{\partial x} = \frac{C(i+1,j)-C(i-1,j)}{2\Delta x} - \sum_{n=1}^{\infty} \frac{\partial^{2n+1} C(i,j)}{\partial x^{2n+1}} \frac{(\Delta x)^{2n}}{(2n+1)!} \tag{15}$$

If we approximate the first derivative by neglecting the higher order terms one obtains:

$$\frac{\partial C(i,j)}{\partial x} = \frac{C(i+1,j)-C(i-1,j)}{2\Delta x} \tag{16}$$

This equation is said to be second order correct since the first term that is neglected is multiplied by the finite variable, delta x, to the second power. To obtain the second derivative one can add (13) to (14), rearrange terms and divide by delta x squared. The following equation results.

$$\frac{\partial^2 C(i,j)}{\partial x^2} = \frac{C(i+1,j)-2C(i,j)+C(i-1,j)}{(\Delta x)^2} - 2 \sum_{n=2}^{\infty} \frac{\partial^{2n} C(i,j)}{\partial x^{2n}} \frac{(\Delta x)^{2n-2}}{(2n)!} \tag{17}$$

If higher order terms are neglected then the second derivative, which is second order correct can be written as:

$$\frac{\partial^2 C(i,j)}{\partial x^2} = \frac{C(i+1,j)-2C(i,j)+C(i-1,j)}{(\Delta x)^2} \tag{18}$$

To obtain a second order correct analog for the time derivative of concentration one uses the same method employed for the spatial derivative. The Taylor series for the concentration is written about the point (i,j+1/2). The resultant equations are:

$$C(i,j) = C(i,j+1/2) + \sum_{n=1}^{\infty} \frac{\partial^n C(i,j+1/2)}{\partial t^n} \left(\frac{\Delta t}{2}\right)^n \frac{1}{n!} \tag{19}$$

$$C(i,j+1) = C(i,j+1/2) + \sum_{n=1}^{\infty} (-1)^n \frac{\partial^n C(i,j+1/2)}{\partial t^n} \left(\frac{\Delta t}{2}\right)^n \frac{1}{n!} \tag{20}$$

Subtracting (19) from (20), rearranging terms, and dividing delta t one obtains:

$$\frac{\partial C(i,j+1/2)}{\partial t} = \frac{C(i,j+1)-C(i,j)}{\Delta t} - 2 \sum_{n=2}^{\infty} \frac{\partial^{2n-1} C(i,j+1/2)}{\partial t^{2n-1}} \left(\frac{\Delta t}{2}\right)^{2n-2} \frac{1}{(2n-2)!} \tag{21}$$

Neglecting the higher order terms one obtains the second order correct analog for the time derivative of concentration given below:

$$\frac{\partial C(i,j+1/2)}{\partial t} = \frac{C(i,j+1)-C(i,j)}{\Delta t} \tag{22}$$

To obtain the analog for the second partial derivative of concentration with respect to distance at the point (i,j+1/2), one takes the simple arithmetic mean of the second derivative at the point (i,j) and (i,j+1).

$$\frac{\partial^2 C(i,j+1/2)}{\partial x^2} = \frac{1}{2}\left[\frac{C(i+1,j+1)-2C(i,j+1)+C(i-1,j+1)}{(\Delta x)^2} + \frac{C(i+1,j)-2(C(i,j)+C(i-1,j)}{(\Delta x)^2}\right] \tag{23}$$

Substituting (22) and (23) into (1) one obtains the Crank-Nicolson finite difference equation for Fick's Second Law. This equation is second order correct in both the time and spatial variables.

The first partial derivative of concentration with respect to distance at the point (i,j+1/2) may be found by taking the average of the derivatives at (i,j) and (i,j+1) and is given below:

$$\frac{\partial C(i,j+1/2)}{\partial x} = \frac{1}{2}\left[\frac{C(i+1,j+1)-C(i-1,j+1)}{\Delta x} + \frac{C(i+1,j)-C(i-1,j)}{\Delta x}\right] \tag{24}$$

Higher order approximations to the derivatives may be obtained by using an off centered approximation(12) rather than a simple arithmetic average of the two analogs. Since these off centered methods bring added complexity with only a small addition in computational accuracy they will not be considered here.

The interior points (points not on a boundary) will follow equation (1). The second order correct analog for this equation can be found by substituting (22) and (23) into (1) at the point (i,j+1/2).

$$\frac{C_o' - C_o}{\Delta t} = \frac{D}{2(\Delta x)^2}\left[C_{+1}' - 2C_o' + C_{-1}' + C_{+1} - 2C_o + C_{-1}\right] \tag{25}$$

where the subscripts "+1", "0", and "-1" are shorthand notation for i+1, i, i-1 spatial values and the superscript " ´ " denotes the unknown time level j = t+Δt, while the absence of the superscript denotes the known time level j=t. A more convenient form of (25) is to group all the unknown terms on the left hand side (LHS) and all the known terms on the right hand side (RHS). By using this grouping a tridiagonal matrix of grid equations can be developed that lends itself to rapid solution by computer algorithm (see von Rosenberg$^{(11)}$). Rearranging (16) one obtains:

$$C_{-1}' + \left(-2 - \frac{2}{R}\right)C_o' + C_{+1}' = -C_{-1} + \left(2 - \frac{2}{R}\right)C_o - C_{+1} \tag{26}$$

A similar equation can be written for the interior grid lines in the gas phase by replacing R with Rg, where

$$Rg = Dg{*}\Delta t/(\Delta xg)^2$$

where delta xg is the spatial increment in the gas phase and is not necessarily equal to the solid phase increment delta x, and Dg is the diffusivity in the gas phase.

The major problem in obtaining solutions for the gas-solid composite system using a numerical approach is that the diffusivity of the dopant in the gas is about twelve orders of magnitude higher than the corresponding diffusivity in the solid. This means that to keep Rg within bounds (to prevent oscillation of the solution at the gas-solid interface one must take delta xg >> delta x. This implies that dopant rejected from the solid at the moving boundary must be incorporated into a very large volume of gas ($S*\Delta xg$, where S is the wafer surface area) resulting in a loss of sensitivity to effects in the gas phase near the solid-gas interface. Another argument against the composite system approach is that small values of delta xg require large amounts of computer core for storing the gas phase information. Therefore this composite system approach was abandoned in favor of a solution that ignored the details of gas phase transport and approximated the fluxes at the gas-solid interfaces using equations (7) and (8).

The CNM equation for the gas-solid interface will now be developed. In order to obtain grid equations that are second order correct at a boundary, the imaginary point concept must be employed. This concept involves the use of a fictitious point, not in the solid body. This imaginary point is eventually eliminated from the boundary equation by direct substitution. The CNM analog for equation (12) is given below, where i=o is the interface.

$$\begin{aligned}
&\frac{D}{4\Delta x}\left[C'_{+1} - C'_{-1} + C_{+1} - C_{-1}\right] = \\
&+ h\left[\frac{C'_o + C_o}{2} - k_e\left(\frac{C'_m + C_m}{2}\right)\right] \\
&- fh\left[\frac{C'_b + C_b}{2} - k_e\left(\frac{C'_m + C_m}{2}\right)\right] \\
&+ v\left[\frac{C'_o + C_o}{2} - k_g\left(\frac{C'_m + C_m}{2}\right)\right]
\end{aligned} \tag{27}$$

where C'_{-1} and C_{-1} are the imaginary points and Cm(t) is a constant over one delta t.

Equation (27) may be simplified by assuming that the time dependence of the mean gas concentration is known or that Cm(t) is not a function of time over the interval delta t. Also since the escape of dopant at the back interface is assumed independent of the dopant transport at the gas solid interface its time dependence can be easily calculated by treating the back surface boundary as a simple evaporation problem. Even if one were to neglect the time dependence effect of the back evaporating impurity over one delta t the error would be vanishingly small after the first few delta t's. This is true since the surface concentration at the back interface C(b,t), rapidly approaches a steady state value, $C(b,t) = C(b,t+\Delta t)$, for any reasonable value of the evaporation coefficient "h". Equation (27) will be rewritten using the following two assumptions: 1) Cm(t) is a constant and 2) $C(b,t) = C(b,t+\Delta t)$. The resultant equation is then solved for the imaginary points:

$$\begin{aligned} C'_{-1} + C_{-1} &= C'_{+1} + C_{+1} \\ &- \frac{4\Delta xh}{D}\left[\frac{C'_o + C_o}{2} - k_e C_m\right] \\ &+ \frac{4\Delta xfh}{D}\left[C_b - k_e C_m\right] \\ &- \frac{4\Delta xv}{D}\left[\frac{C'_o + C_o}{2} - k_g\, C_m\right] \end{aligned} \qquad (28)$$

Substituting (28) into the CNM equation (25) written at the gas-solid boundary and arranging the unknown concentration terms on the LHS and the known terms on the RHS one obtains:

$$\begin{aligned} C'_{+1} + C'_o\left[-1 - \frac{1}{R} - \frac{\Delta x(h+v)}{D}\right] &= \\ -C_{+1} + C_o\left[1 - \frac{1}{R} + \frac{\Delta x(h+v)}{D}\right] & \\ - \frac{2\Delta x}{D}\{hk_e C_m - fh[C_b - k_e C_m] & \\ + vk_g C_m\} & \end{aligned} \qquad (29)$$

The above equation only has two unknowns C'_{+1} and C'_o and therefore meets the requirements of the first equation of a tridiagonal matrix, i.e., the coefficient of the first unknown term is zero. In this case the first unknown term C'_{-1} does not exist.

Using the same imaginary point approach the grid equation for the back boundary (x=b, Figure 2) can be developed in a manner analogous to (29). This equation is given below.

$$C'_{-1} + \left(-1 - \frac{1}{R} - \frac{\Delta xh}{D}\right)C'_o = -C_{-1} + \left(1 + \frac{1}{R} + \frac{\Delta xh}{D}\right)C_o - \frac{2\Delta xhk_eC_m}{D} \qquad (30)$$

In order to solve equations 26, 29, or 30 let ai, bi, and ci be the coefficients of the unknown concentration terms C'_{-1}, C'_o, and C'_{+1} in a particular grid equation, and let gi equal the value of all the known terms on the RHS of a grid equation. The equations for each grid point can be arranged in a tridiagnoal matrix and solved for the unknown concentration values at the time level t plus delta t with the aid of the following computer algorithm outlined below$^{(11)}$:

$$\beta_i = b_i - \frac{a_i c_i}{\beta_{i-1}} \qquad , \ \beta_1 = c_1/b_1$$

$$\gamma_i = g_i - \frac{a_i \gamma_{i-1}}{\beta_i} \qquad , \ \gamma_1 = g_1/b_1$$

$$C_r = \gamma_r \ , \text{ and } \ C_i = \gamma_i - \frac{c_i \ C_{i+1}}{\beta_i}$$

A computer program called CASPER (Computer Aided Semiconductor Processing and Epitaxial Redistribution) was written to solve the diffusion equation (equation (1)) using the boundary conditions of (7) and (12) and non-uniform initial conditions, using the Crank-Nicolson method. A detailed discussion of CASPER along with a six step sequential example is contained in Appendix A.

To test the accuracy of the CNM, a comparison was made with the known analytical solution for the moving boundary and evaporation problem (MBEP) where the gas concentration, Cm, is set equal to zero.

The analytical solution to the moving boundary and evaporation problem as given by Grove et al.,(4) is presented below:

$$C(x,t) = \frac{C_s}{2} \operatorname{erfc} \left(\frac{x}{2\sqrt{Dt}}\right) - \left(\frac{h+v}{2h}\right)$$

$$\cdot \exp\left[\frac{v}{D} (vt-x)\right] \operatorname{erfc} \left[\left(\frac{2vt-x}{2\sqrt{Dt}}\right)\right] + \left[\frac{v+2h}{2h}\right]$$

$$\cdot \exp\left\{\left[\frac{vth}{D}\right]\cdot\left[(vth)t-x\right]\right\} \operatorname{erfc}\left\{\left[\frac{2(v+h)t-x}{2\sqrt{Dt}}\right]\right\} \qquad (31)$$

where C_s is the original concentration level in the solid.

Equation (31) was compared to the solutions obtained by the CNM for the following set of numerical conditions:

dopant --- boron

temperature --- 1294 C

diffusivity --- 0.0500 μ^2/min

$0.01 \leq h/(\sqrt{D/t}) \leq 10^{10}$

$0.00 \leq v \leq 2.0$ microns/min

substrate thickness --- 5.0 microns

time --- 5.0 minutes

First let us consider the evaporation case, (v=0), using the CNM solution. The accuracy of the CNM will depend not only upon the size of the time and spatial parameters delta t and delta x but also upon the rate of change of concentration in the interval delta x. The error relative to the analytical solution is defined below:

$$\text{Relative Error} = \frac{C_{\text{analytical}} - C_{\text{CNM}}}{C_{\text{analytical}}} \times 100$$

A variable delta t Crank-Nicolson solution is used to solve equation (1) under the boundary conditions of equation (12) and the resultant numerical solution is compared to the analytical solution given in equation (31). In this method a very small value of delta t is initially chosen. This value corresponds to an R value of 0.0001. With each successive solution of the grid equations, delta t is increased by forty percent until the total elapsed time is expended. This technique offers good accuracy while allowing one to minimize the amount of computer time per total calculation. Figure 4 graphically displays both the analytical and numerical solutions to equation (1) using the boundary condition of equation (12) with $hn=h/(\sqrt{D/t})=10^{10}$ and v=0 (evaporation only). At the smaller values of hn the curves tend to flatten out. For the numerical solution delta x was varied from 0.005 to 1.0, i.e. the solid which was five microns thick was divided into a number of steps which varied from 1000 to 5. Even for the largest delta x, the numerical solution and the analytical solution cannot be resolved on this plot. The error associated with the evaporation solution is very small over the entire range of delta x that was investigated. The maximum error occurs at the gas-solid interface. For a delta x of 0.05, which is the interval size normally used, the error at the interface is 0.4 percent. The variable delta t solution is highly accurate for the solution of the evapora-

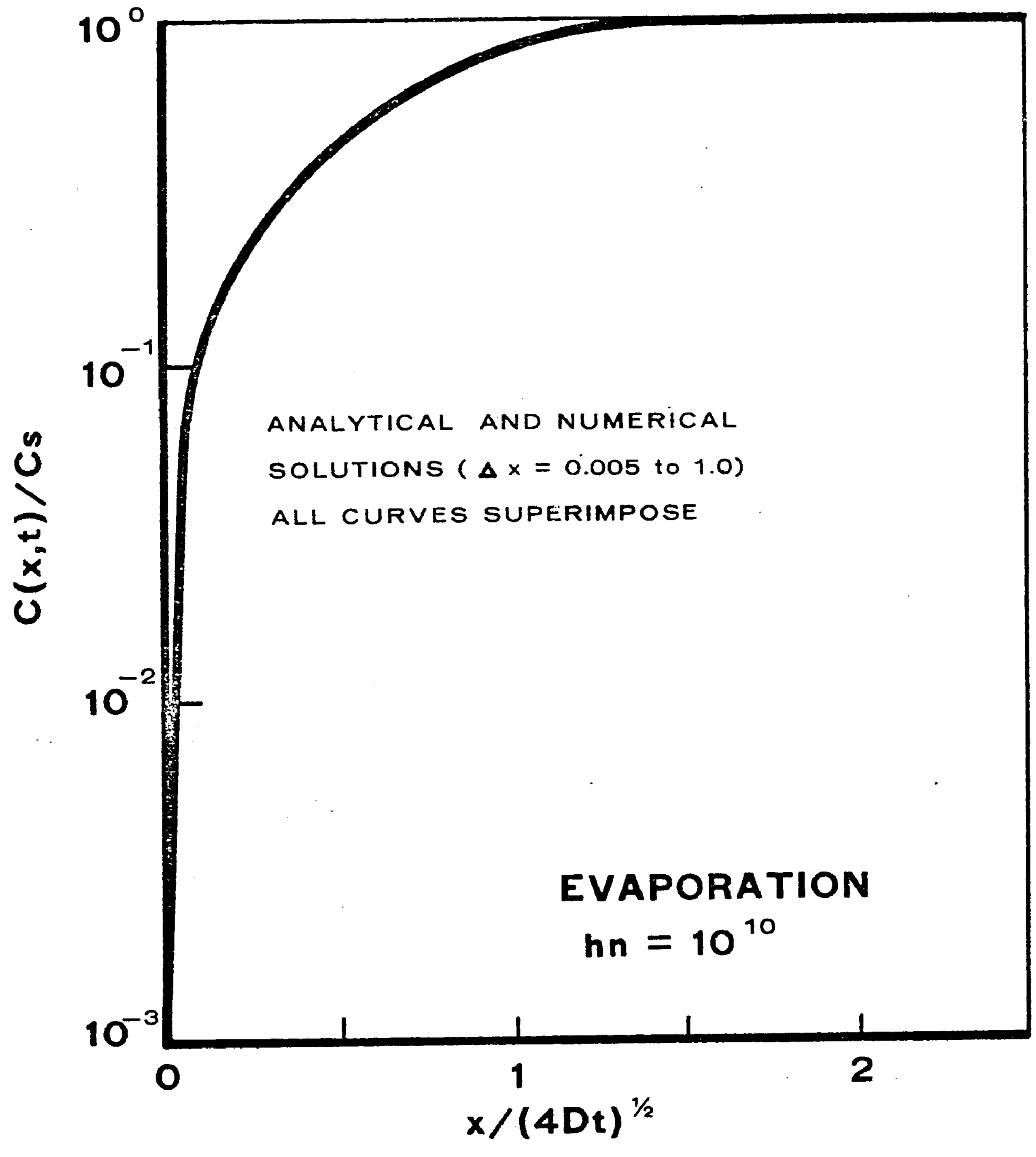

10^0
10^{-1}
10^{-2}
10^{-3}
C(x,t)/Cs
0
1
2
$x/(4Dt)^{1/2}$
ANALYTICAL AND NUMERICAL
SOLUTIONS (Δx = 0.005 to 1.0)
ALL CURVES SUPERIMPOSE
EVAPORATION
$hn = 10^{10}$

FIGURE 4

tion problem. This variable time interval solution is particularly useful in the treatment of long diffusion problems where little or no dopant movement occurs over a large part of the time cycle. For an eight hour oxidation cycle at 1100 C the computer run time was reduced by a factor of 230 when using the variable delta t solution. If the concentration distribution was continuously varying, a fixed interval delta t method would be preferred over the variable delta t solution.

To achieve the highest level of accuracy, using the CNM the smallest value of delta x consistent with the amount of computer core storage available should be chosen. For systems where the active diffusion zone is small relative to the total dimensions of the body under simulation, the smallest practical value of delta x that may be chosen, may still be too large to give the required level of accuracy desired. Therefore a numerical solution that allows the use of small values of delta x in the active diffusion region and larger values of delta x in regions where little or no transport of dopant is taking place, would allow one to conserve large amounts of computer core storage while significantly reducing the calculation time. This split grid or "variable delta x" approach will be developed below. When treating a problem where little change in concentration is expected to occur at the interface (e.g., an evaporation problem with $hn << 1.0$), delta x may be taken large. But if one is working in a region where the concentration gradient is large i.e., the concentration change over one delta x is greater than a factor of two, then a small value of delta x should be used. This would result in a variable delta x solution where delta x would be small in regions of large concentration changes and would be large in regions where the concentration gradient was close to zero. This type of solution can be accomplished as follows.

In Figure 5, let x=m be the boundary between a grid of interval size delta x (on the left) and a grid of interval size delta y (on the right). The flux across the boundary is continuous as is the concentration distribution. Representing these two factors in equation form one obtains:

$$C(x{=}m,t) = C(y{=}m,t) \tag{32}$$

and

$$D\left.\frac{\partial C}{\partial x}\right|_{x=m} = D\left.\frac{\partial C}{\partial y}\right|_{y=m} = M \tag{33}$$

Write the CNM analog for equation (1) at the point x=m in terms of both delta x and delta y. The subscripts will be simplified in the following manner: let 0=m, -1=m-1, and +1=m+1.

$$\frac{C_o' - C_o}{\Delta t} = \frac{D}{2(\Delta x)^2}\left[C_{-1}' - 2C_o' + C_{+1}' + C_{-1} - 2C_o + C_{+1}\right] \tag{34}$$

and

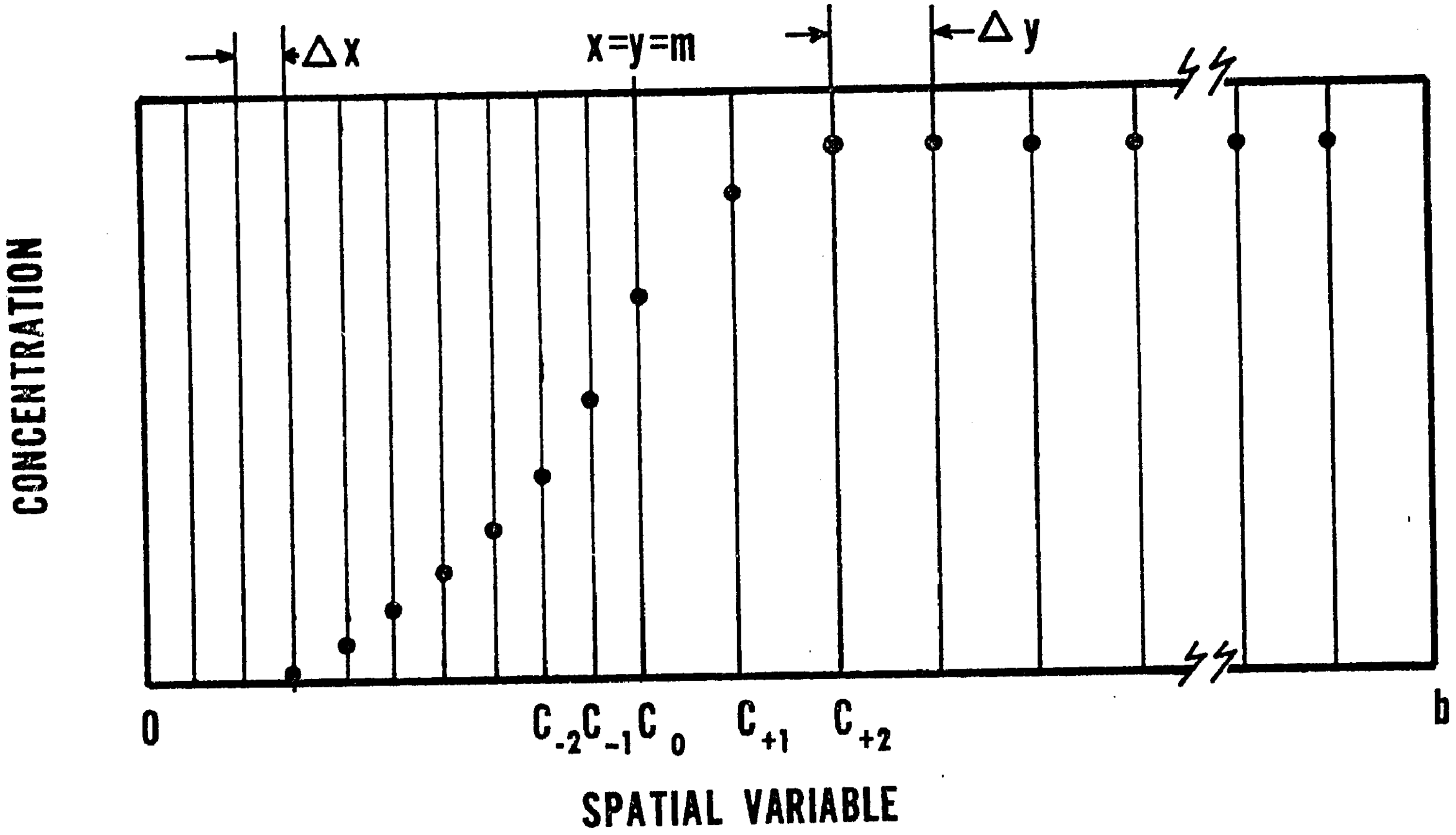

FIGURE 5
VARIABLE SPATIAL GRID

$$\frac{C'_o - C_o}{\Delta t} = \frac{D}{2(\Delta y)^2}[C'_{-1} - 2C'_o + C'_{+1} + C_{-1} - 2C_o + C_{+1}] \tag{35}$$

The imaginary points are those points which do not exist in the grid and will be eliminated from the equations at a latter step. The imaginary points in (34) are C'_{+1} and C_{+1} while the imaginary points in (35) for the y-grid are C'_{-1} and C_{-1}. Writing the CNM analog for equation (33) one obtains:

$$\frac{D}{2}[\frac{C'_{+1} - C'_{-1}}{2\Delta x} + \frac{C_{+1} - C_{-1}}{2\Delta x}] = M \tag{36}$$

and

$$\frac{D}{2}[\frac{C'_{+1} - C'_{-1}}{2\Delta y} + \frac{C_{+1} - C_{-1}}{2\Delta y}] = M \tag{37}$$

where M is a dummy variable. Solving (36) and (37) for the imaginary points one obtains:

$$C'_{+1} + C_{+1} = \frac{4\Delta xM}{D} + C'_{-1} + C_{-1} \tag{38}$$

and

$$C'_{-1} + C_{-1} = \frac{4\Delta yM}{D} + C'_{+1} + C_{+1} \tag{39}$$

Substituting (38) and (39) into (36) and (37) to eliminate the imaginary points one obtains:

$$\frac{C_o' - C_o}{\Delta t} = \frac{D}{2(\Delta x)^2}\left[2C_{-1}' - 2C_o' + 2C_{-1} - 2C_o + \frac{4\Delta x M}{D}\right] \qquad (40)$$

and

$$\frac{C_o' - C_o}{\Delta t} = \frac{D}{2(\Delta y)^2}\left[-2C_o' + 2C_{+1}' - 2C_o + 2C_{+1} - \frac{4\Delta y M}{D}\right] \qquad (41)$$

Multiply (40) and (41) through by D over the grid variable to isolate M:

$$\frac{\Delta x}{D}\,\frac{C_o' - C_o}{\Delta t} = \frac{1}{\Delta x}\left[C_{-1}' - C_o' + C_{-1} - C_o\right] + \frac{2M}{D} \qquad (42)$$

and

$$\frac{\Delta y}{D}\,\frac{C_o' - C_o}{\Delta t} = \frac{1}{\Delta y}\left[-C_o' + C_{+1}' - C_o + C_{+1}\right] - \frac{2M}{D} \qquad (43)$$

Adding (40) to (41) to eliminate 2M/D one obtains:

$$\frac{\Delta x}{D}\,\frac{C_o' - C_o}{\Delta t} + \frac{\Delta y}{D}\,\frac{C_o' - C_o}{\Delta t} = \frac{1}{\Delta x}\left[C_{-1}' - C_o' + C_{-1} - C_o\right]$$

$$+ \frac{1}{\Delta y}\left[-C_o' + C_{+1}' - C_o + C_{+1}\right] \qquad (44)$$

Multiplying (42) through by delta x, and substituting R for $D\Delta t/(\Delta x)^2$

$$\frac{C_o'}{R} - \frac{C_o}{R} + \frac{\Delta y \Delta x}{D}\,\frac{C_o' - C_o}{\Delta t} = C_{-1}' - C_o'$$

$$+ C_{-1} - C_o + \frac{\Delta x}{\Delta y}\left[-C_o' + C_{+1}' - C_o + C_{+1}\right] \qquad (45)$$

Rearranging (45) so that all the terms at time level j+1 are on the LHS and all terms at the known time level j are on the RHS one obtains:

$$C'_{-1} + C'_{o} \left[-1 - \frac{1}{R} - \frac{1}{R}\frac{\Delta y}{\Delta x} - \frac{\Delta x}{\Delta y}\right] + C'_{+1}\frac{\Delta x}{\Delta y} =$$

$$-C_{-1} + C_{o} \left[1 - \frac{1}{R} - \frac{1}{R}\frac{\Delta y}{\Delta x} - \frac{\Delta x}{\Delta y}\right] - C_{+1}\frac{\Delta x}{\Delta y} \qquad (46)$$

Since small values of $\Delta x/(\sqrt{Dt})$ have been shown to lead to higher accuracy one would use this solution in regions where rapidly changing concentration gradients occur. There are savings in both computer time and core, if one has a prior knowledge of where these regions of large concentration changes are occurring throughout the solid. The above approach was developed for a continuous material but it is also extremely useful in treating problems where a boundary or discontinuity exists such as the gas-solid interface or the boundary between two phases. It allows one to choose values of delta x in each region that will result in the minimum total error for the smallest amount of computer core and time. There may be as many breaks in the grid size as is required by the particular problem under study. An example of where this variable grid size solution would be useful is the growth (Figure 6), of a thick epitaxial layer at very low temperatures such that the region between the layer and the substrate would have a very large concentration gradient, while in the substrate and in the layer the concentration gradient would be close to zero. If one tries to model this problem using a large value of delta x the

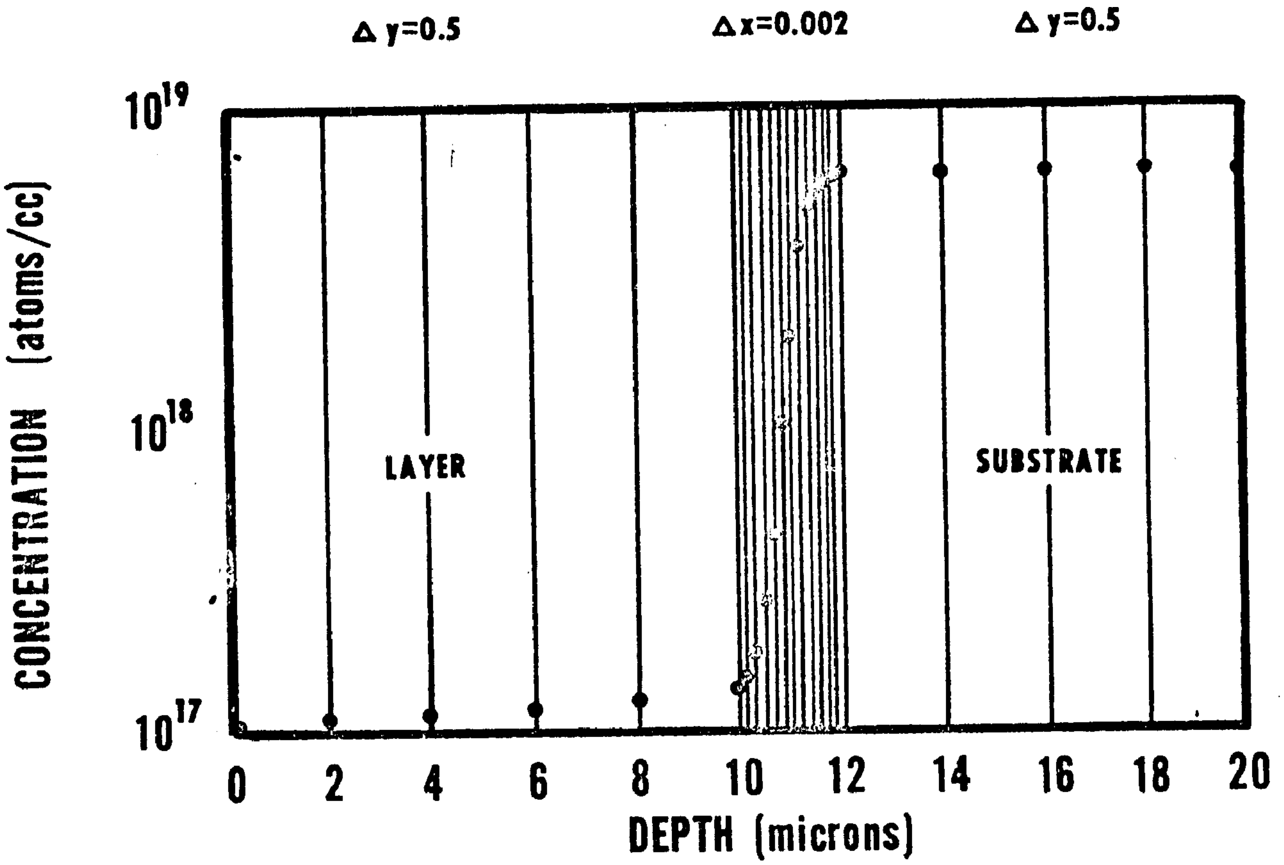

FIGURE 6 EXAMPLE OF VARIABLE GRID SOLUTION

transition region appears more graded than it actually is. If one tries to employ a very fine delta x solution large amounts of core are required since the regions in which the concentration gradient is zero may be twenty microns thick while the transition region may only be 2 microns in size. The optimum treatment of this type of problem is to use a large value of delta x, $\Delta x = 0.5$ in the regions of small concentration change (i.e. the layer and the substrate) and to use a very fine delta x, $\Delta x = 0.002$ microns in the 2 micron transition region. Errors in the numerical solution occurring in the region of fine delta x are comparable to the errors that occurred when using a uniform grid size delta x=0.002. The savings in both computer run time and core storage for this particular problem is almost a factor of 10.

The errors resulting from the CNM treatment of the MBEP will now be discussed. In the growth mode, the following sequence is used to obtain a numerical solution:

a) Add on a growth step equal in size to delta x or some whole number times delta x. These steps are added on using Ca = ke*Cm where Ca is the concentration of the added step. For most elements, ke decreases with temperature and approaches unity with increasing growth velocity.(13)

b) An adjustment is made to the concentration at the prior original interface to conserve mass across the added solid step and a region of equal size already in the solid phase. This is accomplished by averaging the concentration of the added step with the prior interface concentration value.

c) The problem is now solved under static conditions using a fixed delta t method. One time iteration is usually sufficient.

d) Steps "a" through "c" are repeated until the specified growth is complete.

The errors resulting from the CNM solution to the growth case are somewhat larger than one obtains from the evaporation problem. A comparison of the analytical solution and the CNM for the MBEP for a number of values of delta x, and $hn=10^{10}$, $vn = v/(\sqrt{D/t})$ is shown in Figure 7. These results, are representative of values of the normalized growth rates (0.2 to 2.0 microns/min), and are typical of semiconductor epitaxial processing. Since the examples are for boron other elements with smaller diffusivities will experience even smaller errors since $vn \geqslant 50$. Figure 8 is a plot of the absolute relative error in percent plotted over the same depth range as in Figure 7 for values of delta x, from 0.005 to 1.0 microns.

Errors in general are largest at the smallest growth rates and larger values of delta x. While the errors appear larger the further one gets from the original interface (x=0) the concentration gradient at distances far from the interface is also large. At a depth of 3.3 microns from the original boundary the concentration may have dropped by six orders of magnitude, while the concentration change over 0.05 microns is almost a factor of two. Therefore, errors

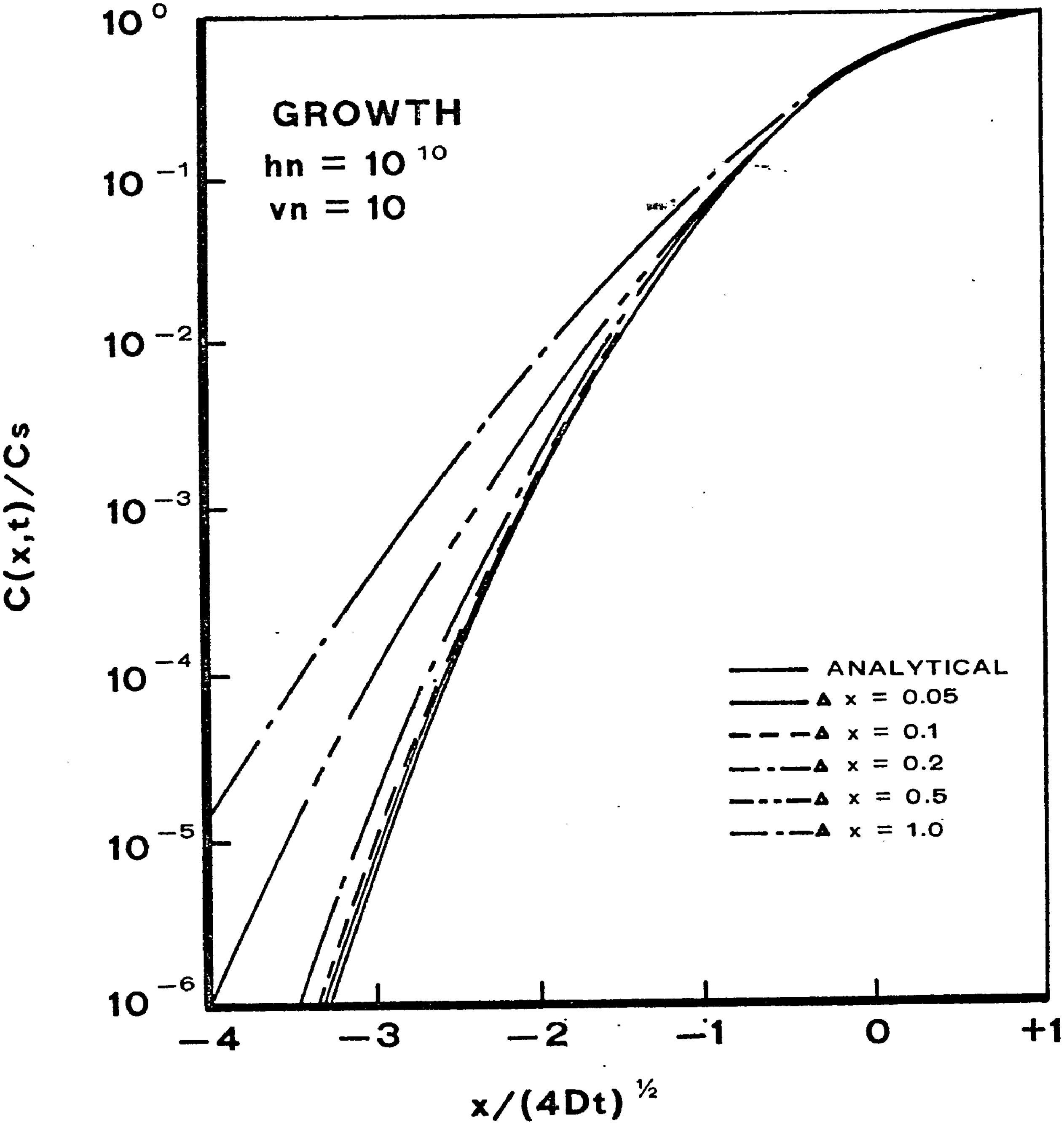

GROWTH
hn = 10^{10}
vn = 10
10^{0}
10^{-1}
10^{-2}
10^{-3}
10^{-4}
10^{-5}
10^{-6}
C(x,t)/Cs
−4
−3
−2
−1
0
+1
x/(4Dt)$^{1/2}$
ANALYTICAL
Δ x = 0.05
Δ x = 0.1
Δ x = 0.2
Δ x = 0.5
Δ x = 1.0

FIGURE 7

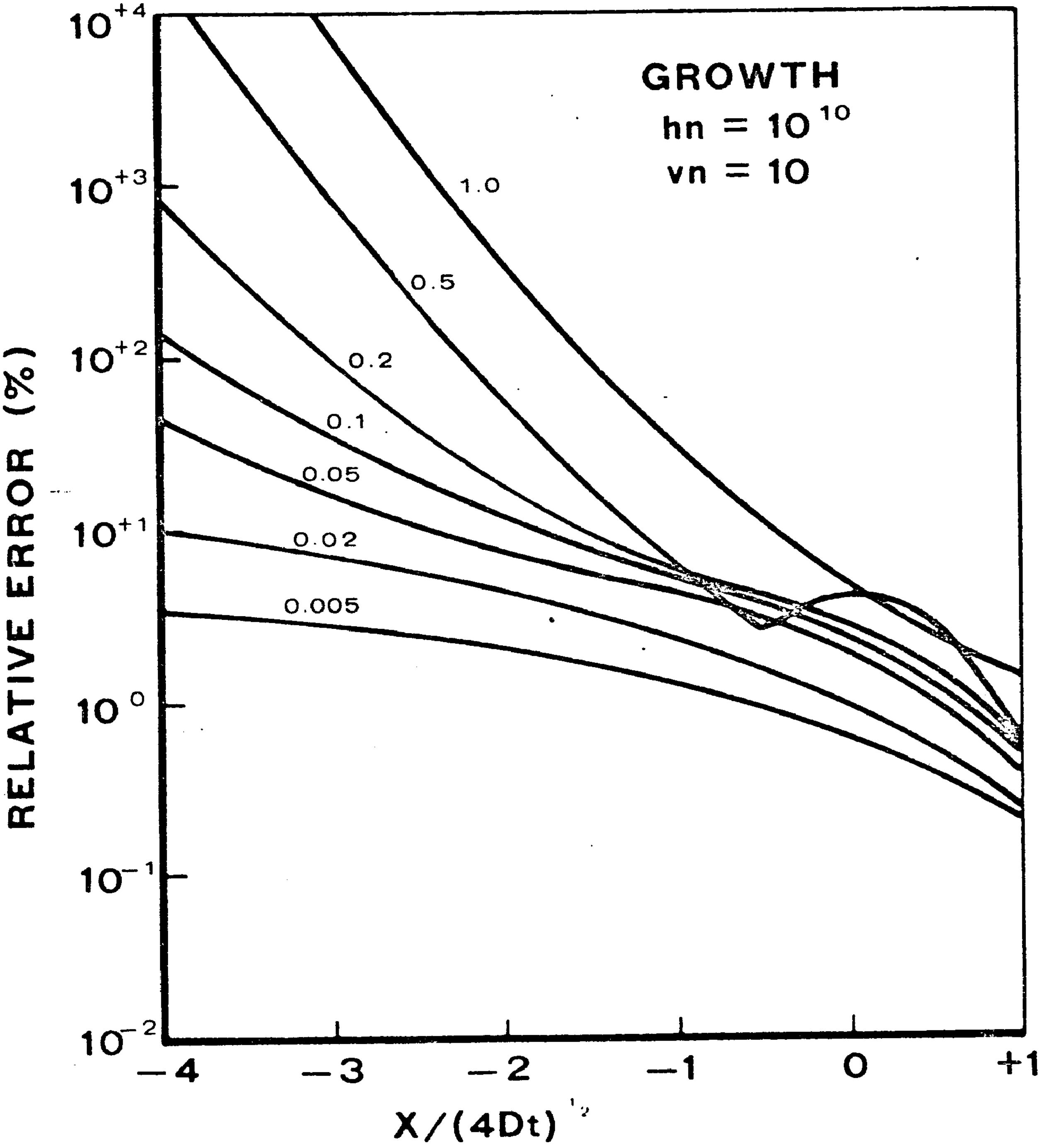
GROWTH
hn = 10^{10}
vn = 10
1.0
0.5
0.2
0.1
0.05
0.02
0.005
RELATIVE ERROR (%)
10^{+4}
10^{+3}
10^{+2}
10^{+1}
10^{0}
10^{-1}
10^{-2}
−4
−3
−2
−1
0
+1
$X/(4Dt)^{1/2}$

FIGURE 8

less than fifty percent are really quite small relative to the large changes in concentration. Even when the calculated error is greater than 1000 percent (Figure 8 at a depth of -3.3 microns) a lateral shift in the concentration distribution of less than one delta x is all that is needed for perfect agreement. For a delta x = 0.005 the calculated error at a concentration level ten orders of magnitude below Cs was only four percent.

In summary a numerical model has been developed that when compared to available analytical solutions yields highly accurate results. The CNM is used to solve the diffusion equation in the solid for arbitrary initial and boundary conditions. Savings in computer time and core storage can be realized by using a variable increment size solution.

To computer actual impurity profiles in semiconductors using CASPER one must experimentally determine the value of the evaporation coefficient "h". In the next section "h" will be determined for boron. Using the experimentally determined values of "h" the transport of boron from the substrate into the layer during epitaxial growth will be studied with both calculations and experiments.

EXPERIMENTAL

Evaporation Experiments

Two different epitaxial reactors were used in this investigation. Figure 9 is a schematic of the first reactor system. This system was used to perform the high temperature cycling for the evaporation experiments. This reactor was of circular cross section and was water cooled. The inner tube was 60 mm i.d. fused quartz. Power was supplied using a 450 kHz radio frequency generator. The susceptor consisted of a graphite slab 25 cm long by 4.8 cm wide. The slab was made from General Electric pyrolytic infiltrated graphite. The susceptor was used uncoated after a one hour bakeout at 1450 C in hydrogen. The susceptor was supported in the reactor on a fused quartz sled. The standard cycle consisted of the following: 10 minutes nitrogen, 10 minutes hydrogen, raise power and stabilize (10 min.), one hour at temperature in 20 liters/min of hydrogen, lower power, 10 minutes hydrogen, 20 minutes in nitrogen. Precautions were taken to prevent moisture from condensing inside the tube when it was opened for loading or unloading of wafers. No cooling water was run through the system when the reactor was open. The flush schedule was arranged so that at least 300 volume changes of dry gas (∿ 1 ppm (parts per million) water) were passed through the reactor before the temperature was raised. Even with these precautions pitting of the silicon surface was observed when the wafers were heated above 1050 C. Therefore silane was introduced during the initial nitrogen flush cycle to getter any residual water that may have condensed on the reactor walls or

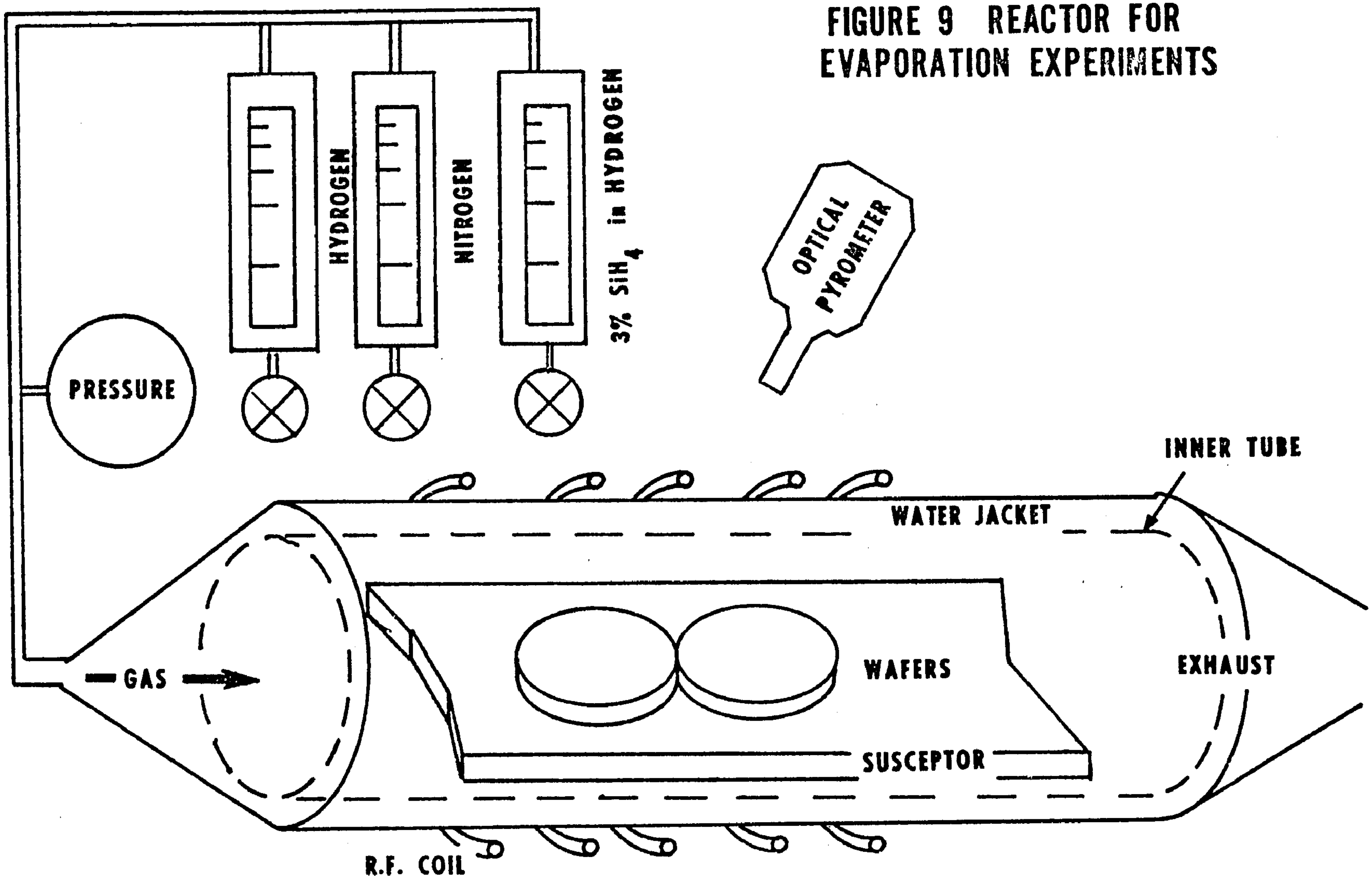

FIGURE 9 REACTOR FOR EVAPORATION EXPERIMENTS

the susceptor. This technique proved completely successful in eliminating the pitting of the silicon surface.

All evaporation samples were held at temperature for one hour. The temperature was recorded using a Leeds and Northrop (L and N) automatic optical pyrometer (model no. 8641) which had been calibrated by L and N at five temperatures against a high precision automatic optical pyrometer traceable to the National Bureau of Standards. The adsorption corrections for the two thickness of fused quartz, the cooling water, and the plexiglass safety shield were determined experimentally in the following manner. A graphite block with two holes in it was placed in a resistance heated diffusion furnace. In one hole a Pt-Pt-10%Rh thermocouple was placed and the pyrometer was sighted on the interior of the second hole. The block was brought to temperature and the fused quartz and plexiglass were placed between the heated block and the pyrometer while the optical temperature was determined. The quartz and plexiglass were withdrawn and the optical temperature was again determined. This procedure was repeated at temperatures from 900 to 1350 C. It was found that a constant adsorption correction of 25 C was sufficient over the experimental range of temperatures used for the evaporation and growth procedures. Emissivity corrections were made using Allen's(14) values for a polished silicon surface in vacuum.

Spreading resistance probe method was used to determine the net carrier concentration both as a function of depth in the epitaxial layer as well as across the surface of the wafer. To perform the spreading resistance determination of the carrier concentration two metal probes, spaced about 10 mm apart, are lowered at a small velocity to the silicon surface. A load is then applied in the range of 40 to 100 grams per point. A small d.c. current is then passed between the points so that a potential drop of about 10 millivolts exists across the probes. The total resistance of this metal probe silicon system is then calculated and it is this quantity that is called the spreading resistance (SR). In order to obtain a silicon resistivity from which the net carrier concentration may be calculated an empirical calibration is required since the geometry of the probe tip and the exact shape of the probe-silicon contact are not precisely known. This empirical calibration is obtained by first measuring the resistivity of bulk silicon wafers (uniform throughout), with a four point probe to determine their resistivity.(26) The SR was then determined on the same wafers and an empirical calibration curve was constructed. The depth resolution of the SR technique is such that when the probes are on the surface one is averaging the SR over about one micron in depth. A modified Schumann(15) multi-layer correction was applied to the calculated resistivity before conversion to carrier concentration was made. This correction factor takes into account the proximity of a concentration gradient or p-n junction along with the concentration level near this gradient relative to the concentration at the point being measured. Conversion of resistivity to concentration was accomplished using Lee's fit to Irvin's data.(21)

In order to determine the evaporation rate of boron from silicon the evaporation rate of silicon, v, must first be known. The silicon evaporation rate is a measure of the loss of silicon from the substrate when it is heated in a flowing gas ambient. To determine the evaporation rate of silicon in a hydrogen ambient the following procedure was used. A lightly boron doped wafer [∿ 10 parts per billion atomic (ppba)], with 7000 A of thermally grown oxide was etched in a buffered hydrofluoric acid solution to remove the oxide film covering one half of the front surface. The rest of the oxide was protected by Kodak Metal Etch Resist during the etch. The photoresist was then removed and the wafers were cleaned using a mixture of nitric and sulfuric acids followed by a rinse in deionized water. The wafers were then scrubbed using a mild detergent, and rinsed again and spun dry. Following the drying, the wafers were heated in the reactor for a period of one hour.

After the high temperature cycle the remaining oxide was completely removed. The step height was then measured between the area protected by the oxide during the high temperature treatment and the area that had been exposed to the ambient (20 liters/min hydrogen stream). This height measurement was performed using a Talysurf profilometer.* Figure 10 schematically shows the evaporated and protected parts of the silicon surface and exactly what quantites were measured in the determination of the evaporation rate. A control

---

*Commercial differential height gauge.

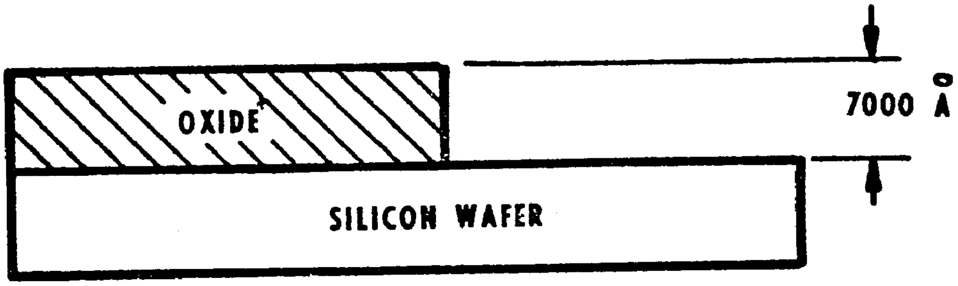

BEFORE SILICON EVAPORATION

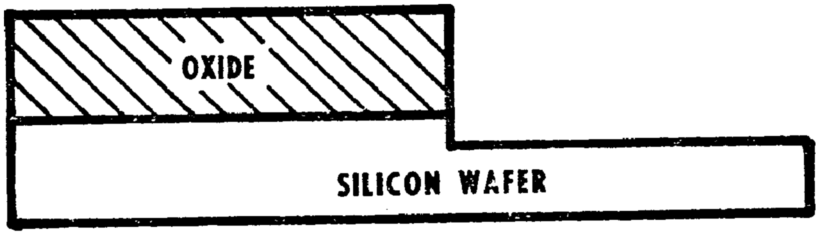

AFTER SILICON EVAPORATION

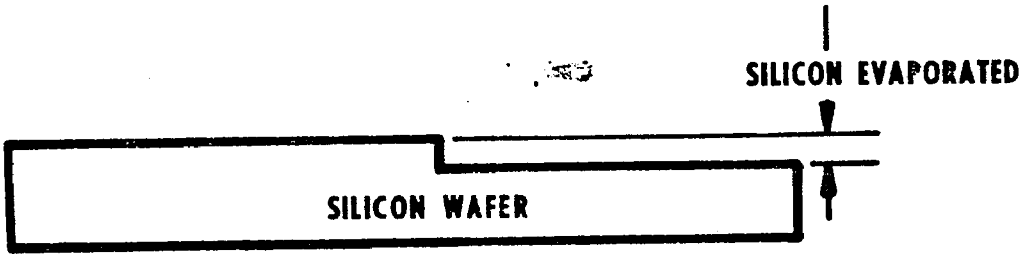

AFTER OXIDE REMOVAL

FIGURE 10
SILICON EVAPORATION EXPERIMENT

was run with no thermal treatment to check for the attack of the buffered hydrofluoric acid solution on the silicon wafer surface. Etching of the silicon by the buffered solution was 0.05 microns or less. Therefore the measured step height was due entirely to the evaporation of silicon.

Once the evaporation rate of the silicon had been determined the next step was the determination of the boron evaporation rate. This was accomplished by measuring the concentration distribution of the boron in the silicon wafer after evaporation had been allowed to occur. This boron distribution was then fitted to calculated boron concentration distributions in which the only variable was the evaporation rate of the boron. The procedure that was used to determine the actual boron concentration distribution in the wafer is given below.

The wafers used to determine the evaporation coefficient of boron had to be heavily doped enough so that the surface concentration after evaporation was still above the background of the reactor. A ten minute deposition run was made at a rate of 0.4 microns/min to determine the reactor background concentration. The resultant resistivity measured by four point probe on the epitaxial structure showed the system background concentration to be 2 ppba n-type. Therefore wafers doped to 4 ppma with boron were chosen for the evaporation study. These wafers were grown by the Czochralski method and were oriented in the (111) direction. The wafers were sawed, chemically etched, and then polished with Syton abrasive (a colloidal suspension of silica in a basic solution). The cleaned wafers were subjected to one hour at temperature in a 20 liters/min hydrogen ambient. The range of temperature used was 1190 to 1380 C. After the evaporation heat treatment the resultant wafers were angle lapped at a nominal 0.5 degree angle using Linde A abrasive on a glass plate, followed by a quick polish with Syton abrasive on a plexiglass plate. The prepared samples were measured on a Solid State Measurements ASR-100 Spreading Resistance Probe test set to obtain plots of spreading resistance versus depth from the wafer top surface. This data was then fed into a computer program containing the empirical calibration data and was converted to uncorrected resistivity. Resistivity values were converted to concentration using Lee's polynomial fit.

Boron Autodoping Experiments

The epitaxial reactor used for the boron "back" surface autodoping studies was a commercial Radyne unit shown in Figure 11. It differed from the first system in two respects: first the cross section was rectangular (38x76 mm), and secondly the gas flow used was 108 liters/min (76 cm/sec). The susceptor was 9.5 mm thick and was tilted at an angle of 1.5 degrees from the horizontal. These two factors result in greater uniformity of deposition rate in both the longitudinal direction (direction of the gas flow), and in the transverse direction (perpendicular to the gas flow) as shown by Takahashi.(18) The susceptor used in this case was silicon carbide coated graphite with a layer of undoped silicon covering all surfaces. Two consecutive runs were made of 10 minutes each. Arsine was intro-

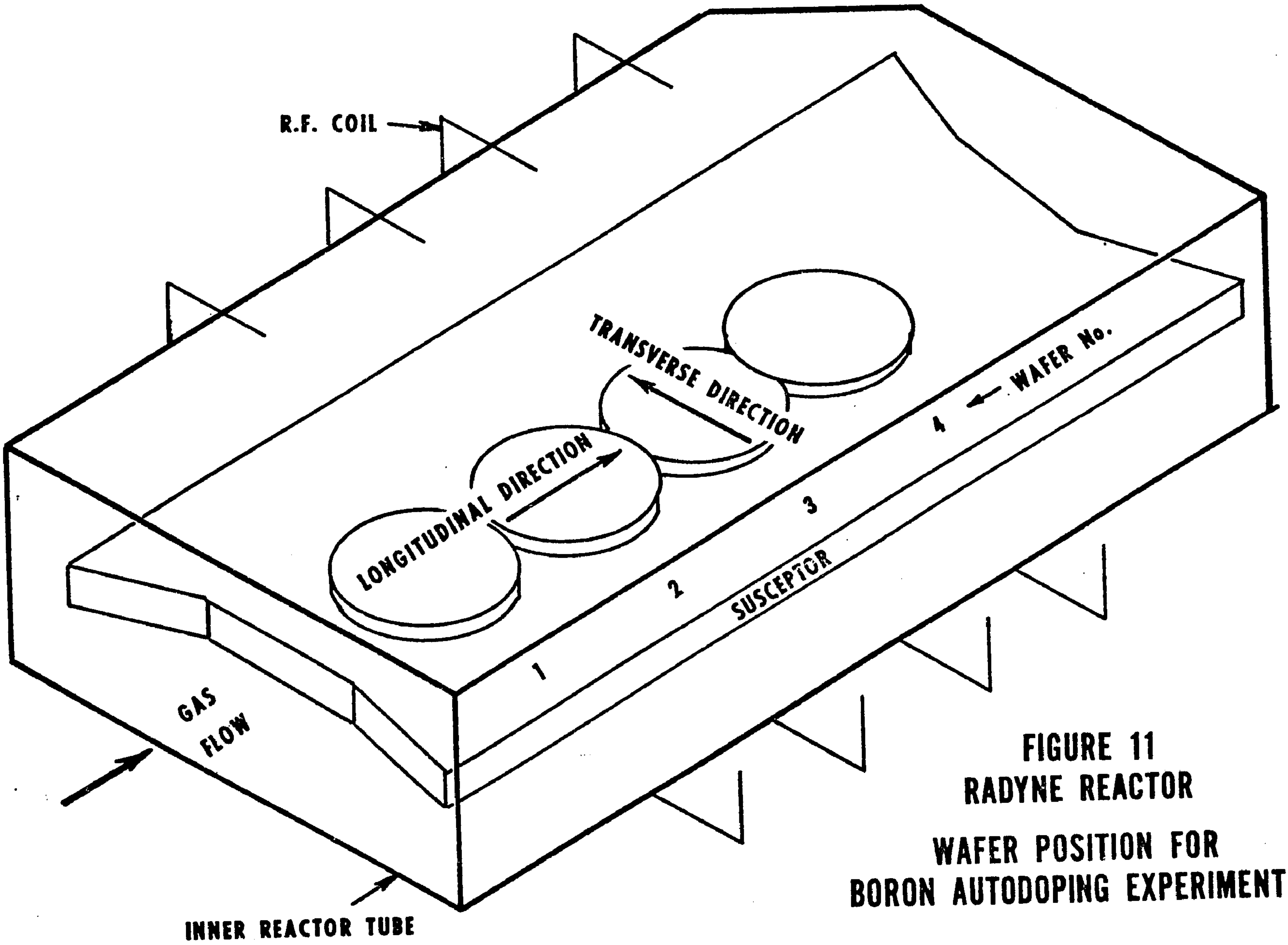

FIGURE 11
RADYNE REACTOR

WAFER POSITION FOR
BORON AUTODOPING EXPERIMENTS

duced during the deposition cycle to achieve an n-type doping level of about 10 ppba. Both runs were made with four 32 mm diameter wafers placed near the center of the susceptor as shown schematically in Figure 11. A deposition rate of 0.92 microns/min was achieved in both runs at a temperature of 1120 C. No preheat, HCl etch, or post epitaxial growth heat cycle was employed. The wafers in the first run were all lightly doped p-type (100 ppba). In the second run the first and third wafers were also lightly doped, while the second and fourth wafers (position relative to gas inlet end) were heavily doped with boron to about 200 ppma. It was these heavily doped wafers that would become the autodoping source. After the layer was deposited all wafers were measured at 25 micron intervals across the surface both in the direction of the gas flow, and in a direction 90 degrees to the gas flow. All measurements were made using an automatic spreading resistance probe with on-line correction capabilities. Selected wafers were also profiled in depth for concentration.

RESULTS AND DISCUSSION

Boron Evaporation

The evaporation coefficient of boron from silicon was determined over the temperature range from 1190 to 1380 C. The measured evaporation coefficient enables one to calculate the movement of boron across gas-solid interfaces so that doping and autodoping during epitaxial growth may be accurately predicted. The following equations gives the value of the evaporation coefficient, h, at a boundary in terms of the concentration at the boundary and the flux of dopant.

$$h = \frac{D}{C(i,t)} \frac{\partial C(i,t)}{\partial x} - v \qquad (47)$$

Assuming the gas phase concentration of boron, $C_g(i,t)$ is negligible compared to the value in the solid, $C(i,t)$, then one only need determine the velocity of movement of the boundary, v, and the concentration distribution as a function of distance into the solid. During the evaporation experiments v is simply the evaporation rate of the silicon. If h is large compared to v, v may be neglected. For some elements this is the case, such as, antimony, arsenic, and phosphorus, but not for boron. The evaporation rate of silicon was measured experimentally and found to be 0.013 ± 0.003 microns/min over the temperature range from 1190 to 1380 C. This measured value is much smaller than the value of 0.023 ± 0.005 microns/min determined by Tung.(17) Tung observed gross nonuniformity of the evaporation effect which was not observed during these experiments. His samples may have experienced etching by residual water vapor in the system. This form of attack had been eliminated in this work by the addition of three percent silane to the room temperature nitrogen flush.

The concentration was normalized using a value determined deep into the wafer ($\sim 3\sqrt{Dt}$), where the concentration gradient was almost zero, while the depth was normalized using the published diffusivity of boron.(22) This normalization was performed so that comparison between experimental and calculated results for the concentration versus depth distribution of boron could be easily accomplished for the determination of the boron evaporation coefficient. The rate of silicon evaporation was also normalized using the diffusivity of boron, D_B, in the following manner.

$$vn = \frac{v}{\sqrt{D_B/t}} \tag{48}$$

Solutions were then obtained to Fick's Second Law for various values of the normalized evaporation coefficient, hn, where:

$$hn = \frac{h}{\sqrt{D_B/t}} \tag{49}$$

These normalized solutions (equation (31)) were then plotted over the experimental data that had also been normalized, and a fit was obtained between these solutions and the experimental values of hn. The normalized calculated concentration versus depth values at different values of the evaporation coefficient are plotted in Figures 12 through 15 at four different temperatures. At each temperature the normalized evaporation rate of silicon is different, varying from -1.0 to 0 and this value is shown on each plot. The symbols (Figures 12 to 15) are the experimental data while the solid lines represent the results of the analytical solution for different values of hn. One can see that by comparing the various analytical solutions that for values of hn over 6 the concentration versus depth plots are almost indistinguishable. Therefore it is extremely difficult if not impossible to distinguish between high evaporation coefficients (hn > 20) using this type of data analysis. If one neglects the effect of the evaporation rate of silicon (largest effect at the lowest temperature), then no reasonable fit can be obtained between the experimental data and the calculations at temperatures below 1380 C. Exact analysis of errors is difficult since some parts of a given concentration versus depth curve fit better than others. To obtain more precise results at larger values of hn, one must determine the concentration of boron right at the interface. This surface concentration value cannot be determined experimentally by the spreading resistance technique that was used. Usually the first two or three points adjacent to the interface are lost as one traverses from the surface of the wafer to the beveled area. Also the concentration gradient is largest in this region so that the correction factor is playing a larger role and the resultant corrected values of concentration are less precise. If small times were used to limit the normalized value of h, then the

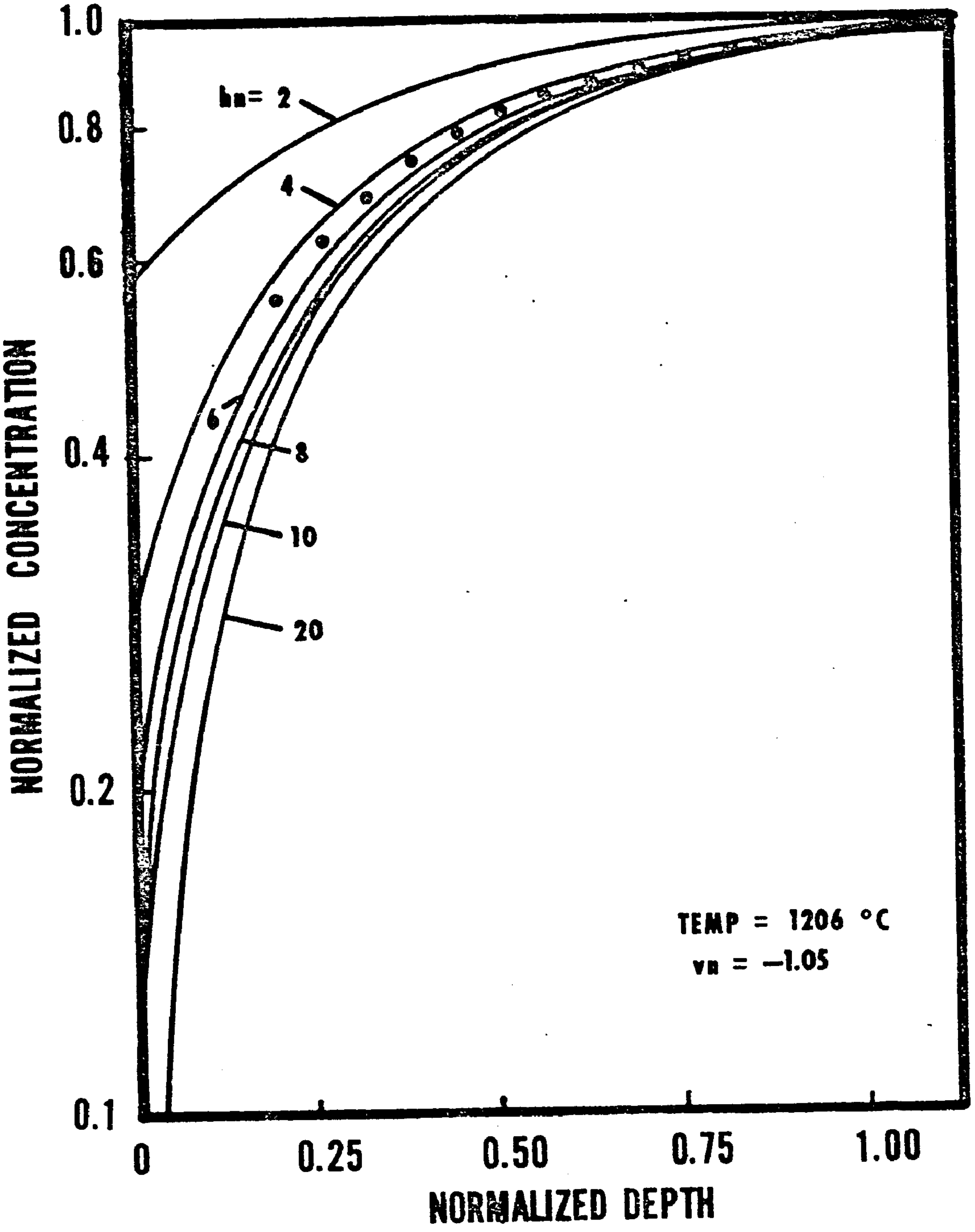

1.0
0.8
0.6
0.4
0.2
0.1
0
0.25
0.50
0.75
1.00
NORMALIZED CONCENTRATION
NORMALIZED DEPTH
hn= 2
4
6
8
10
20
TEMP = 1206 °C
vn = –1.05

FIGURE 12

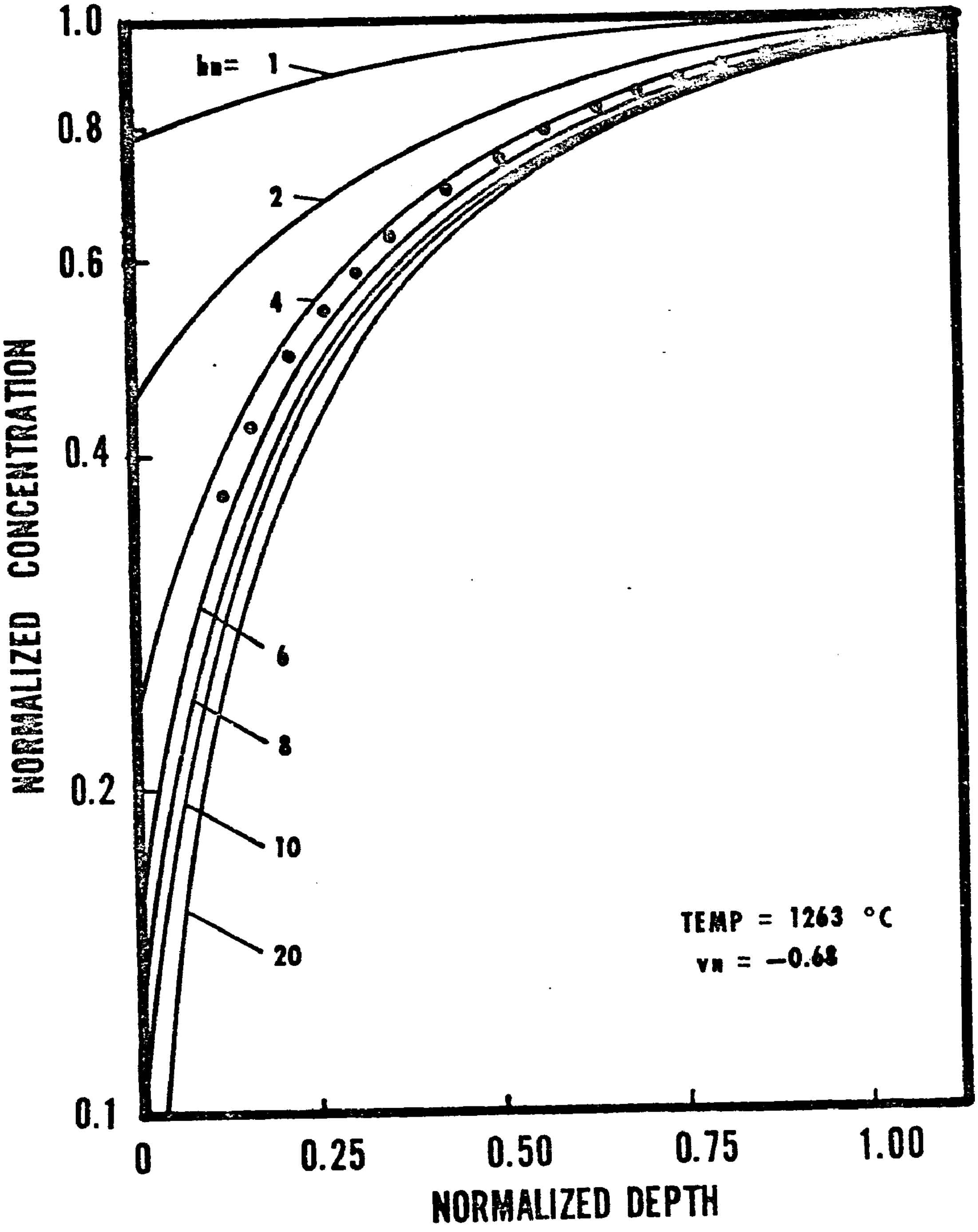
1.0
0.8
0.6
0.4
0.2
0.1
NORMALIZED CONCENTRATION
hn= 1
2
4
6
8
10
20
TEMP = 1263 °C
vn = -0.68
0
0.25
0.50
0.75
1.00
NORMALIZED DEPTH

FIGURE 13

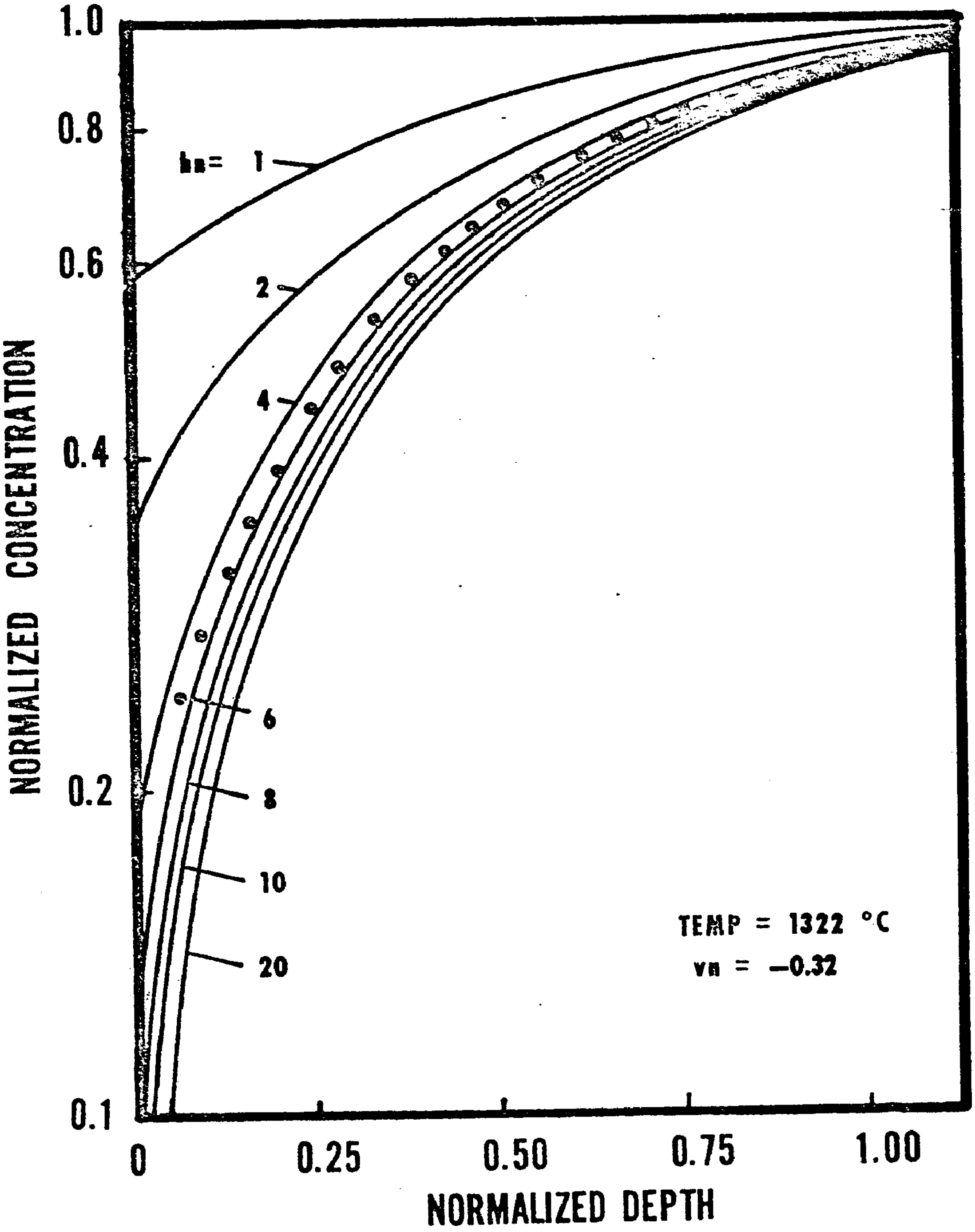
1.0
0.8
0.6
0.4
0.2
0.1
NORMALIZED CONCENTRATION
0
0.25
0.50
0.75
1.00
NORMALIZED DEPTH
hn= 1
2
4
6
8
10
20
TEMP = 1322 °C
vn = −0.32

FIGURE 14

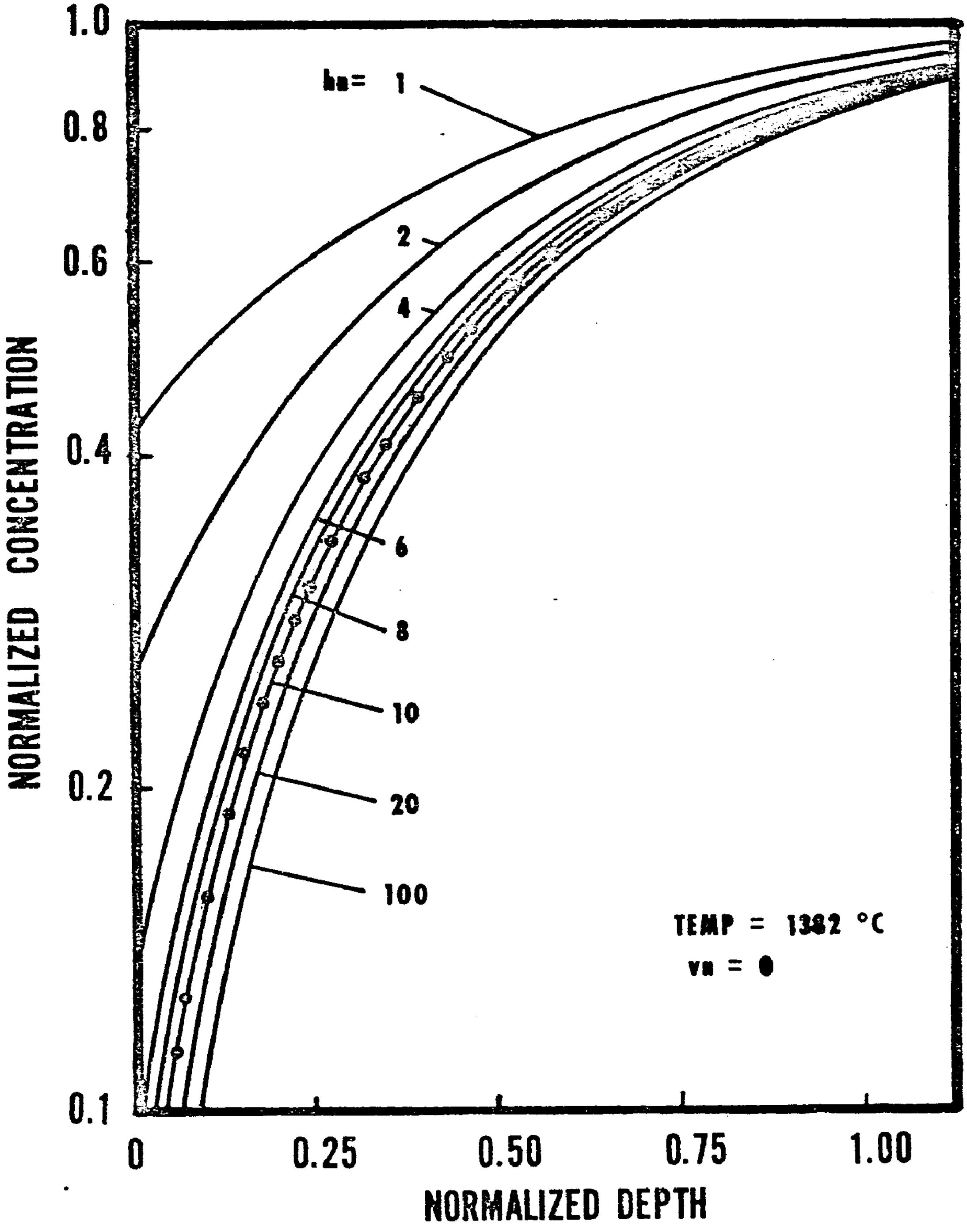
1.0
0.8
0.6
0.4
0.2
0.1
NORMALIZED CONCENTRATION
hn= 1
2
4
6
8
10
20
100
TEMP = 1382 °C
vn = 0
0
0.25
0.50
0.75
1.00
NORMALIZED DEPTH

FIGURE 15

evaporation effect would occur so close to the surface that no results (meaningful) could be obtained. The normalized values of hn were then converted to evaporation coefficients, by multiplying by $\sqrt{D/t}$, and these results are summarized in Table 1.

The experimentally determined values of h are plotted against one over the temperature in Figure 16. A least square first order polynomial was fit to an Arrenhius type of equation to produce:

$$h = 1.674 \times 10^{7} e^{-2.48/kT} \tag{50}$$

where h is given in units of microns/min, the energy is in eV, the temperature is in ^{o}K, and the value of k used was 8.62×10^{-5} eV/^{o}K. An analysis of the errors in h_o and E were made using the Arrenhius form of the equation

$$h = h_o e^{-E/kT}$$

Two worst case graphical fits were made to the data in Figure 16 and the values of h_o and E were determined. The difference between the worst case fits and the least squares analysis was found to result in a worst case error of ± 28% in h. This error is based upon a variation in h_o from 2.4×10^{5} to 1.2×10^{10} microns/min, while E varied from 1.9 to 3.4 eV. The value of h at 1275 C is within 20 percent of the value determined by Grove$^{(4)}$ at that temperature.

Boron Autodoping

To completely test the numerical model the contribution to layer doping from dopant escaping from the back and edges of the wafer

TABLE I

Boron Evaporation Data

Temp °C	Run/ Wafer	$\sqrt{D/t}$	$-V_n$	h_n	h µm/min
1188	29D	0.011	1.15	4.4	0.048
1206	29U	0.013	1.05	5	0.065
1246	31D	0.095	0.80	5	0.095
1263	31U	0.11	0.68	5	0.11
1305	30D	0.034	0.43	5	0.17
1322	30U	0.036	0.32	5.1	0.184
1365	32D	0.050	0.05	10	0.50
1382	32U	0.057	0	10	0.57

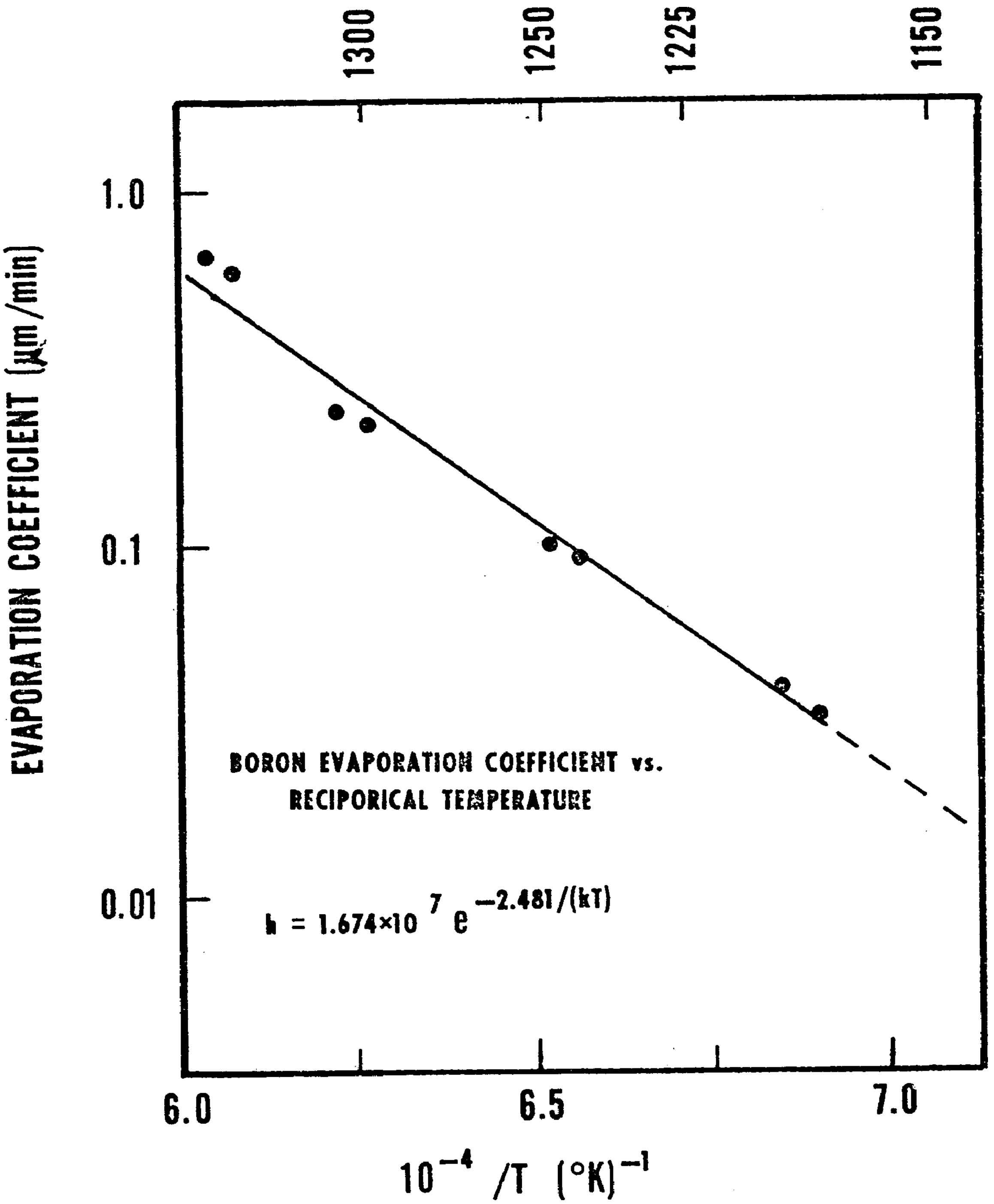1300
1250
1225
1150
1.0
0.1
0.01
EVAPORATION COEFFICIENT (µm/min)
BORON EVAPORATION COEFFICIENT vs.
RECIPORICAL TEMPERATURE
$h = 1.674\times10^{7}\, e^{-2.481/(kT)}$
6.0
6.5
7.0
$10^{-4}/T\ (°K)^{-1}$

FIGURE 16

was calculated and is shown in Figure 17. The numerical model predicts that when a heavily doped boron substrate (200 ppma) is used a level of about 120 ppba is predicted for the epitaxial layer. A major difficulty arises when trying to simulate back surface (back and sides) autodoping, i.e., one does not know what fraction of the back surface (effective area) of the wafer is contributing dopant to the gas stream. This fraction has been estimated by other workers studying arsenic as between 0.9(8) and 4(7) percent. The smaller value of effective area represents work done using silane in a single wafer reactor at 1050 C. Since only one wafer was present it was impossible to assess the results of the evaporated dopant on other wafers in the system. The authors also used a rather small total gas flow, i.e., 2 liters/min. The larger value of effective area represents the results of a multi-wafer system using silicon tetrachloride at 1200 C. Both heavily and lightly doped substrates were present in the system. The way in which Shepherd calculated the effective source area for back surface autodoping, this area would increase as the number of wafers went up, and also as the wafer diameter decreased. All of his data was taken at the center of the wafers.

Two factors had been neglected by the previous authors in their treatment of back surface autodoping. The first factor is that dopant released from the sides of the wafer must also be considered as a potential autodoping source, since this side area represents two to four percent of the wafer to surface area for normal semiconductor wafers. The second factor is that since the effective area of the

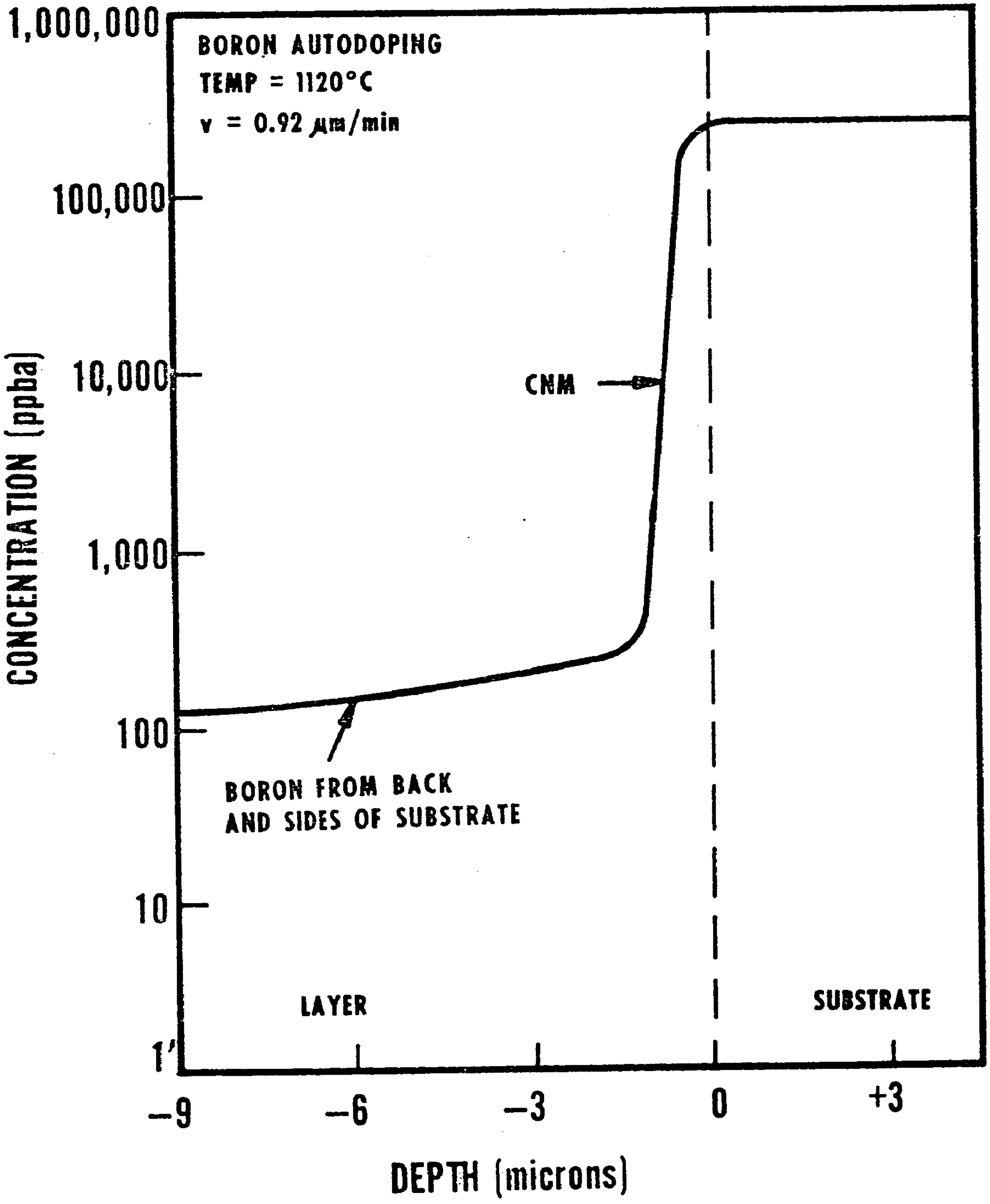
1,000,000
100,000
10,000
1,000
100
10
1
CONCENTRATION (ppba)
BORON AUTODOPING
TEMP = 1120°C
v = 0.92 μm/min
CNM
BORON FROM BACK
AND SIDES OF SUBSTRATE
LAYER
SUBSTRATE
−9
−6
−3
0
+3
DEPTH (microns)

FIGURE 17

source (back and sides) is much smaller than the area of the sink (top surface) one would expect to see a large decrease in transferred dopant as one moved further from the source. If diffusion was the only transport mechanism in the gas phase adjacent to the wafer then the radial concentration profile (from the center of a given wafer out in any direction), of transferred dopant would be the same in any direction relative to the gas flow. If other dopant transport mechanisms are present, dopant from upstream wafers would effect the ambient gas phase concentration and appear to give effects similar to intentionally added dopant with the effect increasing in the downstream direction.

To test the back autodoping model and the evaporation coefficient of boron two consecutive epitaxial runs were made. The first run (control run) only contained lightly doped wafers (0.1 ppma). The first and third wafers in the second run were also lightly doped while the second and fourth wafers were heavily doped with boron to a level of about 200 ppma. The surface concentration results across all wafers in the direction of the gas flow for the first run (all lightly doped substrates) are plotted in Figure 18. The results in Figure 18 were obtained by spreading resistance measurements from the upstream (inlet) edge of wafer one, going in the direction of the gas flow, to the downstream edge of wafer four (exit end of reactor). Data was taken every 25 microns at the surface of the 9.2 micron thick epitaxial layer. For this section longitudinal or axial will mean in the direction of the gas flow (inlet to outlet), while transverse will

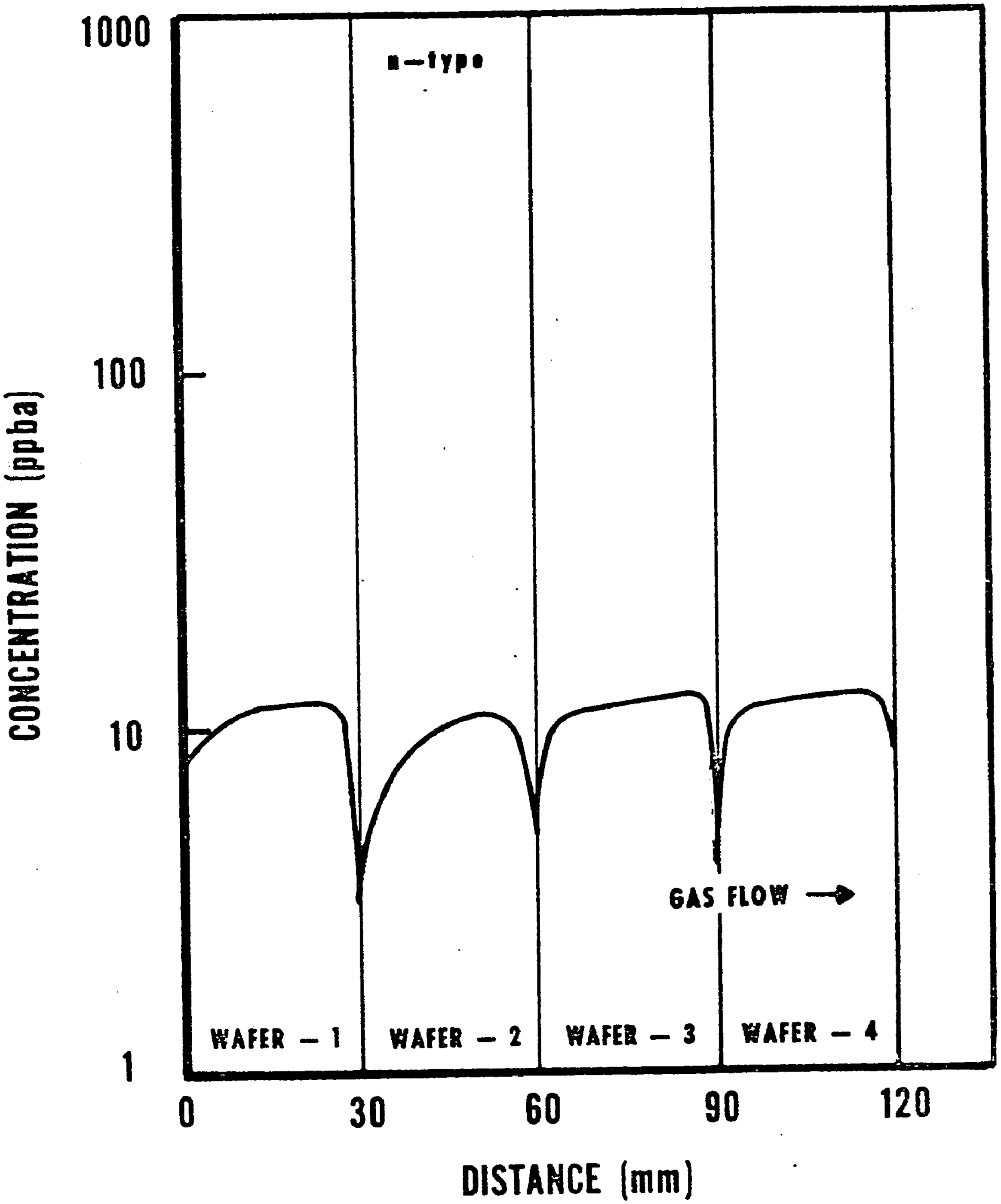

LONGITUDINAL SECTION RUN No. 1

FIGURE 18

refer to data obtained perpendicular to the gas flow across the center of a given wafer. The concentration results displayed in Figure 18 for run number one show a level of about 10 to 12 ppba, n-type, with a small rise in the dopant level from the leading edge of each wafer. This increase in concentration may be caused by boron autodoping from the lightly doped substrates or contamination from the susceptor. Since this run will be used as a control no further attempt will be made to explain the concentration profiles across these wafers. These results will be compared to the results of the second run and the differences in concentration level and type will be used to characterize any autodoping that is present. Figure 19 is a transverse surface section taken across the center of the third wafer, and shows about a twenty percent difference in concentration from the center to the edge of the wafer. These results do not show the presence of any back autodoping effect.

The second run (wafers two and four heavily doped), showed some very interesting autodoping effects. The longitudinal concentration profile across all the wafers on the susceptor is shown in Figure 20. The first wafer is n-type until about 8 mm from its trailing edge (Figure 20). The concentration level over the first 20 mm (in the direction of the gas flow) shows no signs of autodoping and is characteristic of the results of the first epitaxial run (control run). It establishes that the intentionally added dopant is n-type. Continuing across wafer no. 1 in the direction of the gas flow a p-n junction is encountered. The concentration then rises above 200 ppba, p-type, as

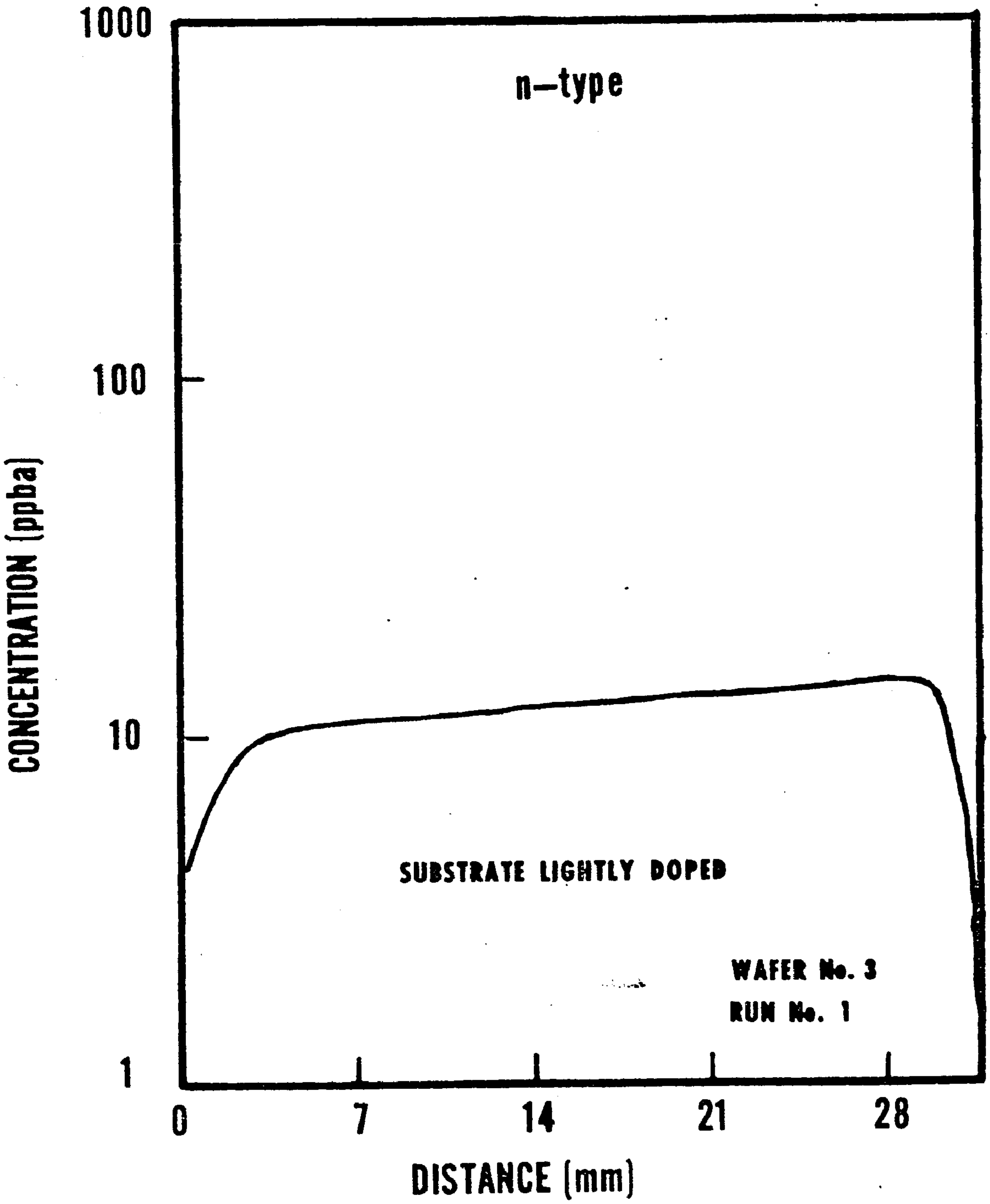

TRANSVERSE SECTION

FIGURE 19

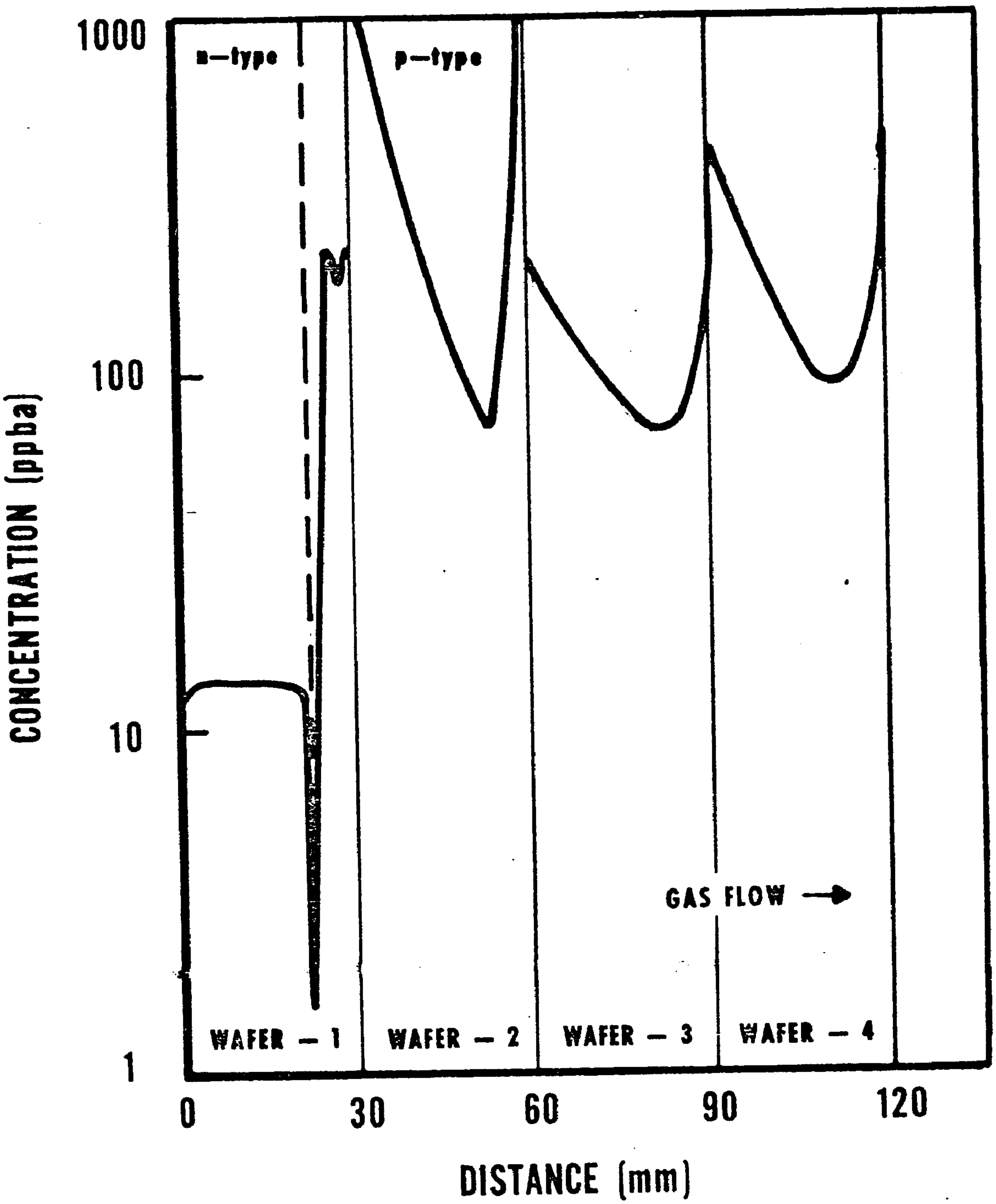

LONGITUDINAL SECTION RUN No. 2

FIGURE 20

one approaches the boundary between the first and the second wafer.

The second wafer (heavily doped) is completely p-type with extremely high values of concentration seen at both the leading and trailing edges. It appears that dopant released at the leading edge of the wafer is swept downstream across the wafer by the ambient gas because the autodoping effect is much more pronounced in the direction of the gas flow. Therefore diffusion is not the only mechanism for the transport of dopant in the gas phase. Looking at the transverse concentration profile (Figure 21) across the center of wafer no. 2 one again sees an autodoping effect at both edges of the wafer and a small peak in concentration in the central region. The transverse section does not exhibit the large directional effect seen in the longitudinal profile. Also the size of the autodoped region at the transverse edges is comparable to the size of the autodoped region at the trailing edge. This indicates that the effect of the gas flow on diffusion of released dopant is negligible. The implication of this is that dopant released at an edge does get into the mean gas phase well above the surface of the wafer where the temperatures are lower and the gas velocities higher. The shape of the transverse profile (Figure 21) near the center of the wafer may be due to the transverse variation in gas velocity above the susceptor.(18) The increased concentration near the edges (Figure 21) is due to dopant transported from the back and sides of the wafer and diffusing perpendicular to the gas flow during epitaxial growth of the layer. The concentration above the surface of the third wafer (lightly doped) which does not contri-

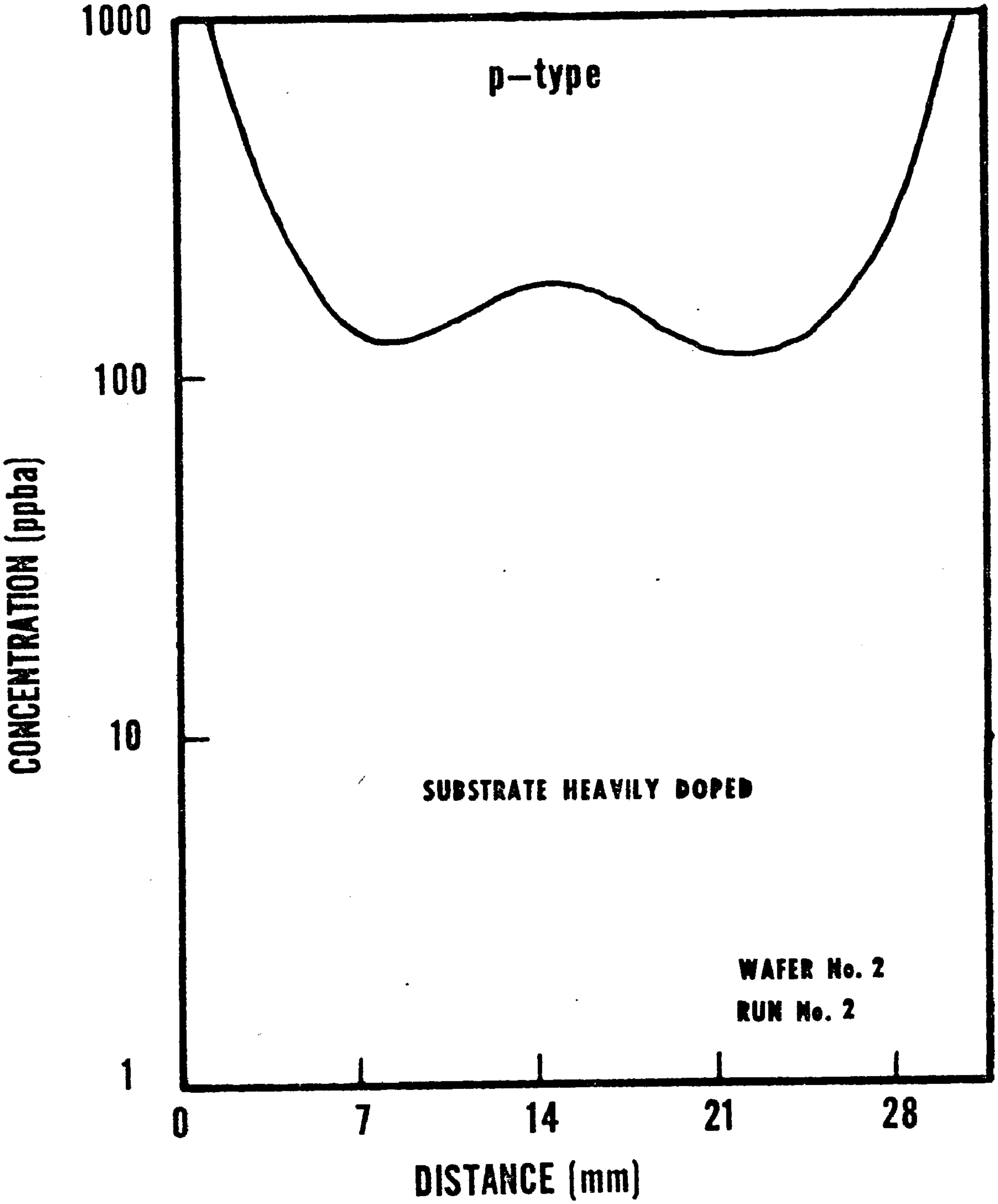

TRANSVERSE SECTION

FIGURE 21

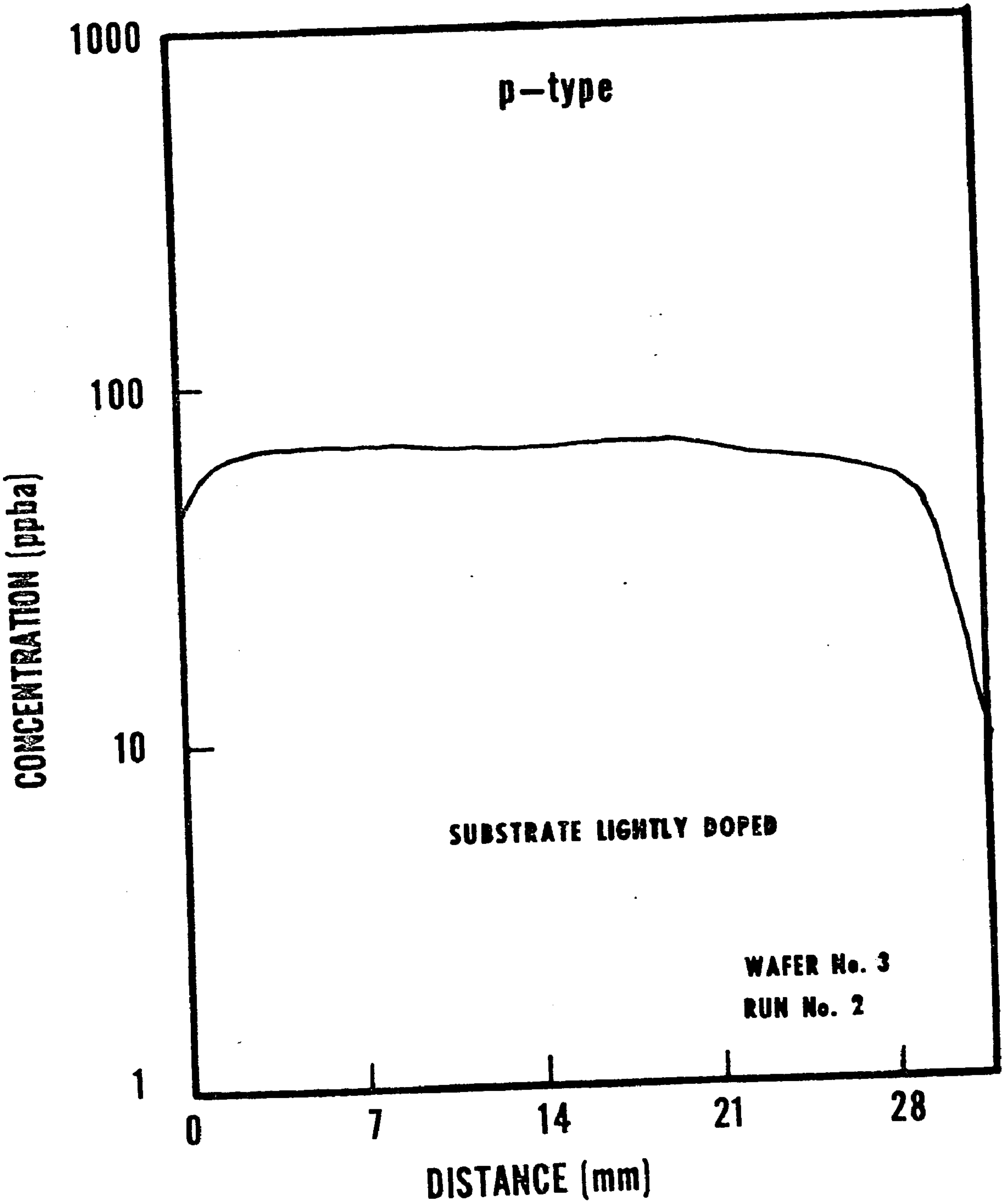

TRANSVERSE SECTION

FIGURE 22

bute boron to the reactor ambient is also completely p-type. Again one sees the smearing of dopant (Figure 20) from the leading edge toward the downstream end of the wafer. The transverse profile (Figure 22) of this wafer (no. 3) does not show an increased edge concentration. This is expected since this wafer is lightly doped and therefore cannot contribute dopant to the gas stream for reincorporation through the autodoping process. The p-type dopant in this layer comes from wafers no. 2 and no. 4. At the trailing edge of wafer no.3 dopant released from wafer no. 4, and diffusing upstream against the gas flow is present. The maximum concentration at both the leading and trailing edges of the wafer is less than on either of the heavily doped structures. The fourth wafer (heavily doped) also shows the smearing effect of the autodoped species. Also the minimum concentration found on the wafer is higher than the minimum concentrations found on any of the previous wafers. This is further evidence that dopant released from the sides and the back of the heavily doped upstream wafer (no. 2) is also effecting the mean gas phase concentration downstream from the source.

The concentration versus depth plot taken at a point 15 mm from the leading edge on wafer no. 4, parallel to the gas flow is shown in Figure 23 along with the results of the numerical simulation using the CNM. The simulation was performed assuming one percent of the back and side area was acting as a source of the autodoping species. Errors in the simulation involve not only the source area but also the effective distribution coefficient between the gas and the solid as well as the value of the evaporation coefficient. Even though agreement between calculations and theory (Figure 23) is excellent the presence of the large transverse and longitudinal concentration gradients tend to complicate the interpretation. As one can see from Figure 20 (wafer 2) the concentration at the surface varies by a factor of ten from the leading edge of wafer to a point about 20 mm downstream. Therefore the problem can no longer be described by a one dimensional model and a more complex interpretation is needed. One could empirically determine f (the fraction of effective area acting as a source) as a function of position in the reactor. This approach could give a reasonable first approximation to the concentration profiles measured. A one dimensional approach would still be valid in systems (antimony substrates) that do not exhibit large transverse and longitudinal concentration gradients.

The concentration gradient over the top few microns of the layer for a multi-wafer system may also vary as a function of position from the source of the autodoping species. This is due to the fact that the time rate of change of the mean gas phase autodoping component is different from that dopant that is transferred without going through the mean gas phase. Therefore downstream wafers should show a smaller slope in the gradient near the surface than upstream wafers due to the larger component of the mean gas phase effect with downstream position. This change in slope was experimentally observed even within one wafer.

As a check on the evaporation coefficient determined in the previous series of experiments these results are not valid due to the

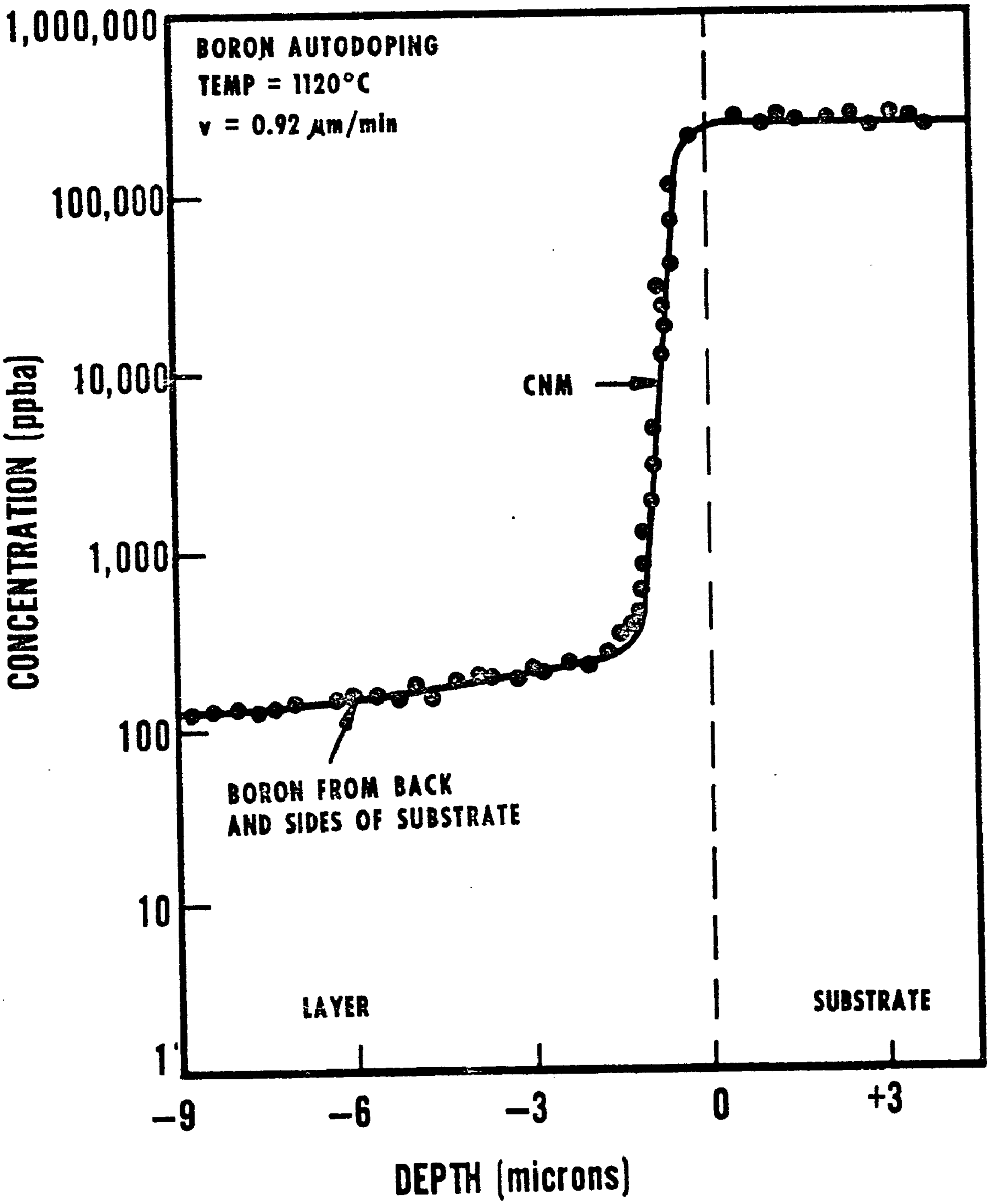
BORON AUTODOPING
TEMP = 1120°C
v = 0.92 µm/min
1,000,000
100,000
10,000
1,000
100
10
1
CONCENTRATION (ppba)
CNM
BORON FROM BACK AND SIDES OF SUBSTRATE
LAYER
SUBSTRATE
−9
−6
−3
0
+3
DEPTH (microns)

FIGURE 23

presence of the large transverse and longitudinal concentration gradients. These results do indicate that the product, ke•f•h was chosen correctly as can be seen from the agreement between theory and data in Figure 23.

The extension of these results to a system in which chlorine atoms are present during the deposition cycle (e.g., silicon tetrachloride, or dichorosilane) is not straightforward. Bloem(16) has shown that additions of HCl to a reactor ambient will result in decreased doping efficiency of diborane. He postulates the formation of a stable boron chloride compound which ties up some of the available boron that would normally be available for doping or autodoping. This may explain why Grove(4) using silicon tetrachloride as his silicon source did not report any autodoping when using heavily boron doped substrates. Oxide masking may not be as effective in preventing autodoping of boron as with n-type elements since the segregation coefficient for boron between the oxide and the silicon is about 10(19). Therefore the concentration of boron in the oxide layer would be larger than in the silicon. Depending on the relative diffusivity of boron in the oxide to the evaporation rate of boron from the oxide, one might even postulate that an oxide layer would act as a larger source of dopant during the initial stages of epitaxial growth than the exposed silicon wafer back and edges. The addition of HCl to the ambient during epitaxial growth over heavily doped boron substrates may significantly reduce the boron autodoping effects.

In summary a set of equations (1, 7, and 12) has been developed to describe the redistribution of dopant in a silicon wafer during semiconductor device fabrication. This set of equations was solved using the CNM. A computer program called CASPER (appendix A) was developed to facilitate the use of the CNM solution on actual sequential processing problems. The evaporation rate of boron was determined as a function of temperature and these experimental results were used to predict the back autodoping phenomenon from heavily boron doped substrates. Though the numerical model was unsuccessful in characterizing the distribution of dopant over the entire wafer diameter due to the large longitudinal and transverse concentration gradients it was very successful in predicting the in-depth distribution at the center of the wafer where these gradients were negligible.

In the next section the computer program CASPER will be applied to a number of actual sequential device fabrication problems.

ANALYSIS OF PROCESSING PROBLEMS

To design or modify a semiconductor device the single most important parameter is the concentration distribution in the wafer. This distribution affects every single electrical function of the device. Unfortunately, at present, no experimental method exists to determine this concentration distribution. Also, due to the complex boundary conditions and the non-uniform initial conditions that describe the concentration distribution, no analytical solutions to the redistribution problem exist. A typical integrated circuit device may experience 200 discrete processing steps and spend from four to eight months in the manufacturing line.

Historically, semiconductor device design has been a purely experimental procedure. A designer would start with a crude estimate of his final concentration distribution. From this estimate and the use of computer programs to calculate how the device would function electrically, the designer then fabricated a materials specification (i.e., epitaxial layer thickness and resistivity) along with a lengthy processing sequence (i.e., oxidation, diffusions, implants, and photolithographic steps). Since the estimate of the concentration distribution was very crude, the electrical properties of the initial experimental devices were usually not what the designer required. In most cases the device did not function at all. Since he could not calculate the affect of the processing sequence on the distribution of impurities in the wafer, the designer had to rely solely on experience and judgment. He usually based his materials and processing changes on the measured distributions of simple parameters such as: junction depth, sheet resistance, breakdown voltage, and gain. In an integrated circuit, this may not always be a wise choice, but no other parameters are available. Usually a good designer will accomplish his goal in from one to three years. When the initial design is complete, the device is then transferred to the manufacturing line at low volume of production. If the device can be manufactured at a reasonable yield (one to ten percent) further optimization may be difficult. The manufacturing organization knows that a change in one part of the process to improve a certain parameter may have detrimental effects on other electrical parameters. Therefore the manufacturing organization resists further "improvements" by the designer. The cost of converting a device from a designer's conception into something that is manufactured at the level of over one million per year is extremely large. The high cost is primarily due to the inability of the designer to calculate how any processing sequence will affect the concentration distribution in the wafer, and consequently, the operation of the device. Therefore a cheaper and much faster method of device designer is sorely needed.

To design and optimize a semiconductor device one does not require an exact knowledge of the concentration distribution. The designer needs some means of performing experiments to optimize his design in a short time at a reasonable cost. Even though the designer cannot accurately describe his boundary conditions, he must be able to determine how the material's parameters and the processing sequence affect the electrical operation of his device. In many cases he would be satisfied if he could only predict whether a certain region were n or p-type even if he did not know the exact concentration level.

The computer program CASPER (Appendix A) offers the designer a powerful tool for performing processing experiments in a short time at a reasonable cost. With CASPER the designer can easily perturb a particular set of materials' properties or a given processing sequence to optimize the electrical charactersitics of the device.

In this section CASPER is applied to actual semiconductor processing problems supplied to the author by device designers. In most cases the designers could not accurately define the boundary conditions for the diffusion and "drive-in" operations. All experimentally determined electrical parameters were obtained from the device engineers and represent averages taken over hundreds of thousands of processed devices. For every device that was simulated using CASPER the designers were extremely impressed by the speed and ease in which CASPER could deliver concrete suggestions for processing changes. In one case the confidence in CASPER's predictive powers was so high (and the alternatives very time consuming and expensive) that a particular standard processing sequence was completely abandoned based solely upon the computed results. The use of CASPER to alter and optimize semiconductor processing offers a whole new approach to device design. CASPER has the potential of reducing the time from initial conception to high level manufacture of any new device with a tremendous reduction in cost.

In treating certain steps in the device fabrication sequence specific simplifying approximations were used. During a step involving oxidation of the silicon surface it is assumed that all n-type dopants have zero evaporation coefficients, i.e., no dopant is lost through the oxide. For p-type dopants the evaporation coefficient is modified (lowered) and thirty percent of the dopant consumed by the oxide is lost to the silicon. The values of the segregation coefficient, k, were taken from the work of Shepherd.(13) The limiting concentration allowed in the solid in all cases is the solubility limit of the individual dopant species taken from the work of Trumbore.(20) Conversions from concentration to resistivity were made using the polynomial fit developed by T. P. Lee,(21) which is used in the calculation of sheet resistance. Emitter diffusions were carried out under a constant surface concentration boundary condition, while base diffusions were simulated as a two step process consisting of a predep at low temperature followed by a high temperature drive-in step.

Example 1

In the first example, a p-n-p-p+ transistor, the fabrication sequence given in Table II was used. This example shows the power of CASPER in handling a sequential processing problem with up to eleven processing steps. This fabrication sequence is characteristic of most bipolar transistors with only the temperatures being varied. The starting substrate (initial conditions for the first process step) was uniformly doped with boron to the 10^{19} atoms/cc level. The first five process steps occur in the epitaxial reactor where the only added dopant is boron. All other processing steps except step number 8 are carried out in a standard fused quartz tube diffusion furnace.

Table III contains the calculated and experimental values of junction depth and sheet resistance for this device at various stages in the fabrication sequence. Figure 24 shows the net calculated concentration versus depth distribution in the device after boron emitter diffusion. The agreement with the results of the calculation using the accepted values of diffusivity(22) is not particularly good, because certain effects have been neglected in developing the model. Among the neglected effects are the concentration dependence of the diffusivity, field aided diffusion due to the motion of charged carriers, and defect generation (dislocations and vacancies) due to the strain associated with the large mismatch in size between the boron atom and the silicon atom in the lattice. Since all values of diffusivity that were used in the calculation had been derived assuming some form of concentration versus depth distribution that characterizes

TABLE II

P-N-P Processing Sequence

Description	Step No.	Temp. °C	Time Min.	Gas Conc. Atms/CC	Element
Bakeout	1	1250	5	0	
Vapor Etch	2	1300	5	0	
Flush	3	1300	3	0	
Epitaxial Growth	4	1250	30	5×10^{15}	Boron
Flush	5	1250	3	0	
Oxidation	6	1100	60	0	
Base Predep	7	745	30	1.5×10^{20}	Phosphorus
Chemical Etch	8	25	-	0	
Drive-in	9	1200	45	0	
Oxidation	10	1050	120	0	
Boron Diffusion	11	1100	20-25	1×10^{21}	Boron

TABLE III

Calculated and Experimental Results

Description	Oper. No.	Sheet Resistance (ohms/sq)			Junction Depth B-C (Microns)		
		Exp.	Calc.	Calc.* Modified	Exp.	Calc.	Calc.* Modified
Phosphorus Predep	7		281	281			
Chemical Etch (88Å)	8		323	323		0.075	0.075
Phosphorus Drive-in**	9	110	93.5	100	2.86	3.525	2.975
Phosphorus Oxidation	10	115	99.5	106.3		3.375	2.825
Boron Diffusion	11	8.5±1.5	13.9	6.22	2.8±0.2	3.425	2.925

	Exp.	Calc.	Calc.* Modified
Junction Depth E-B (Microns)	1.6±0.2	0.675	1.875
Base width (Microns)	1.18	2.75	1.05
Gummel number (atoms/cm^2)	3×10^{12}	9.9×10^{13}	2.6×10^{12}

*Phosphorus Drive-in - Diffusivity of Phosphorus multiplied by 0.70
Boron Diffusion - Diffusivity of Boron multiplied by 5.0

+Sheet Resistance due to Boron

**In oxidizing ambient

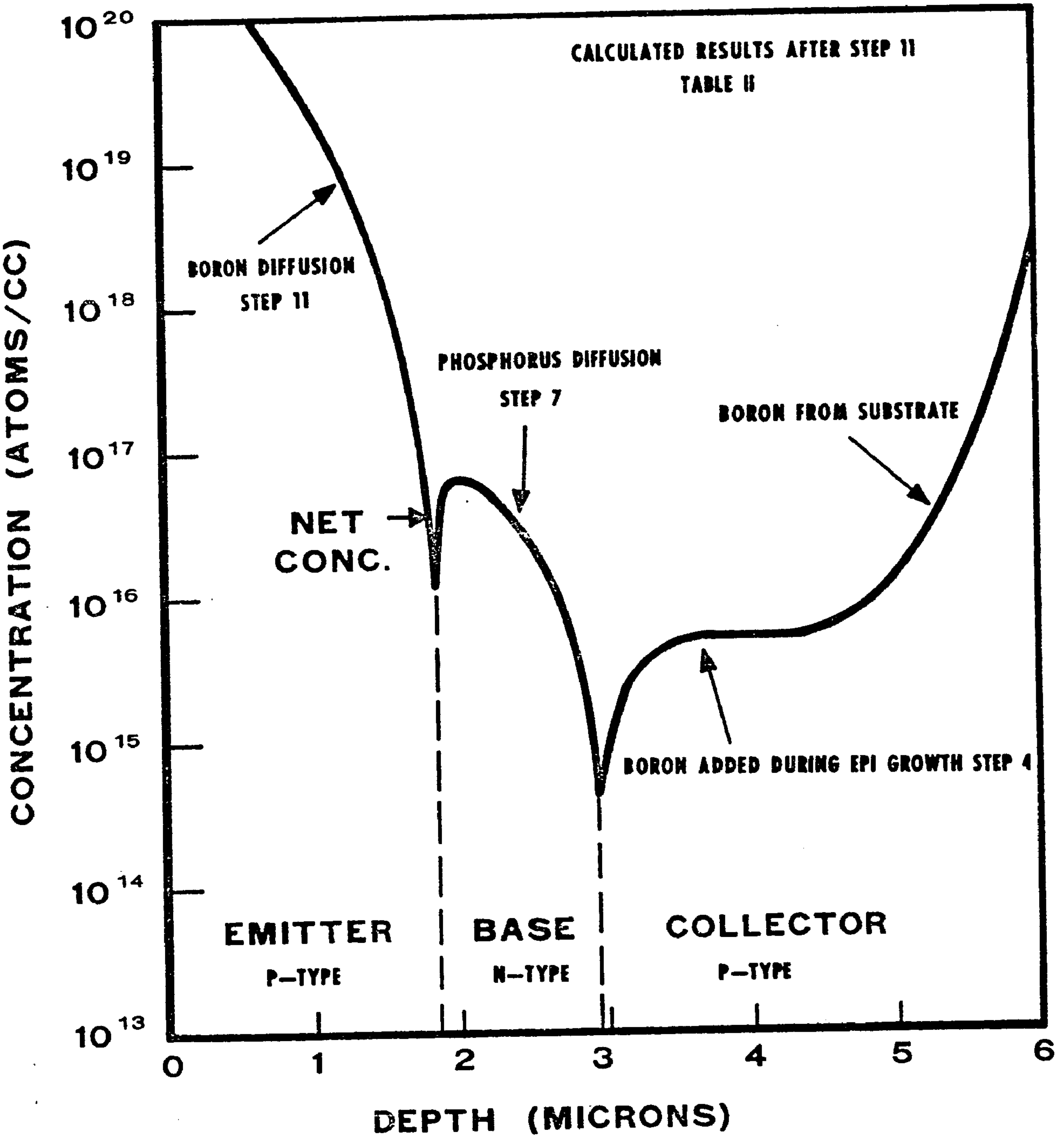

CALCULATED RESULTS AFTER STEP 11
TABLE II
BORON DIFFUSION
STEP 11
PHOSPHORUS DIFFUSION
STEP 7
BORON FROM SUBSTRATE
NET
CONC.
BORON ADDED DURING EPI GROWTH STEP 4
EMITTER
P-TYPE
BASE
N-TYPE
COLLECTOR
P-TYPE
CONCENTRATION (ATOMS/CC)
10^20
10^19
10^18
10^17
10^16
10^15
10^14
10^13
0
1
2
3
4
5
6
DEPTH (MICRONS)

FIGURE 24

the diffusion process, any experimental deviation from this function by the diffusing species will lead to an inaccurate value of the diffusivity. For most calculated emitter impurity profiles the only region where one would expect the calculated concentration distribution to differ markedly from reality would be the high concentration region near the surface. In this region concentration dependent and field aided diffusion effects are probably present during the diffusion process. One would therefore expect a flatter profile than is calculated with a steeper dropoff into the region where the concentration dependent mechanism would not be operative ($C(x,t) < 1x10^{19}$ atoms/cc). On this p-n-p device the high frequency charactersitics are greatly affected by the slope of the concentration distribution near the base collector junction. Good agreement between the calculated and measured values of the device parameters can be obtained by using the CNM. To achieve this agreement one must modify the phosphorus diffusivity by a factor of 0.7 during the drive-in operation (step 9), while the diffusivity of the boron should be enhanced by a factor of five during the emitter diffusion. Using these enhancement and retardation factors to obtain effective values of the diffusivity, one obtains excellent agreement not only with the junction depth measurements but with the sheet resistance and Gummel number values as well, as can be seen in the columns designated "modified" in Table III. The CNM technique easily lends itself to an analysis of the predep, etching and drive-in cycles to optimize the high frequency response of the device.

Example 2

In the second example an integrated circuit device pictured in Figure 25 is analyzed. This example shows how CASPER is used to isolate a critical step in the processing sequence relative to a given parameter (buried layer sheet resistance), that can be easily calculated from the resultant concentration versus depth distribution. In this structure the sheet resistance of the antimony buried layer must be kept below 20 ohms/square. It was found in some devices after processing that the sheet resistance had exceeded this value. Since the antimony distribution itself was formed by a deep predep and drive-in process no analytical solution existed for the impurity distribution. Therefore the CNM was used to calculate this distribution and subsequently integrate it to obtain the sheet resistance of the structure at all subsequent processing steps. R_s is defined below:

$$R_s = \{\int_{x_1}^{x_2} q\,\mu(x)\,C(x,t)\,dx\}^{-1} ,$$

where q is the electronic charge and $\mu(x)$ is the majority carrier mobility. Table IV shows the change in antimony sheet resistance as a function of high temperature processing. Since this calculation established that the HCl vapor etch was the principal culprit, further analysis was undertaken to reveal the extent of this effect. Calculations were performed simulating the HCl vapor etching of the silicon surface, removing from none to two microns of silicon. Figure 26 shows

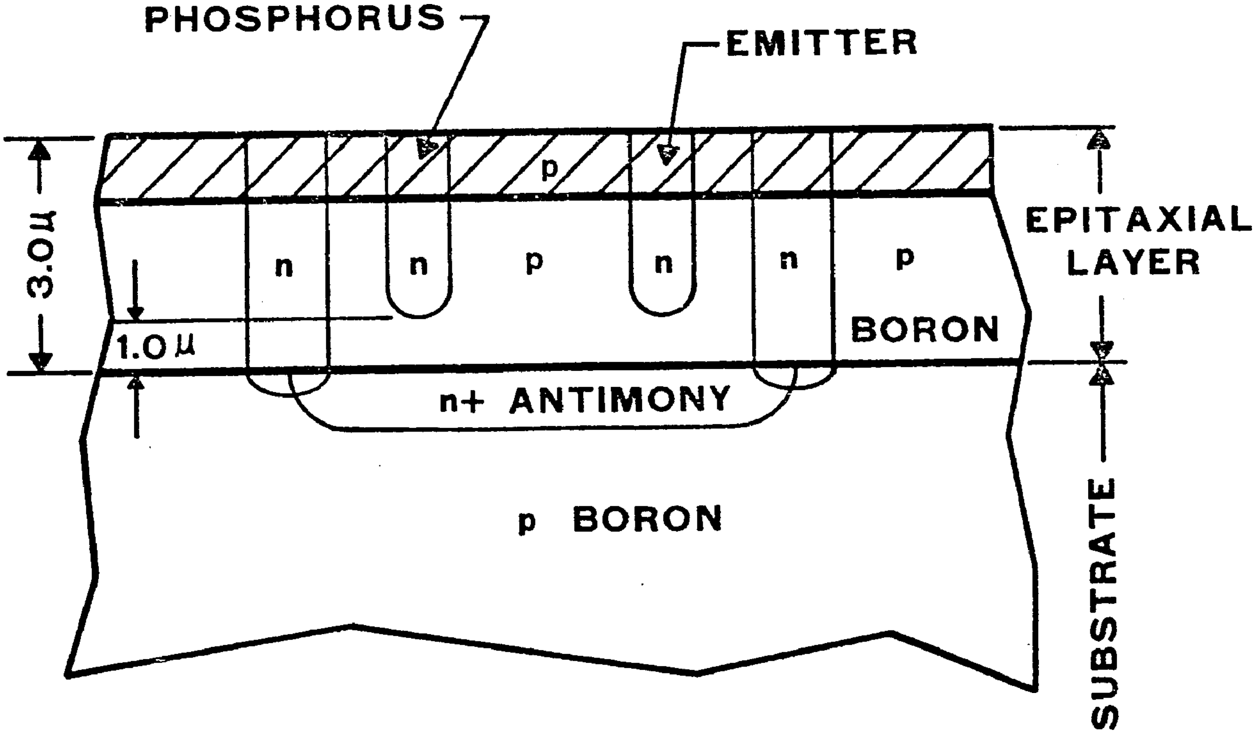
PHOSPHORUS
EMITTER
p
3.0µ
n
n
p
n
n
p
EPITAXIAL LAYER
1.0µ
BORON
n+ ANTIMONY
p BORON
SUBSTRATE

FIGURE 25

TABLE IV

Sheet Resistance Change vs. Processing Step

Step No.	Sb Sheet Resistance	Width of Sb Region	Max. B.L. Conc. Atm/CC x 10^{19}
Steam Oxid.			
Sb. Predep	16.71	4.15	5.50
Cap. Oxid.	16.48	4.30	4.52
Drive-in	13.14	9.15	1.61
HCl Etch* (0.75 μm)	17.34	8.45	1.48
Epi Growth (3 μm)	16.96	8.85	1.46
Steam Oxid.	16.91	8.90	1.41
Phos. Diff.			
BN Predep			
B Drive-in			
Steam Oxid.			
Emitter Diff.	16.79	9.00	1.37

*32% change in sheet resistance on HCl etching.

both the calculated and experimental results for the percentage change in R_s versus the amount of silicon removed. The agreement between the predicted increase in R_s and the measured values is excellent. This calculation enabled the specification of the HCl cycle as a function of the sheet resistance and therefore resulted in the more efficient utilization of the subdiffused wafers.

Example 3

Example three explored the movement of a minor impurity in a heavily doped substrate during epitaxial growth and subsequent high temperature processing. Again one is confronted with a problem with non-uniform initial conditions for the second and all subsequent steps. In this case the substrate was doped to $5\text{x}10^{18}$ atoms/cc with antimony and the layer was intentionally doped with 2×10^{14} atoms/cc of phosphorus. The boron in the substrate (due to contamination of the polycrystalline silicon raw material or contamination during crystal growth) was believed to diffuse out during growth and form a p-region about one micron from the original interface in the epitaxial layer. In some cases this region apparently escaped detection after epitaxial growth but appeared to form sometime during subsequent high temperature processing. Figure 27 shows the calculated concentration distribution for $1\text{x}10^{16}$ atoms/cc of boron originally in the substrate. The CNM solution showed that the p-layers did indeed grow with subsequent processing by almost a factor of 2.5. The calculation also showed that if the boron level in the substrate was less than 5×10^{15} atoms/cc no

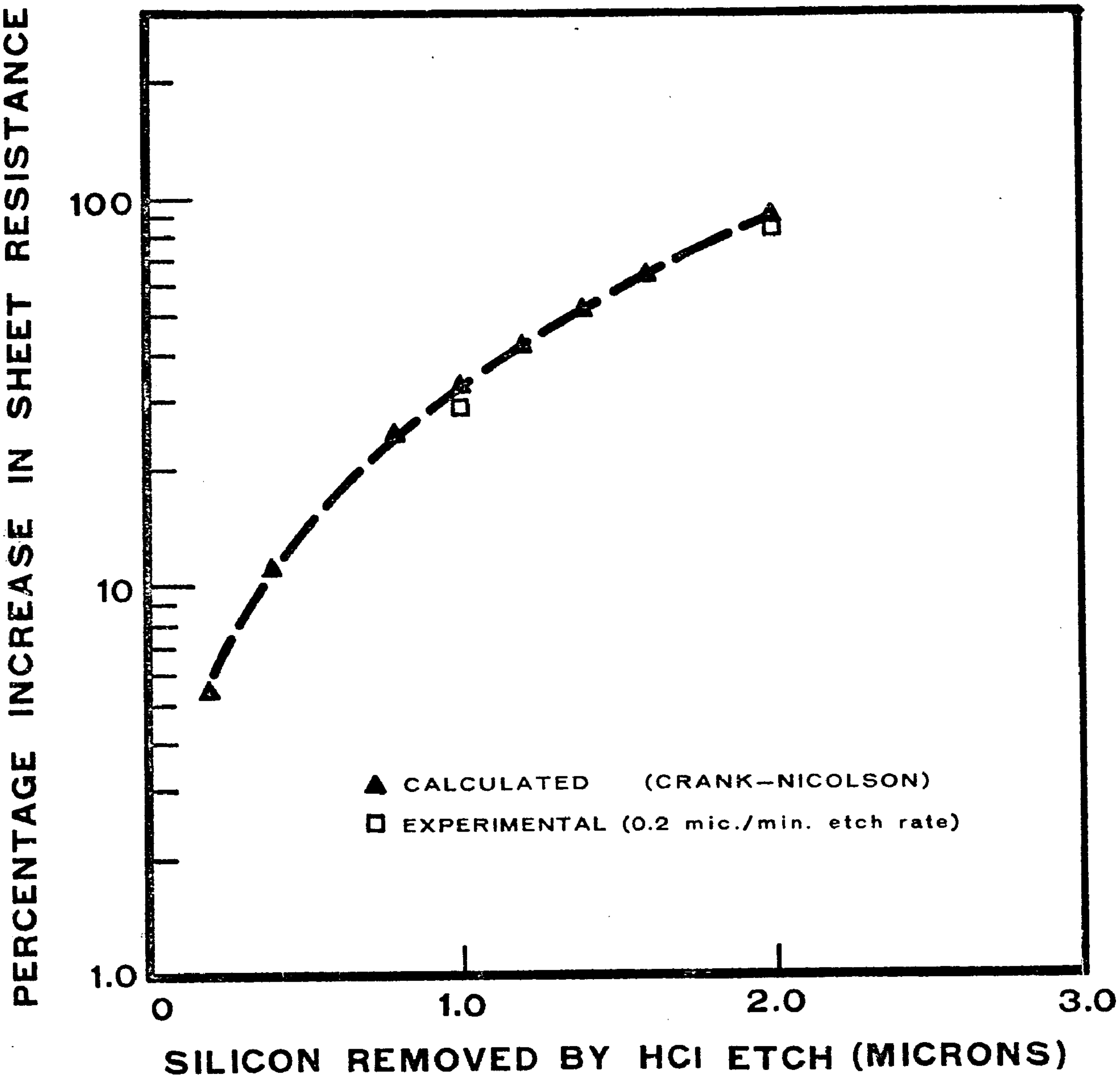
PERCENTAGE INCREASE IN SHEET RESISTANCE
100
10
1.0
0
1.0
2.0
3.0
SILICON REMOVED BY HCl ETCH (MICRONS)
▲ CALCULATED (CRANK–NICOLSON)
☐ EXPERIMENTAL (0.2 mic./min. etch rate)

FIGURE 26

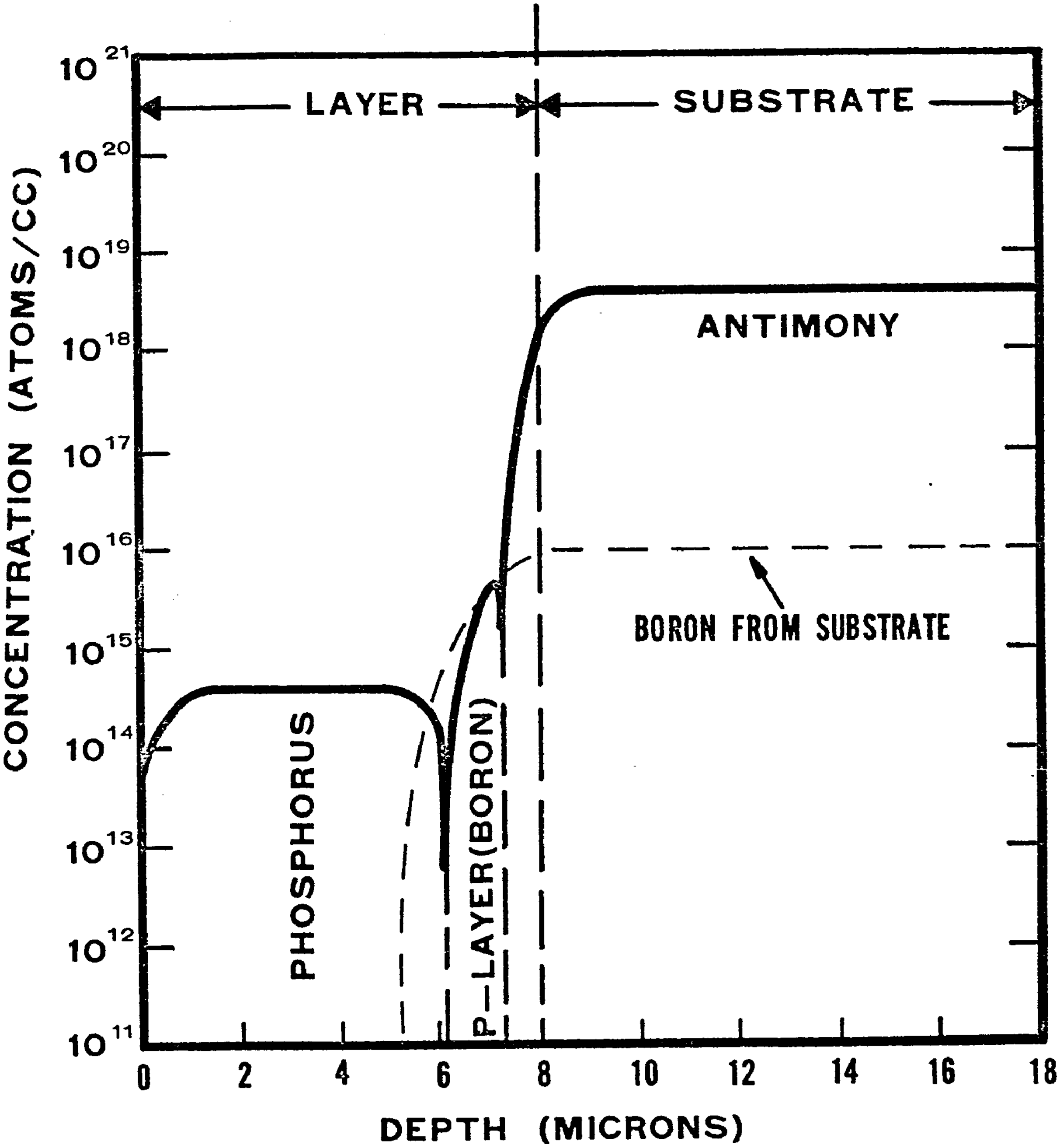
LAYER
SUBSTRATE
ANTIMONY
BORON FROM SUBSTRATE
PHOSPHORUS
P—LAYER(BORON)
CONCENTRATION (ATOMS/CC)
10^{21}
10^{20}
10^{19}
10^{18}
10^{17}
10^{16}
10^{15}
10^{14}
10^{13}
10^{12}
10^{11}
0
2
4
6
8
10
12
14
16
18
DEPTH (MICRONS)

FIGURE 27

layer could be detected by the MOS capacitance technique being used. This suggested that slices should be subjected to a high temperature soak directly after epitaxial deposition to enhance the presence of the p-layers if they existed. Figure 28 shows the comparison between the calculated width of the p-region before and after the high temperature processing steps. These calculated p-region widths are in good agreement with the boron concentrations found in the substrates using the ion microprobe.(23)

Example 4

Example four treats the problem of front surface antimony autodoping. This example explores a transport mechanism for antimony over and above the predictions of normal diffusion theory. The calculation of the concentration gradient between a substrate and an epitaxial layer should follow a simple ERFC function if the normalized values of evaporation coefficient and growth rate are both large.(4) Therefore when one requires a steep concentration gradient between the layer and the substrate for a particular device application, lower deposition temperatures coupled with faster deposition rates would achieve the desired result. Also to minimize the presence of any back autodoping effects a substrate dopant with a small segregation coefficient should be chosen to prevent reincorporation from the ambient gas phase. Antimony fits all of these requirements.

It was therefore very surprising when one experimentally determined the concentration gradient over a diffused antimony region and

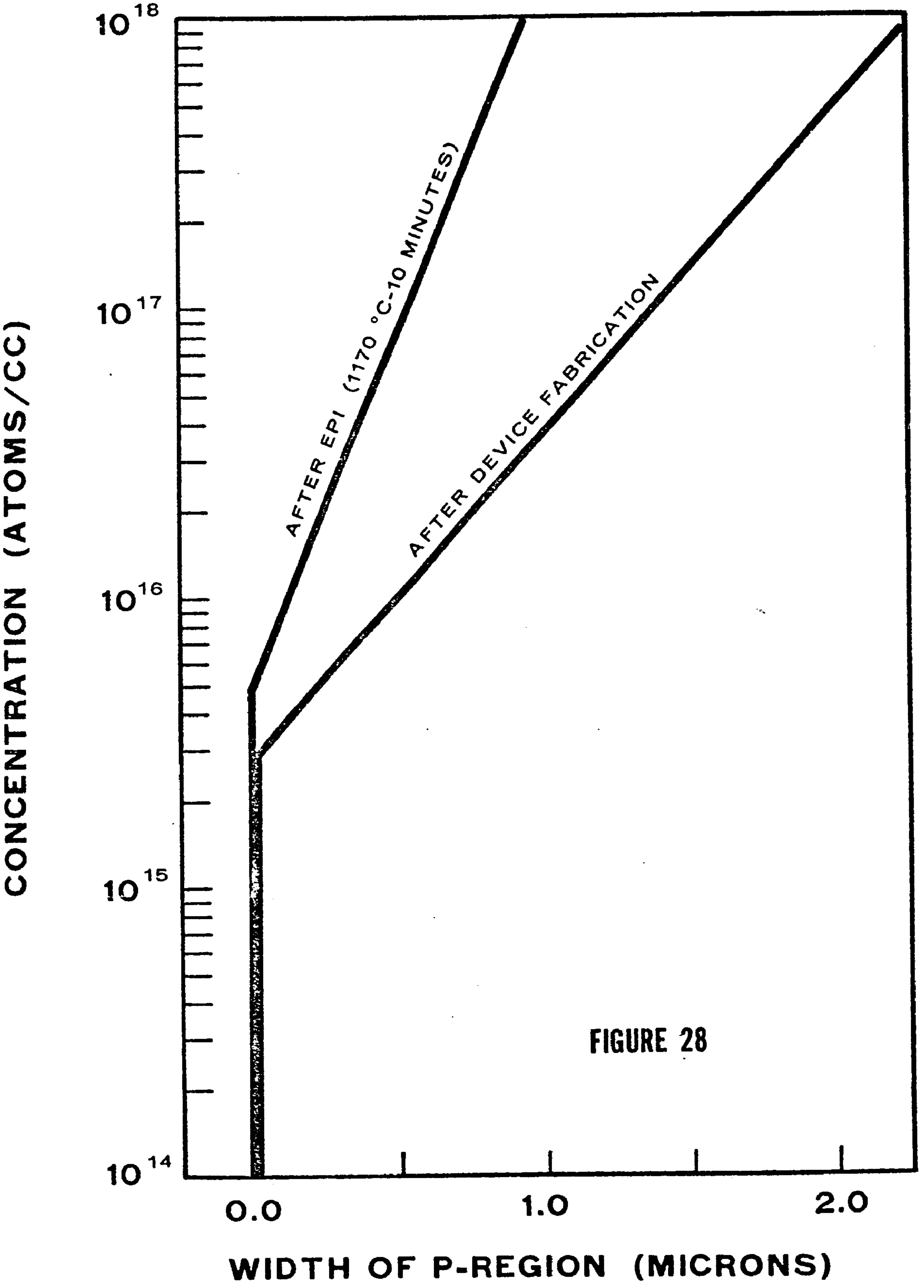

10^{18}
10^{17}
10^{16}
10^{15}
10^{14}
CONCENTRATION (ATOMS/CC)
AFTER EPI (1170 °C-10 MINUTES)
AFTER DEVICE FABRICATION
0.0
1.0
2.0
WIDTH OF P-REGION (MICRONS)

FIGURE 28

found that the substrate dopant had moved ten to twenty times further into the epitaxial layer than was predicted from simple diffusion theory. When one looked at the segregation coefficient for antimony, it is indeed lower than that of arsenic, phosphorus, or boron by at least an order of magnitude. Therefore a large activation energy must be required to transport antimony across a silicon gas-solid interface. Even though the evaporation coefficient of antimony is large an adsorbed antimony layer may exist at the moving gas solid interface. This adsorbed layer would modify the concentration distribution between the layer and the substrate resulting in a flattening of the gradient instead of a monotonic increase in slope.

To account for the observed dopant anomaly by an enhanced diffusion phenomenon a factor of between twenty and two hundred would have to be applied to the accepted diffusivity.(22) This type of explanation was used to explain the anomalous movement of phosphorus during epitaxial growth by Joyce.(6) Since no valid reason exists for using an enhanced diffusion mechanism in this case the adsorbed surface layer analysis was employed to treat this problem. CASPER was used to simulate an adsorbed surface layer whose transfer characteristics with the bulk of the solid had the same velocity dependence as the segregation coefficient. A layer was epitaxial grown over a lightly doped boron substrate containing a deep antimony diffusion (10 microns) in the top surface only. Therefore back autodoping was not possible since the back surface and edges of the wafer were lightly doped with boron. A three micron layer was deposited in 4.5 minutes at 1120 C using silane. The results of the simulation and the corrected spreading resistance probe measurements are plotted in Figure 30.

These results clearly show excellent agreement between the experimental data and the CNM solution assuming an adsorbed surface layer. For comparison the simple diffusion theory results (equation (13)), are also plotted. This effect over and above the movement of dopant predicted from normal diffusion theory shall be referred to as "front surface autodoping". To further check the model another epitaxial run was made over the same type of diffused structure except that a smaller deposition rate was used to achieve the same three micron total layer thickness. These results are shown in Figure 31 along with the accompanying simulation containing the front autodoping effect. Again the agreement between prediction andd experimental results is excellent.

Another startling fact is that even though the second run experiences a factor of four longer time at temperature, the position of the concentration gradient is almost the same. This makes sense in light of the fact that diffusion of antimony is a negligible quantity at this temperature, so that the movement of dopant is due almost entirely to the front autodoping effect. The absence of almost any time dependence precludes an enhanced diffusion effect. At higher temperatures the front autodoping effect decreases as diffusion begins to predominate. At lower temperatures where diffusion is absent the front autodoping effect may explain the anomalous movement of antimony

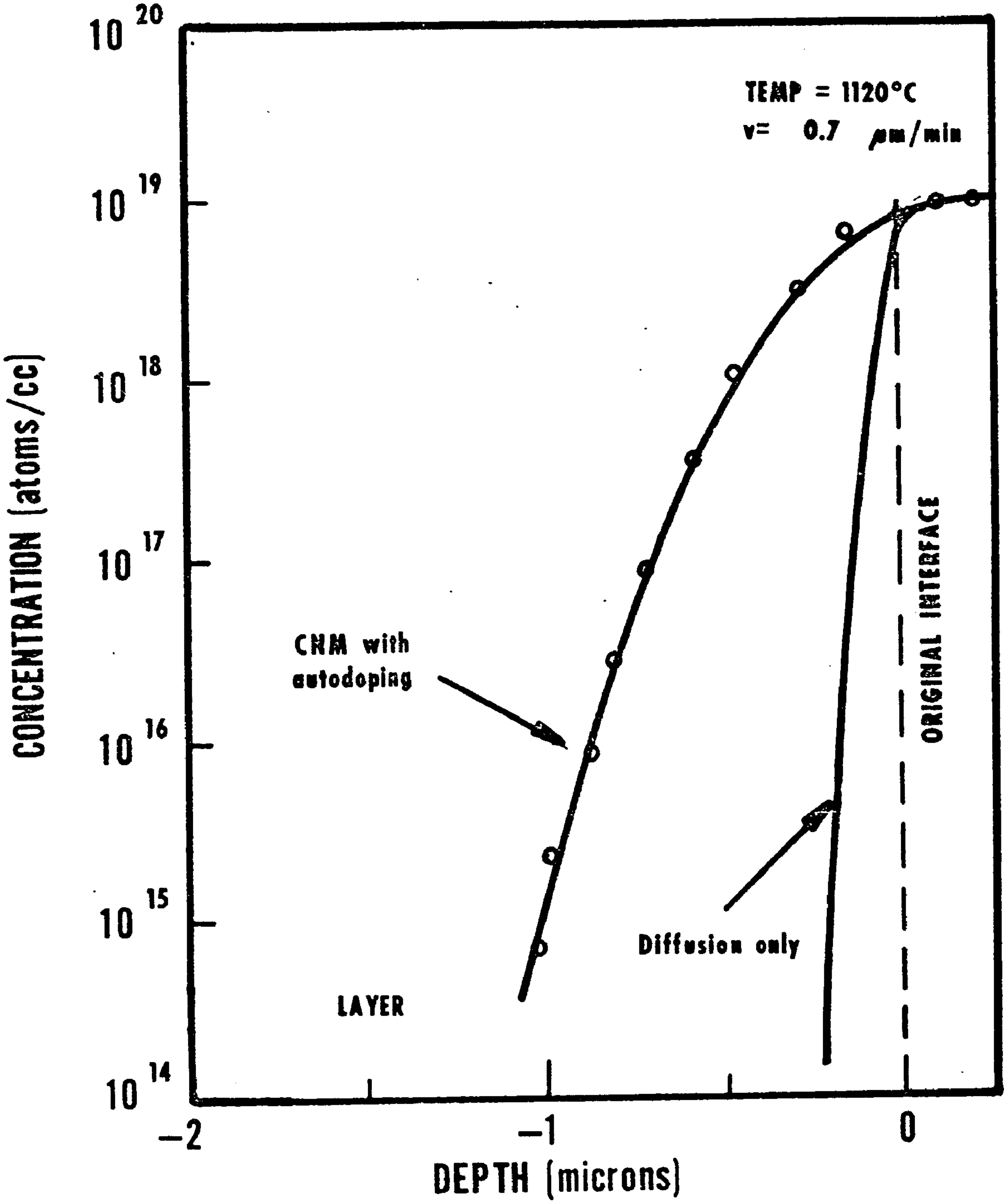

TEMP = 1120°C
v= 0.7 µm/min
CNM with autodoping
Diffusion only
LAYER
ORIGINAL INTERFACE
CONCENTRATION (atoms/cc)
10 20
10 19
10 18
10 17
10 16
10 15
10 14
−2
−1
0
DEPTH (microns)

FIGURE 30

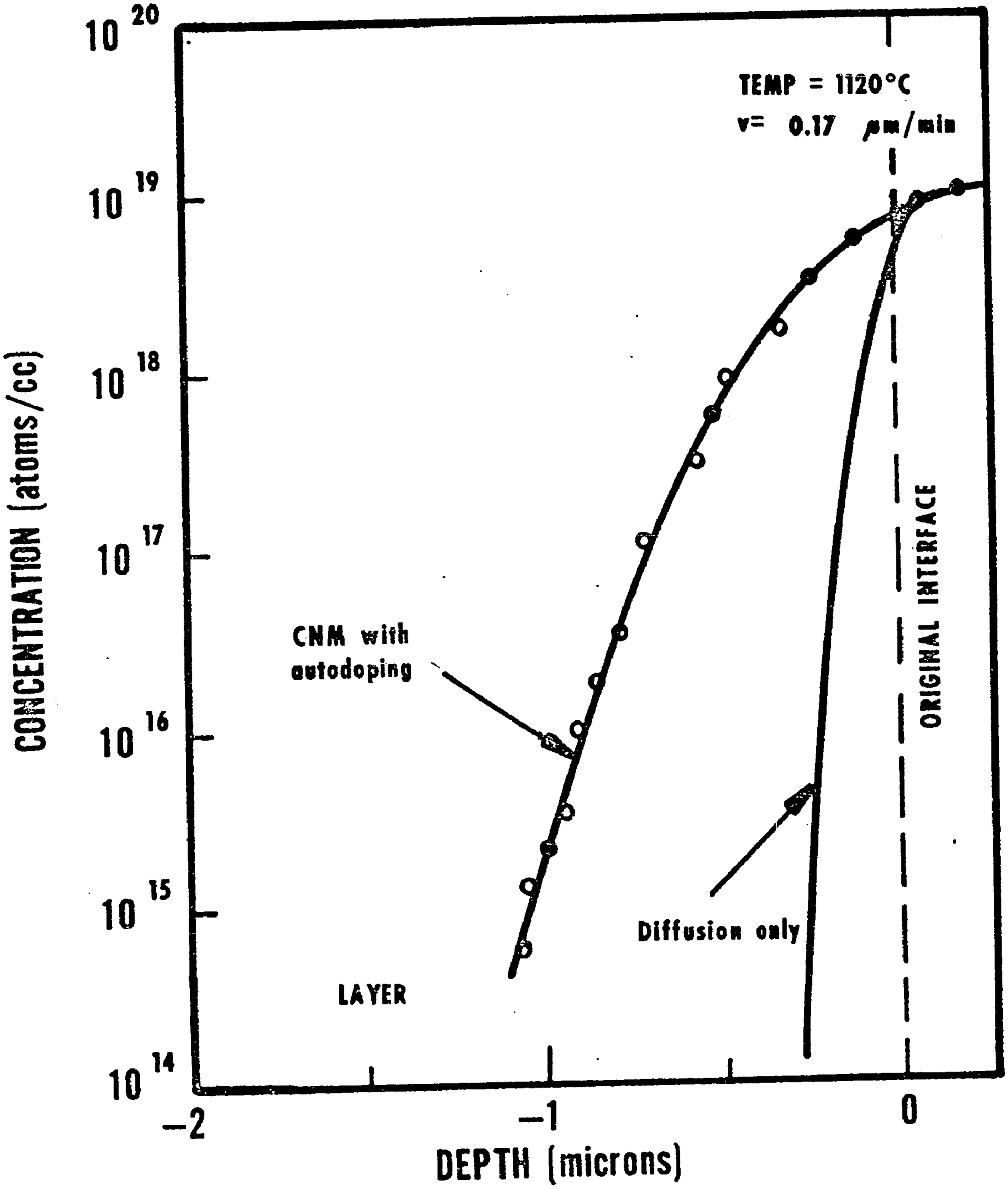

TEMP = 1120°C
v= 0.17 µm/min
CNM with autodoping
Diffusion only
LAYER
ORIGINAL INTERFACE
CONCENTRATION (atoms/cc)
10 20
10 19
10 18
10 17
10 16
10 15
10 14
−2
−1
0
DEPTH (microns)

FIGURE 31

reported by Gittler.(24)

Example 5

The fifth example deals with the back autodoping phenomenon. This example shows how CASPER may be used on a problem where multiple sources of dopant are present (i.e., intentionally added to the gas phase, diffusing from the substrate into the layer, and transported through the gas phase from the sides and back of the substrate). This effect involves the transport of dopant originally in the substrate through the gas phase and back into the growing layer. Therefore epitaxial layers deposited on lightly doped substrates would have a lower layer doping level than layers deposited on heavily doped substrates in the same reactor. Dopant from one substrate may affect other wafers in the reactor with the effect decreasing as the distance from the heavily doped wafer in question. The back of the substrate which is unsealed during the deposition cycle is usually the prime source of this extra dopant after the first micron or two of growth. Subdiffused regions on the surface have been shown by Pogge(25) to also give rise to the same autodoping effect though this source of dopant modifies the impurity profile near the original interface more than in the layer far from the interface. Shepherd(7) developed a mathematical treatment of the autodoping problem that considered the back surface of the wafer as the sole source of dopant that could enter the growing epitaxial layer over and above the transport of dopant by solid state diffusion. Using this approach and the initial conditions that the distribution of dopant originally in the substrate was uniform he developed a calculation that involved a knowledge of the growth rate and the transport parameters of the dopant in both the gas and solid system. His final equation ignores the effects of solid state diffusion so that his model is applicable from about two diffusion lengths from the original interface to the surface of the epitaxial structure. Figure 32 is a comparison between the autodoping model developed by Shepherd and the CNM solution of the same problem. The agreement is quite good between the two approaches. Both calculations were performed assuming that four percent of all dopant leaving the back surface was available for reincorporation into the growing layer. The conditions of growth were as follows: temperature 1200 C, time 6 minutes at a growth rate of 0.75 microns/min, and 114 minutes at a growth rate of 0.13 microns/min. The scatter in Shepherd's data is a factor of five greater than the disagreement between his calculation and the results of the numerical model.

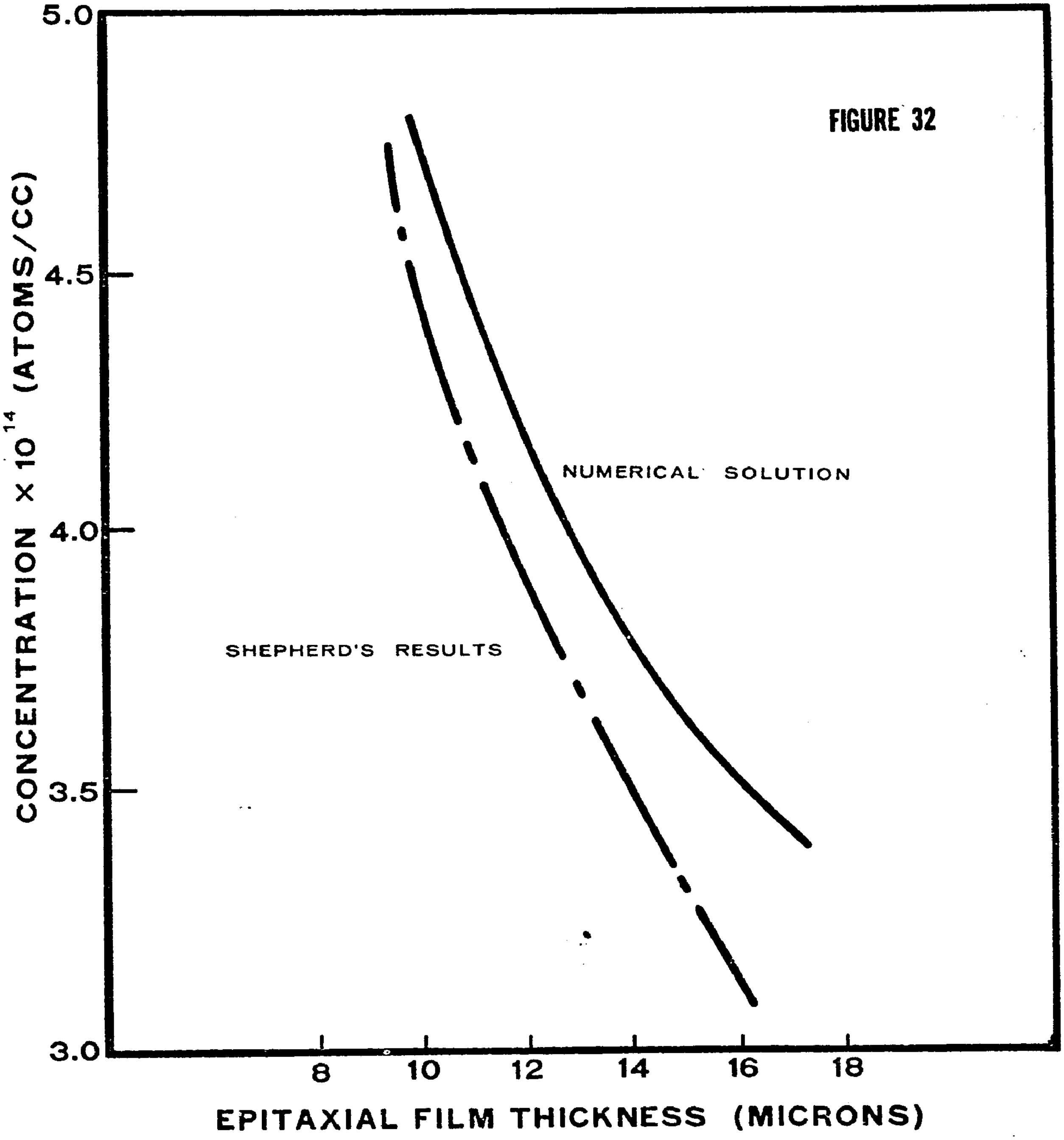
FIGURE 32
NUMERICAL SOLUTION
SHEPHERD'S RESULTS
CONCENTRATION × 10^14 (ATOMS/CC)
5.0
4.5
4.0
3.5
3.0
8
10
12
14
16
18
EPITAXIAL FILM THICKNESS (MICRONS)

CONCLUSIONS

In conclusion a one dimensional computer model has been developed that can predict the impurity distribution in a silicon wafer that has been subjected to a sequence of high temperature device processing steps. Particular attention has been paid to the modeling of dopant transport during epitaxial growth in order to explain both front and back surface autodoping phenomenon. The Crank-Nicolson method has been used to solve the resultant equations numerically to a high order of accuracy with the aid of a split grid approach to minimize computer run time. The evaporation coefficient of boron in silicon has been determined in the temperature range from 1190 to 1380 C. Using these evaporation coefficient results it was shown that boron doped substrates are a large source of contamination during silane epitaxial growth. No front surface autodoping effects were observed and the concentration gradient between the heavily doped substrate and the lightly doped layer appears to follow normal diffusion theory. At present the accuracy of the predictions is only limited by the experimental values of the constants employed in the analysis, e.g., diffusivity, evaporation coefficient, and segregation coefficients. A better understanding of the dopant interchange at the gas solid interface will permit extension of this model to the analysis of sub-micron epitaxial structures.

REFERENCES

1) Thomas, C. O., Kahng, D., and Manz, R. C., "Impurity Distribution in Epitaxial Silicon Films", Jl. Electrochem. Soc., vol. 109, p. 1055, 1963.

2) Grossman, J. J., "A Kinetic Theory for the Autodoping for Vapor Phase Epitaxial Growth of Germanium", ibid, vol. 110, p. 1065, 1963.

3) Rice, W., "Diffusion of Impurities During Epitaxy", Proceedings IEEE, vol. 52, p. 284, 1964.

4) Grove, A. S., Roder, A., and Sah, C. T., "Impurity Distribution in Epitaxial Silicon Growth", Jl. Appl. Phys., vol. 36, p. 802, 1965.

5) Abe, T., Nishi, Y., Sato, K., and Oi, N., "Impurity Distribution in Silicon Epitaxial Films", Denki Kageku, vol. 35, p. 142, 1967, Translated by Associated Technical Services, 1968.

6) Joyce, B. A., Weaver, J. C., and Maule, D. J., "Impurity Redistribution Process in Epitaxial Silicon Layers", Jl. Electrochem. Soc., vol. 112, p. 1100, 1965.

7) Shepherd, W. H., "Autodoping of Epitaxial Silicon", ibid, vol. 115, p. 652, 1968.

8) Skelly, G., and Adams, A. C., "Impurity Atom Transfer During Epitaxial Deposition of Silicon", ibid, vol. 120, p. 116, 1973.

9) Hu, S. M., "Redistribution of Diffused Layers During Epitaxial Growth and Other Processing Steps", Jl. Appl. Phys., vol. 39, p. 3844, 1968.

10) Monnier, J., Stern, M., Maffei, A., and Vandorpe, D., "Numerical Analysis of Simultaneous Diffusion of Several Impurities in Silicon and Silicon Dioxide", Electronics Letters, vol. 8, p. 517, 1972.

11) von Rosenberg, D. U., Numerical Methods for the Solution of Partial Differential Equations, American Elsevier Publishing Co. New York, chaps. 2 and 5, and appendix A, 1969.

12) Carnsahan, B., Luther, H. A., and Wilkes, J. O., Applied Numerical Methods, John Wiley Publishing Co., New York, P. 451, 1969.

13) Shepherd, W. H., "Doping of Epitaxial Silicon Films", Jl. Electrochem. Soc., vol. 115, p. 541, 1968.

14) Allen, F. G., Emissivity at 0.65 microns of Silicon and Germanium at High Temperatures", Jl. Appl. Phys., vol. 28, p. 1510, 1957.

15) Schumann, P. A., and Gardner, E. E., "Spreading Resistance Corrections Factors", Solid State Electronics, vol. 12, p. 371, 1969.

16) Bloem, J., "The Effect of Trace Amounts of Water Vapor on Boron Doping in Epitaxial Silicon", Jl. Electrochem. Soc., vol. 118, p. 1837, 1971.

17) Tung, S. K., "Influence of Process Parameters on the Growth of Epitaxial Silicon", Metallurgy of Semiconductor Materials, edited by J. Schroeder, published by Interscience, p. 95, 1961.

18) Takahashi, R., Hoga, Y., and Sugawara, K., "Gas Flow Patterns and Mass Transfer Analysis in a Horizontal Flow Reactor for Chemical Vapor Deposition", Jl. Electrochem. Soc., vol. 119, p. 1406, 1972.

19) Kato, T. and Nishi, Y., "Redistribution of Diffused Boron in Silicon by Thermal Oxidation", Jap. Jl. Appl. Phys., vol. 3, p. 377, 1964.

20) Trumbore, F. A., "Solid Solubilities of Elements in Germanium and Silicon", Bell System Tech. Jl., 39, p. 205, 1960.

21) Lee, T. P., "Calculations of Cutoff Frequency, Breakdown Voltage, and Capacitance for Diffused Junctions in Thin Epitaxial Layers", IEEE Trans., Electron Devices, vol. 13, p. 881, 1966.

22) Kendall, D. L., and DeVries, D. B., "Diffusion in Silicon", Semiconductor Silicon, edited by R. R. Haberecht and E. L. Kern, published by the Electrochemical Society, New York, p. 358, 1969.

23) Edwards, J., Member of Technical Staff, Bell Telephone Laboratories, private communication, January 1972.

24) Gittler, F. L., "Epitaxial Deposition of Silicon in Nitrogen", Jl. of Crystal Growth, vol. 17, p. 271, 1973.

25) Pogge, H. B., Boss, D. W., and Ebert, E., "Autodoping During Epitaxial Silicon Growth", Chemical Vapor Deposition, published by the Electrochemical Society, New York, p. 767, 1970.

26) American Society for Testing and Materials, 1972 Annual Book of Standards, vol. 8, F-84-72, p. 688, 1972.

27) Gibbons, J. F., "Ion Implantation in Semiconductors - Part I Range Distribution Theory and Experiments", Proc. IEEE, vol. 56, 295, 1968.

28) Crank, J., Mathematics of Diffusion, published by Oxford University Press, London, p. 38, 1967.

29) Grove, A. S., Physics and Technology of Semiconductor Devices, published by John Wiley and Sons, New York, p. 65, 1967.

30) Evesteyn, F. C., Severin, P. J., v.d. Brekel, C. H., Peek, H. L., "A Stagnant Layer Model for the Epitaxial Growth of Silicon from Silane", J. Electrochem Soc., vol. 117, p. 925, 1970.

APPENDIX A

Computer Program

The program CASPER* (Computer Aided Semiconductor Processing and Epitaxial Redistribution) performs the sequential numerical solution of the diffusion equation using the Crank-Nicolson Method (CNM). The program can handle up to five dopant elements simultaneously. CASPER consists of a main program and fifteen major subroutines. The major functions of these routines are given below along with an example of the input and output of the program. This example will contain sufficient information so that it may be used as a manual for the operation of the program.

MAIN: Inputs data such as temperatures, times, growth rates, dopant species and concentrations. Calculates the diffusivities of all elements from stored data. Diffusivities may be supplied externally or modified by the user. Contains many input parameter default options. Guards against specifying a spatial grid too large for the program. Calls most of the major subroutines.

DEPTH: Calculates the depth from the front gas-solid interface to each grid line. For all processing steps except epitaxial growth, the zero value of depth is the gas-solid interface. For epitaxial growth simulations the original gas-solid interface is defined as the zero of depth. Depth values are not stored by the program in order to minimize core storage.

---

*Available from Lehigh University Computer Center.

INITIAL: This routine initializes the concentration to a uniform level in the substrate for up to four different dopant elements.

HEADING: This routine prints out the heading information on each page of printed output.

IONIMP: This routine calculates and loads into core the ion implanted profile from the following information: ion dose and accelerator voltage. Second order polynomials have been fitted to Gibbons(27) data for the range and the standard deviation of gaussian implanted profiles. The stored values may be overridden by the user simply by specifying the range and standard deviation on the appropriate element card (see discussion of input and output below). No thermal treatment occurs during an ion implantation step. Only one dopant species may be implanted per step.

JNDPTH: This routine detects changes in the net concentration distribution between n and p type material. The depth at which this transition occurs is defined as the junction depth.

OTPT: This routine outputs the concentration versus depth information for the net or total concentration (absolute value of the sum of the n-type dopants minus the p-type dopants). The concentration distributions of each element is also printed out in column form. This line printer output may be deleted for all steps but the last step.

GENPLT: This routine performs the coding of the concentration versus depth information for plotting on a CALCOMP 900 off-line digital plotting system. It allows the output of any size plot up to 30x125 inches.

PLT: This routine plots the net concentration, for each processing step, as well as the concentration of each dopant species using a different symbol. Junction depths, sheet resistances and integrated net concentration are printed on each plot. Time, temperature, diffusivity, evaporation rate, growth rate, and oxide thickness are printed on every plot.

QPLT: This routine permits the plotting of the net concentration versus depth distribution under the control of the user for size and scaling of the plot. No heading information is supplied.

OXIDE: This routine assumes a parabolic oxidation rate for the oxide thickness and time specified. It then calculates the time necessary to oxidize away one delta x of silicon as a function of the amount of oxide already removed.

REMOVE: This routine is employed to simulate chemical etching operations in which no transport of dopant is occurring by diffusion.

SHTRES: This routine calculates the sheet resistance and integrates the net concentration distribution between all junctions and between a junction and the nearest gas-solid interface. When no junctions are present these parameters are calculated between the front and back boundaries. Lee's fit to Irvin's curve is used to convert concentration to resistivity.

SUBSLN: This routine computes the analytical solution to the moving boundary and evaporation problem. The difference between the analytical solution and the results of the CNM are displayed in percent on the printed output.

TTIME: This routine computes the delta t for the fixed time case based upon a given value of "R". This initial delta t is then reduced by a factor of four orders of magnitude and is used as the starting point in the variable delta t solution. Epitaxial growth and vapor phase etching are fixed delta t operations while other types of processing steps are solved using a variable delta t solution.

THOMAS: This routine contains the algorithm for solving the tridiagonal matrix of equations for the concentration values at the next time interval. It also contains the evaporation coefficient and equilibrium segregation coefficient data by element as a function of temperature. The velocity dependence of the segregation coefficient is also calculated in this routine. Redistribution due to thermal oxidation at the front interface is also computed in this program. Adjustments to the size of the spatial grid due to oxidation, growth, or etching are made in this routine.

A typical set of input data for a six step sequential processing problem is given below in Table A1. The sequence consists of

1) epitaxial growth, 2) oxidiation, 3) phosphorus implant, 4) oxidation, 5) boron diffusion, and 6) oxidation. The substrate is doped with antimony while boron is added during epitaxial growth to form a p-type layer with a p-n junction. Pileup of n-type dopants at the front interface is seen to occur during the oxidation steps while the p-type dopant near the interface is depleted. Phosphorus is implanted into the silicon at step three while boron is again added at step five.

The solution of this six step problem using CASPER, involving approximately 400 grid points per step to describe the solid, took 0.772 minutes of effective elapsed time on an IBM 370/165 computer. This included the line printer output as well the coding for a CALCOMP plot of the concentration versus depth for each processing step.

The following detailed description of the input stream found in Table A1 will constitute a user's manual for CASPER. For this section all numbers found between brackets {} will refer to column numbers on the input card under discussion.

The first card contains twelve columns of literal information {1-12}, that will be printed on each plot and page of printed output for each step. For this example the word "EXAMPLE" will be printed on each page and plot. The next parameter on this card is the ratio of delta y to delta x {22-28} and is 10 for this problem. The third parameter on this card is the number of spatial steps delta x wide {30-32}, and is 100 for this problem. The remainder of the spatial steps will be delta y large. When the epitaxial layer is grown it will

TABLE A1

Example of Input

```
Card No.

    1        EXAMPLE
    2        5.00D18            10.0            100
    3        6 01 4  1.00D12
    4        1 01 3  1.00D15
    5        7 03 2  1.00D14   150.0
    6        1 05 1  1.00D20     5.0
    7        9
    8        0.01
    9                    EPI GROWTH
   10        1120.00  6.000  3.0000          0.5000
   11        7           OXIDATION
   12        1100     60.0                                    5000
   13        7           PHOSPHORUS IMPLANT
   14        100.00   1700
   15        7           OXIDATION
   16        1050     120.0                                   5000
   17        7           BORON DIFFUSION
   18        900.0    30.00
   19        7           OXIDATION
   20        1050.00  120.0                                   5000
   21        9
```

be composed of spatial steps delta x wide. The only limit on size is the core storage allocated by the program. The version of CASPER used for this solution contains 2500 core locations for each of the five elements that could be used in a particular problem.

The second input card contains the concentration of the dopant in the substrate {1-7, 9-15, 17-23, 25-31}. Up to four different dopants may exist in the substrate at the beginning of the problem.

The next few cards, (four cards, there may be up to 39), are called "element cards" (EC). An EC is required every time a new dopant is introduced into the system and also to define the dopant species initially in the substrate. The EC are set up as follows. The first parameter is the code for a given element (dopant) species {1}. This code is given below.

1 = boron

2 = aluminum

3 = indium

4 = gallium

5 = arsenic

6 = antimony

7 = phosphorus

9 = end EC input stream

The second parameter on this EC {3-4}, is the number of the processing step at which the dopant defined in {1} is introduced into the gas phase or the solid. There is no limit on the number of processing steps in a particular problem. The third parameter is the boundary condition (BC) code {6}, and is given below.

1 = Constant surface concentration in the solid

2 = Ion implantation step

3 = General boundary condition, dopant is transferred through the gas phase.

4 = Same as BC-3, except that back surface autodoping is considered.

In using BC 3 or 4 one must remember that the concentration supplied by the user is not the value of concentration that will occur in the solid. These input values are first multiplied by the effective segregation coefficient and then must undergo transport across the gas-solid interface which is controlled by the evaporation coefficient. The fourth parameter on an EC is the concentration in atoms/cc for boundary conditions 1, 3, and 4. For boundary condition 2 (ion implantation) this parameter becomes the ion dose in ions/cm^2. This parameter is found in columns {8-14}. The last parameter on an EC again has a dual role. For ion implantation it is the accelerator voltage in KEV {16-22}, while for any other type of BC this parameter becomes a factor which multiplies the internally calculated value of the diffusivity for that particular element. This parameter is usually used to obtain better agreement between the calculated and actual values of sheet resistance and junction depth for high surface concentration diffusions when the concentration dependence of the diffusivity is ignored in the solution.

The next card (number 8), contains the value of delta x, the spatial variable, expressed in microns {1-7}. For this example the value is set equal to 0.01 microns.

The following six pairs of cards (9-20) are called "step cards" (SC). The first card of each pair contains a number code {1}, and 72 columns of literal information {2-73} that will appear on the CALCOMP plot as well as each page of printed output for the particular step. The second SC in each pair contains the following input parameters: temperature (degrees C) {1-7}, time (minutes) {9-15}, substrate thickness (microns) {17-32}, (this parameter needed only appear on the first SC). The rest of the input parameters are optional depending upon the type of processing step that is being simulated. The growth rate (microns/min) {33-39}, and the oxide thickness (angstroms) {41-47} are two commonly used optional parameters. Vapor phase etching is accomplished by supplying a negative growth rate to the program. The code number that appears in the first column of the description card and the operations that it controls are given below.

0 = initial step, not an oxidation
4 = chemical etch - removal without thermal treatment
5 = initial step, an oxidation
6 = non-initial oxidation step, no oxide thickness supplied
7 = any other non-initial step
8 = terminal card for a particular processing sequence

9 = end job card

The CALCOMP output for each processing step is given in Figures A1 through A6. All elements as well as the net concentration at the end of each step are shown using separate symbols. The curves consist of short straight line segments connecting all calculated points. At every tenth point a symbol is plotted. Pertinent information is printed on each plot.

A brief step by step description of the CALCOMP output Figure A1 to A6) will now be given for the input example shown in Table A1.

Figure A1 shows the concentration versus depth results after step 1 (epitaxial growth). The concentration distributions for the substrate dopant (antimony), the layer dopant (boron), and the net concentration are all shown using different symbols. At a concentration level of $\sim 10^{17}$ atoms/cc evidence of antimony front surface autodoping can be seen. A p-n junction occurs at -0.765 microns from the original interface or 2.24 from the front surface. From a depth of $\geqslant$ 1.0 microns, the symbols are spaced 10 times further apart. This depth point corresponds to the break in the spatial grid between a Δx of 0.01 and a Δy of 0.1 microns. There is one symbol plotted for every ten grid points.

In Figure A2 (step 2) after a 5000 angstrom oxidation the zero value of depth is now set at the front surface. During the oxidation boron has been depleted from the first 0.4 microns and the junction is now at 1.96 microns. The oxidation consumed 0.22 microns of silicon so that the junction has only moved 0.06 microns by diffusion of the antimony.

In Figure A3 (step 3) one can see the ion implanted phosphorus distribution near the surface. CASPER has calculated the input dose and reports it as -1.00E14 (third column second line on plot) while the sheet resistance of the implant is 486 ohms/sq. Two new junctions are now formed due to the phosphorus implant and they occur at 0.03 and 0.34 microns respectively.

Figure A4 (step 4) shows the redistribution of the phosphorus at 1050 C due to a 5000 angstrom oxidation. The junction nearest the surface (step 3) has disappeared as the phosphorus was piled up in the silicon at the oxide-silicon (front) interface. The second junction has moved in from 0.34 to 1.31 microns, while the sheet resistance of the phosphorus region has now dropped to 289 ohms/sq. The junction between the antimony from the substrate and the boron added in step 1 has moved from 1.96 (step 3) to 1.70 microns, but only 0.06 microns of this junction movement is caused by diffusion. The rest of the apparent dopant movement is due to the loss of silicon at the front surface due to the oxidation (0.22 microns). The net concentration distribution (triangular symbols) no longer contains any region characteristic of the original boron distribution, since diffusion of antimony and phosphorus have almost completely compensated the layer. Only the small region between 1.31 and 1.70 is still p-type as can be seen from the positive value of the integrated dopant (column three on plot).

In step 5 (Figure A5) boron is again added, this time by means of a constant surface concentration diffusion (Card 6, Table A1). The boron diffusing in from the surface has formed a new p-n junction with the phosphorus at 0.13 microns. The phosphorus has been depleted due to evaporation from about the first 0.1 microns of the solid. The number of atoms/cm^2 of boron added during the diffusion is 4.22E14.

After the oxidation in step 6 (Figure A6) a large amount of the boron has been lost from the silicon through escape into the oxide. The concentration of boron has dropped below that of the phosphorus at the surface such that the first 0.41 microns are again n-type and a new p-type compensated region has been formed between 0.41 and 0.59 microns. The compensated p-type region from step 5 has disappeared due to diffusion of phosphorus from the surface to a depth of 1.5 microns where a minimum in the net concentration now exists instead of the p-region seen in Figure 5A.

A sample of the printed output (step 6 page 2) is reproduced in Table A2. The negative sign in the total concentration column, column 3, just indicates that the material at this depth is n-type. Junction depths, sheet resistance values and integrated net concentration values are found at the end of each printout for a given step.

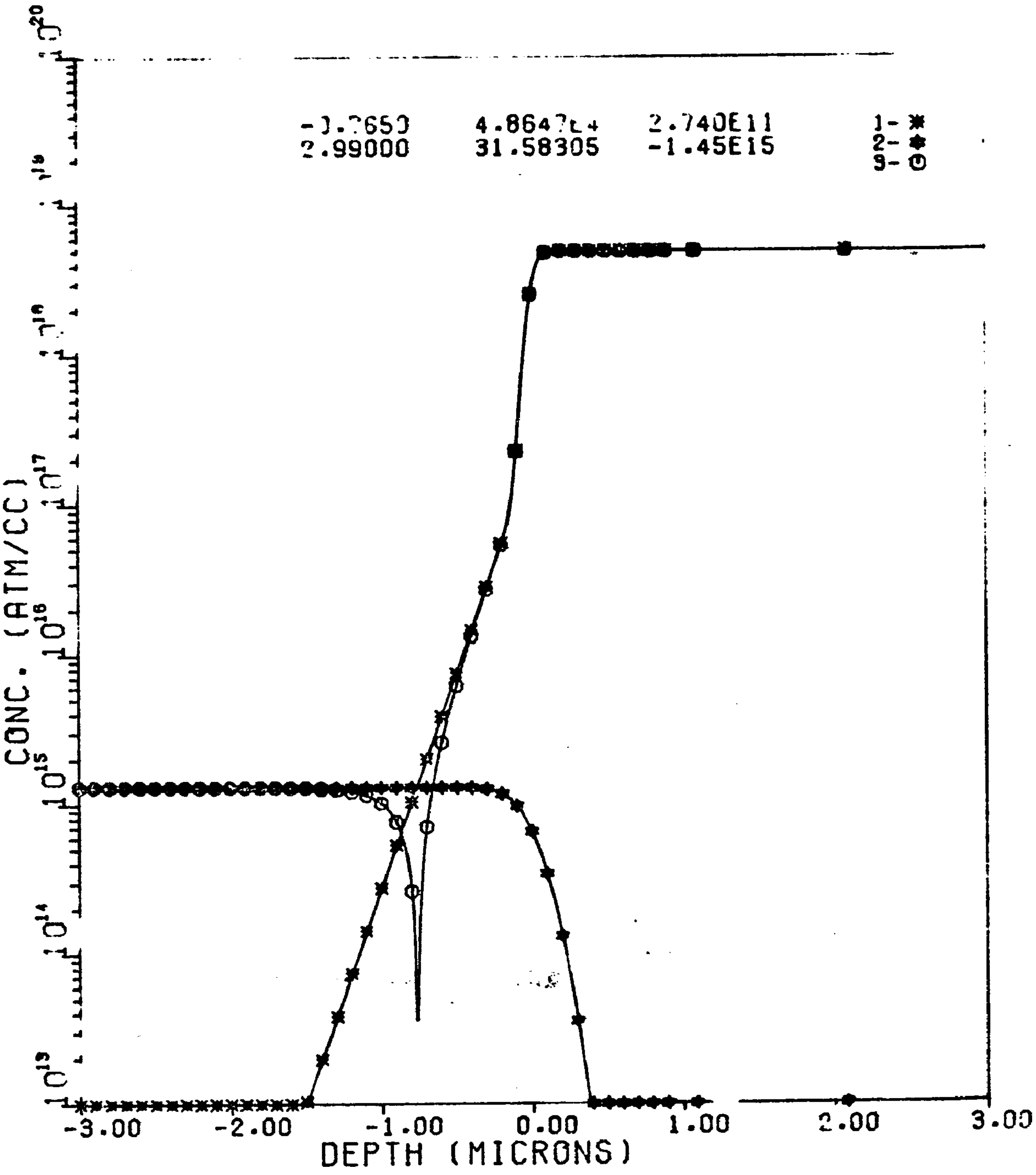

```
STEP = 1                     EPI GROWTH
EXAMPLE               DX = 0.0100        DT = 0.0200
TEMP = 1120 C           TIME = 6.0000
EVAP RATE = 0.0000       GROWTH RATE = 0.5000
FAUTO = 0.00E60     FINTF = 0.00E60     K0 = 1.44544      KE = 1.31579

1- ✱   -     0C = 2.200E-4    ANTIMONY     HP = 32.94887    VP = 82.56781
2- ✱   -     0C = 1.991E-3    BORON        HP = 0.97952     VP = 27.44775
```

FIGURE A1

DATE 04/16/73 10:06:44

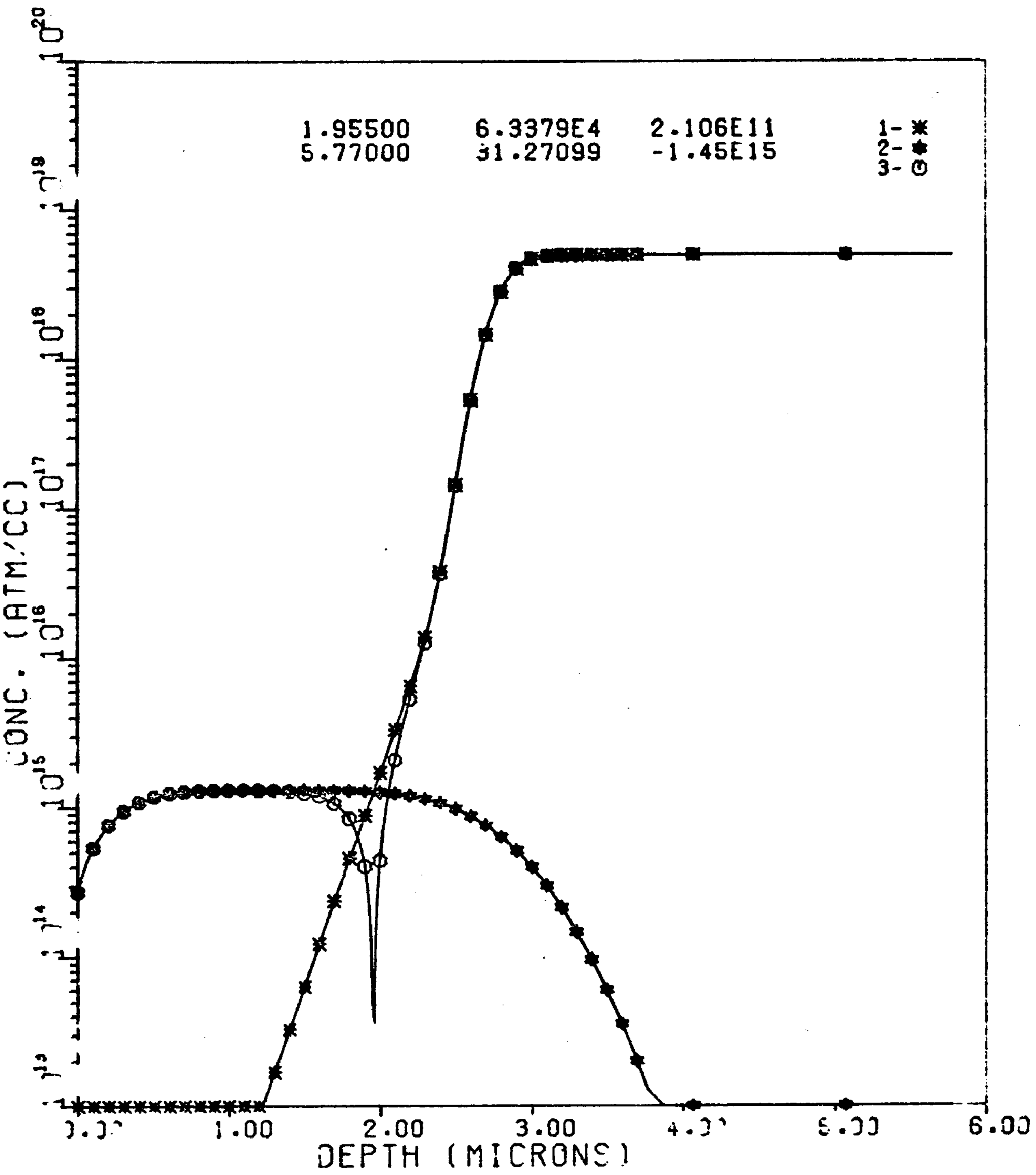

```
STEP = 2                    OXIDATION
EXAMPLE               DX = 0.0100
TEMP = 1100 C            TIME = 60.0000
EVAP RATE = 0.0000
OXIDE THK. = 5000 ANGSTROMS

1- ✱  -    DC = 1.367E-4   ANTIMONY    HP = 6.62E-58
2- ✱  -    DC = 1.304E-3   BORON       HP = 2.83318
```

FIGURE A2

```
DATE  04/16/73       10:07:05
```

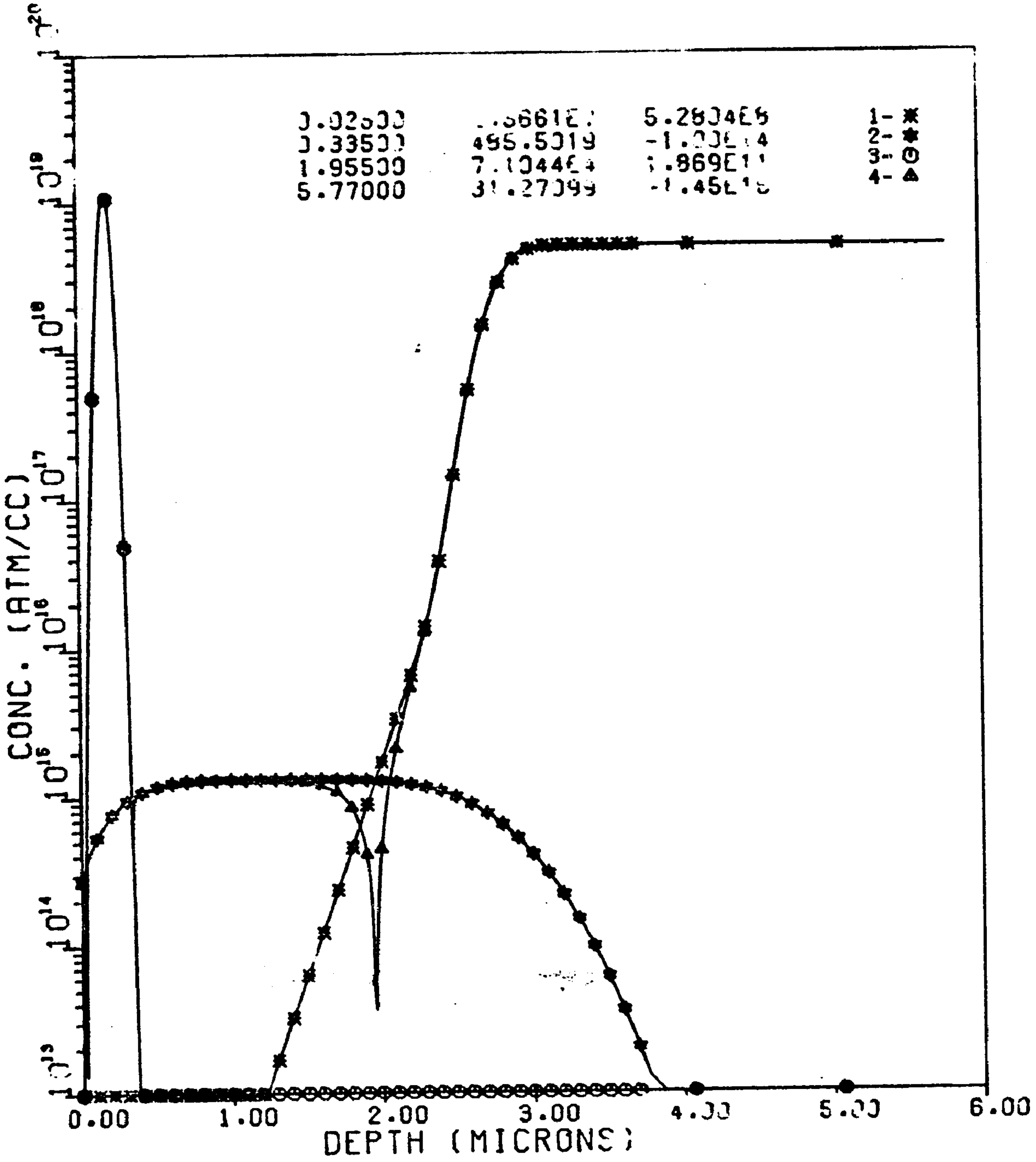

STEP = 3 PHOSPHORUS IMPLANT
EXAMPLE DX = 0.0100
TEMP = 100 C TIME = 5.0000
EVAP RATE = 0.0000

1- ✱ - DC = 3.73E-43 ANTIMONY MP = 2.83318
2- ✱ - DC = 6.15E-38 BORON MP = 2.83318
3- ⊙ - DC = 1.49E-38 PHOSPHRS MP = 2.83318

FIGURE A3

DATE 04/16/73 10:07:15

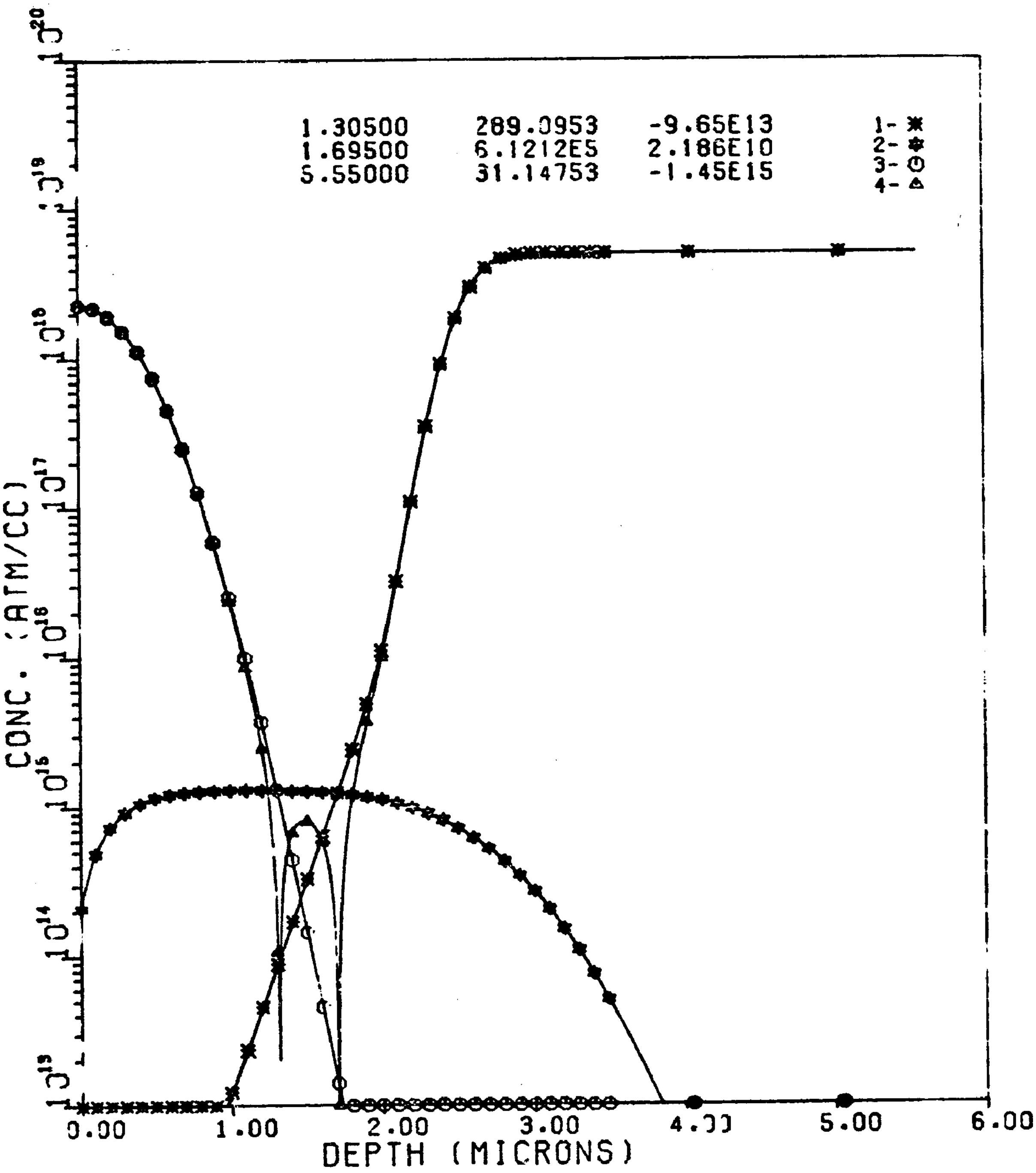

```
STEP = 4                   OXIDATION
EXAMPLE               DX = 0.0100
TEMP = 1050 C            TIME = 120.0000
EVAP RATE = 0.0000
OXIDE THK. = 5000 ANGSTROMS

1- ✱  -    DC = 3.909E-5    ANTIMONY    HP = 1.75E-57
2- ✱  -    DC = 4.277E-4    BORON       HP = 3.16826
3- O  -    DC = 4.629E-4    PHOSPHRS    HP = 5.09E-58
```

FIGURE A4

DATE 04/16/73 10:07:33

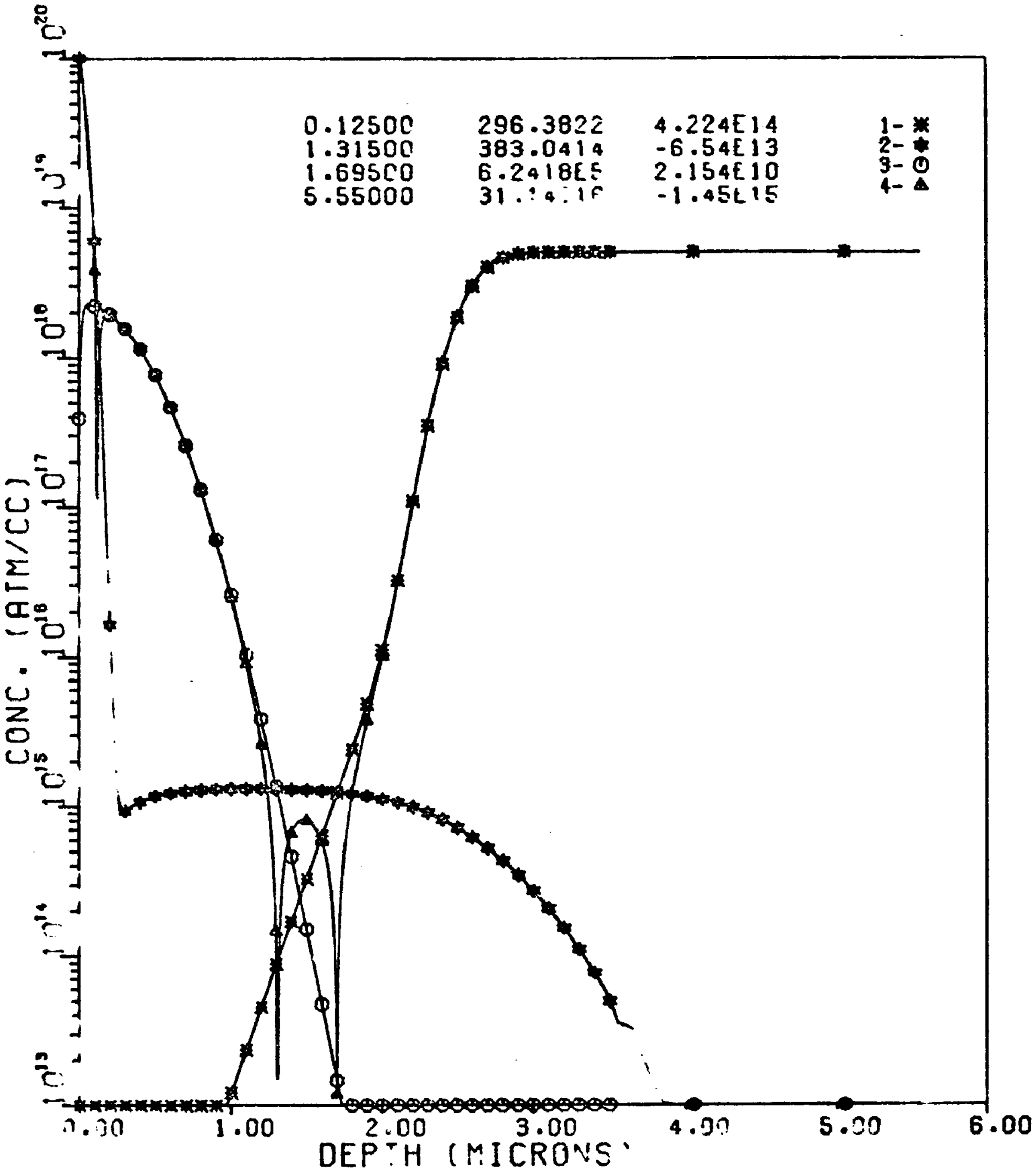

```
STEP = S                    BORON DIFFUSION
EXAMPLE           DX = 0.0100
TEMP = 900 C        TIME = 30.0000
EVAP RATE = 0.0000

1- ✱   -    DC = 4.815E-7   ANTIMONY    MP = 443.8741
2- ✸   -    DC = 4.270E-5   BORON       MP = 0.31063
3- ⊙   -    CC = 8.573E-6   PHOSPHRS    MP = 5.91538
```

FIGURE A5

DATE 04/16/73 13:37:49

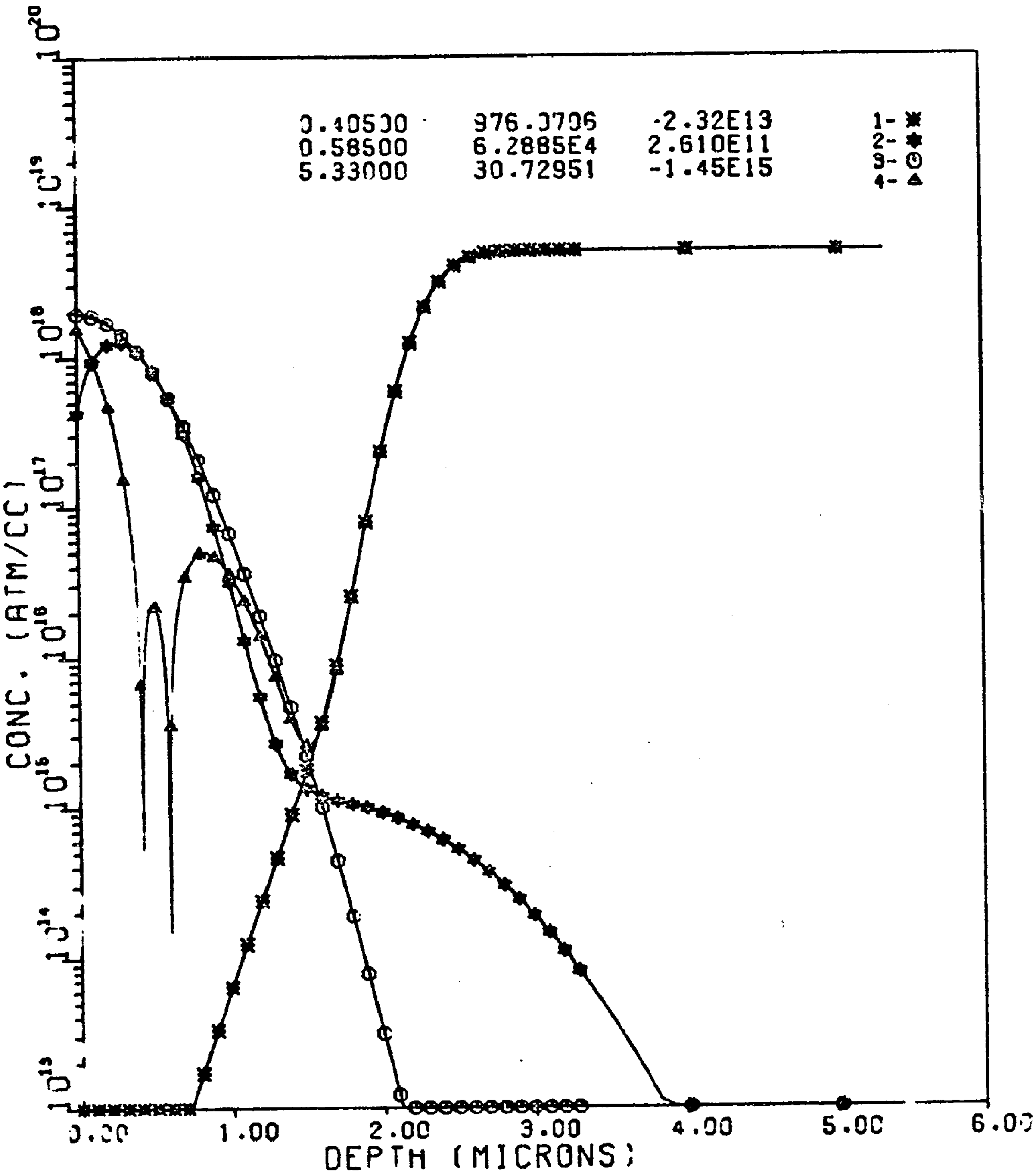

```
STEP = C                         OXIDATION
EXAMPLE                  DX = 0.0100
TEMP = 1050 C              TIME = 120.0000
EVAP RATE = 0.0000
OXIDE THK. = 5000 ANGSTROMS

1- ✱   -     DC = 3.909E-5   ANTIMONY    HP = 1.75E-57
2- ✸   -     DC = 4.277E-4   BORON       HP = 3.16826
3- ⊙   -     DC = 4.629E-4   PHOSPHRS    HP = 5.09E-58
```

FIGURE A6

DATE 04/16/73 10:08:13

TABLE A2

```
STEP....   6                 OXIDATION                                              DATE  04/13/73     TIME - 20:36:01
EXAMPLE
     TEMP=  1050.0 C                                                                        PAGE =    2

      ELEMENT       STEP       BC SURF CONC/DOSE     ENHANCE        STDDEV       EVAP COEF        DIFFUSIVITY

   1   ANTIMONY       1         3      1.0000D 12     0.0            1.7110-01    1.0000D-60      3.9090-05
   2   BORON          1         3      1.0000D 15     0.0            1.9950 00    5.9810-03       4.2770-04
   3   PHOSPHRS       3         3      1.0000-60     1.0000-60       1.9050 00    1.0000-60       4.6290-04

TIME      =  120.00000 MINUTES                            COEF1 =     5.000000 18
THICK     =    3.00000 MICRONS                            COEF2 =     0.0
EVAP RT   =  0.0       MIC/MIN                            COEF3 =     0.0
GRWT RT   =    0.0     MIC/MIN                            COEF4 =     0.0
OX THK    =    5000.00 ANGSTMS                            COEF5 =     1.000000 21
FAUTO     =  0.0                                          CMEAN =     1.111110 05
FINTF     =  0.0                                          DOSE  =     1.000000-02
NSP/2     =   59.00000                                    MAX.CONC    1.164700 19
     KO =     1.90546                                     DPMAX =     1.000000-60
     KE =     1.90546                                     STDEV =     4.856170-02

  DX =     0.0100      DT =  2.558051      R=    0.80270
  NSP =       353      NTS =       37      JCNT =   0  1  3  1  1  0  0  1  3  0  0  0  0  3  0  1  6  6  0100

     DEPTH    D/Z        TOT CON         ANTIMONY        BORON           PHOSPHRS

     0.280    0.594     -2.03630 17     6.38890 11     1.27420 18     1.47810 18     0.0          0.0          0.0
     0.290    0.615     -1.78400 17     6.74250 11     1.26910 18     1.44750 18     0.0          0.0          0.0
     0.300    0.636     -1.54740 17     7.12660 11     1.26190 18     1.41660 18     0.0          0.0          0.0
     0.310    0.658     -1.32820 17     7.54170 11     1.25260 18     1.38540 18     0.0          0.0          0.0
     0.320    0.679     -1.12610 17     7.98900 11     1.24130 18     1.35390 18     0.0          0.0          0.0
     0.330    0.700     -9.40560 16     8.46960 11     1.22810 18     1.32220 18     0.0          0.0          0.0
     0.340    0.721     -7.71270 16     8.98510 11     1.21310 18     1.29030 18     0.0          0.0          0.0
     0.350    0.742     -6.17730 16     9.53750 11     1.19650 18     1.25830 18     0.0          0.0          0.0
     0.360    0.764     -4.79440 16     1.01290 12     1.17820 18     1.22620 18     0.0          0.0          0.0
     0.370    0.785     -3.55930 16     1.07610 12     1.15850 18     1.19410 18     0.0          0.0          0.0
     0.380    0.806     -2.46270 16     1.14380 12     1.13740 18     1.16200 18     0.0          0.0          0.0
     0.390    0.827     -1.50130 16     1.21610 12     1.11500 18     1.13010 18     0.0          0.0          0.0
     0.400    0.849     -6.67210 15     1.29340 12     1.09150 18     1.09820 18     0.0          0.0          0.0
     0.410    0.870      4.65900 14     1.37590 12     1.06700 18     1.06650 18     0.0          0.0          0.0
     0.420    0.891      6.47080 15     1.46420 12     1.04150 18     1.03500 18     0.0          0.0          0.0
     0.430    0.912      1.14130 16     1.55850 12     1.01520 18     1.00380 18     0.0          0.0          0.0
     0.440    0.933      1.53620 16     1.65920 12     9.88210 17     9.72850 17     0.0          0.0          0.0
     0.450    0.955      1.83480 16     1.76680 12     9.60610 17     9.42220 17     0.0          0.0          0.0
     0.460    0.976      2.05590 16     1.88180 12     9.32520 17     9.11960 17     0.0          0.0          0.0
     0.470    0.997      2.17420 16     2.00470 12     9.04020 17     8.82070 17     0.0          0.0          0.0
     0.480    1.018      2.26040 16     2.13590 12     8.75220 17     8.52610 17     0.0          0.0          0.0
     0.490    1.039      2.26110 16     2.27610 12     8.46200 17     8.23590 17     0.0          0.0          0.0
     0.500    1.061      2.20260 16     2.42590 12     8.17070 17     7.95040 17     0.0          0.0          0.0
     0.510    1.082      2.09130 16     2.58590 12     7.87910 17     7.66990 17     0.0          0.0          0.0
     0.520    1.103      1.93320 16     2.75690 12     7.58790 17     7.39450 17     0.0          0.0          0.0
     0.530    1.124      1.73440 16     2.93960 12     7.29800 17     7.12450 17     0.0          0.0          0.0
     0.540    1.146      1.50040 16     3.13470 12     7.01010 17     6.86000 17     0.0          0.0          0.0
     0.550    1.167      1.23630 16     3.34320 12     6.72490 17     6.60120 17     0.0          0.0          0.0
```

VITA

Paul H. Langer was born to Beatrice and David M. Langer on September 6, 1941 in New York, New York. After receiving his basic education in the public schools of Brooklyn, he was graduated from Brooklyn Technical High School in June of 1959. After graduation from high school he enrolled in the metallurgy curriculum at the Polytechnic Institute of Brooklyn. He was active in student affairs throughout his undergraduate career, serving as captain of the fencing team and president of his fraternity. In 1963 he was elected to Who's Who in American Colleges and Universities. He graduated in June of 1963 with a Bachelor of Science degree in Metallurgical Engineering having made the Dean's List for eight consecutive semesters. In August of 1963 he married the former Elaine Lipton who became the mother of his sons Jeffrey in 1967 and Eric in 1970.

In 1963 he started work on his masters degree also at the Polytechnic Institute of Brooklyn. His Master's thesis concerned the effects of ultra high pressure on the precipitation in iron based superalloys. Mr. Langer received his Master of Science degree in Metallurgical Engineering in June of 1964. In July of the same year he started his association with the Allentown Works of Western Electric as an engineer in the Semiconductor Materials Engineering group specializing in the area of semiconductor crystal growth. In 1965 he was promoted to Planning Engineer and to Senior Engineer in 1969. For the last four years he has been involved with the measurement of electrical and optical properties of semiconductors.

He holds membership in Tau Beta Pi, Sigma Xi, The American Society of Metals, The American Institute of Mining, Metallurgical, Petroleum Engineers, The American Society for Testing Materials, and the Electrochemical Society, and has co-authored the following papers:

1. Niehaus, W. C., van Gelder, W., Jones, T. D., and Langer, P. H., "Variations of a Basic Voltage-Capacitance Technique for Determination of Impurity Profiles in Semiconductors", Silicon Device Processing, edited by C. P. Marsden, National Bureau of Standards Special Publication 337, p. 256, 1970.
2. Langer, P. H., and Goldstein, J. I., "Impurity Redistribution During Epitaxial Growth and Semiconductor Device Processing", accepted for publication in the Jl. Electrochem. Soc., March 1973.
3. Langer, P. H., and Pearce, C. W., "Epitaxial Resistivity", accepted for publication in Standardization News, March 1973.